Synthesis of Shape Morphing Compliant Mechanisms

by

Kerr-Jia Lu

A dissertation submitted in partial fulfillment
of the requirements of the degree of
Doctor of Philosophy
(Mechanical Engineering)
in The University of Michigan
2004

Doctoral Committee:

       Professor Sridhar Kota, Chair
       Professor Debasish Dutta
       Professor Peretz P. Friedmann
       Associate Professor Kazuhiro Saitou

For Mom, Dad, my sister, Kerr-Hsin,

and

My loving husband, Jia-Hsuan.

Thank you for all your love and support.

Thank you for being my best friends and always being there for me.

ACKNOWLEDGEMENTS

Joel Hetrick and Dr. Jinyong Joo have enhanced my understanding of the fundamental design issues in compliant mechanisms. I am also very grateful for their advices for my future career plan. I want to thank Mr. Charles Kim, Mr. Brian Trease, Mr. Tanakorn (Tony) Tantanawat, Ms. Christine Vehar, Mr. Michael Cherry, and Mr. Zackary Kreiner, whom I see day in and day out in CSDL, for always letting me bounce ideas off of them. The countless discussions in the lab have always been very inspiring. All the other non-academic activities in the lab have also made my graduate study unforgettable.

I want to thank Mr. Kuei-Yuan (Miles) Chan, for his suggestions on local search algorithms. Thanks to Mr. Cheng-Yu (Shower) Lin for motivating the structural design examples and to Mr. Shih-Fen Cheng for offering advice on various optimization algorithms.

TABLE OF CONTENTS

LIST OF FIGURES

xiii

CHAPTER 1

INTRODUCTION TO COMPLIANT MECHANISMS

1.1 Compliant Mechanisms

A compliant mechanism is a single-piece flexible structure with mobility of a conventional mechanisms and stiffness of conventional structures. As shown in Figure 1-1(a), a conventional rigid-link mechanism is comprised of a number of discrete links connected by kinematic joints. The mobility in a mechanism is obtained from the relative rigid-body motion between links, due to the degrees of freedom at the joints. On the other hand, as shown in Figure 1-1(b), a structure is generally designed to be rigid and stiff to sustain external loads. Thus, the structural deformation induced by the external load is considered undesirable. As can be seen in Figure 1-1(c), a compliant mechanism is similar to a conventional mechanism in that it functions as a transmission between the input actuation and the output to the environment. But instead of deriving its mobility from the relative rigid-body motion between links, a compliant mechanism utilizes the structural deformation, induced by an input actuation, to transmit force or deliver motion. Due to the absence of joints, a compliant mechanism can also be seen as a structure that is stiff enough to bear loads. However, the structural deformation is now considered a desirable effect, providing mobility to work against the external loads.
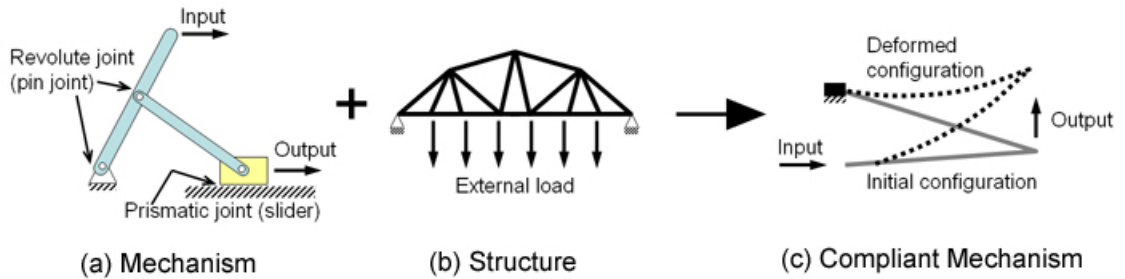
Figure 1-1: (a) A conventional mechanism; (b) a load-bearing structure; (c) a compliant mechanism.

In other words, a compliant mechanism is a combination of a structure and a mechanism, since the jointless feature resembles a structure, while the function of the structure resembles a mechanism. It is a single-piece flexible structure that gains its mobility from structural deformation due to an input actuation. It is a monolithic device that is capable of what conventional mechanisms can do with multiple links and hinges. It is also designed to be flexible enough to transmit motions, yet stiff enough to withstand external loads.

1.1.1   Classification of Compliant Mechanisms

Compliant mechanisms can be classified into *lumped compliant mechanisms* and *distributed compliant mechanisms*, depending on the distribution of compliance in the structure. As shown in Figure 1-2(a), a lumped compliant mechanism is characterized by thin flexural segments (lumped compliance) that mimic the revolute joints seen in rigid-link mechanisms. The localized deformation due to bending at these flexural segments (flexural pivots) provides the required mobility in the compliant mechanism. In Figure 1-2(b), a distributed compliant mechanism is characterized by the smooth profile with gradual dimension changes (distributed compliance). The mobility of the compliant

2

mechanism is derived from the structural deformation that is more evenly distributed over the entire structure.
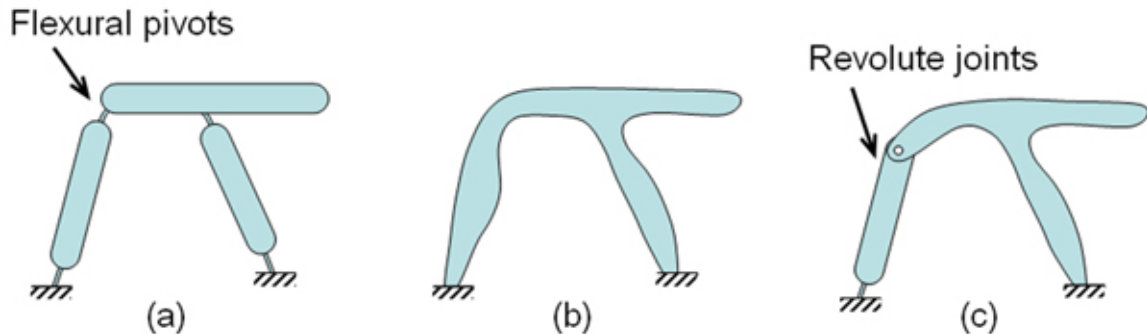
Figure 1-2: (a) A fully compliant mechanism with lumped compliance; (b) a fully compliant mechanism with distributed compliance; (c) a partially compliant mechanism with both lumped and distributed compliance features.

Since a lumped compliant mechanism can be seen as a traditional mechanism with flexural pivots replacing the revolute joints, the lumped compliant mechanism can take advantage of the foundation laid by traditional mechanism, including analysis and synthesis techniques. In a distributed compliant mechanism, the deformation is no longer localized, thus the structural deformation has to be solved for analytically or using finite element analysis (FEA). Although lumped compliant mechanism can benefit from the wealth of knowledge in traditional mechanism, the localized deformations at the flexural pivots give rise to high stress concentration, which, in turn, limit the range of motion and load bearing capacity. On the contrary, a distributed compliant mechanism is less susceptible to stress concentration, thus providing a more robust and reliable design.

Compliant mechanisms can also be classified based on where the mechanism mobility is obtained. When the compliant mechanism gains its mobility entirely from structural deformation (compliance), they are termed as *fully compliant mechanisms*. Both examples in Figure 1-2(a) and (b) belong to this category. When the mobility is derived partly from kinematic joints, in addition to structural deformation, they are

3

termed as *partially compliant mechanisms*. Figure 1-2(c) shows a partially compliant

mechanism with both lumped and distributed compliance. In this dissertation, the

discussion will focus mainly on the fully distributed compliant mechanisms.

1.1.2 Advantages of Compliant Mechanisms

Due to the hingeless nature, compliant mechanisms offer numerous advantages

over traditional mechanisms. Figure 1-3 is an example illustrating how compliant

mechanism reduces the number of parts. The ability to store strain energy in compliant

mechanism eliminates the need of return springs; the monolithic feature reduces the

number of joints and fasteners in the assembly, leading to weight savings. In addition, the

absence of joints greatly simplifies the manufacturing and assembling process, in that the

compliant parts can be injection molded and there is little or even no assembly required.

This not only significantly reduces the cost but also improves the quality and robustness

of the design. Furthermore, the absence of joints in compliant mechanisms eliminates the

backlash seen in kinematic joints, thus providing high precision and highly repeatable

motion. The noise and wear associated with kinematic joints are also eliminated, which

further reduces the cost for maintenance and enhances performance.

Figure 1-3: A compliant stapler significantly reduces the number of parts in a traditional stapler (Ananthasuresh and Saggere, 1994).

1.1.3 Areas of Applications

The use of compliant mechanism is actually quite common in many everyday items, such the flexural hinge on a shampoo cap and the flexible structure that holds the CD in place in a jewel case. These designs take advantage of the compliant mechanism for its simplicity in manufacturing and low cost. As indicated in the previous section, compliant mechanisms have many other desirable features that can potentially benefit designs ranging from micro- to macro-scales. While new applications are constantly being explored, several application areas that can benefit from compliant mechanism are introduced in the following.

Design-for-No-Assembly

The quality of a product is directly related to the number of parts and the number of required assembly processes. Due to the additional manufacturing and assembly error introduced in each step, reducing the number of parts and assembly process is essential to improving the quality and robustness of the design. The monolithic nature of compliant mechanism provides a good paradigm of design-for-no-assembly. The compliant stapler shown in Figure 1-3 is an excellent example demonstrating how compliant mechanisms can reduce the part count. Figure 1-4 gives another example on part reduction. Figure 1-4(a) shows a traditional eyeglasses frame with kinematic joints; Figure 1-4(b) shows a hingeless frame that replaces the 3-part joint-temple (arm) assembly with the one-piece compliant arm. The compliant arms are strong enough to support the weight of the glasses; they are also compliant to fold and deploy into the required position. The

compliant arms can be seen as spring loaded joints, thus are less susceptible to damage from moderate impact.
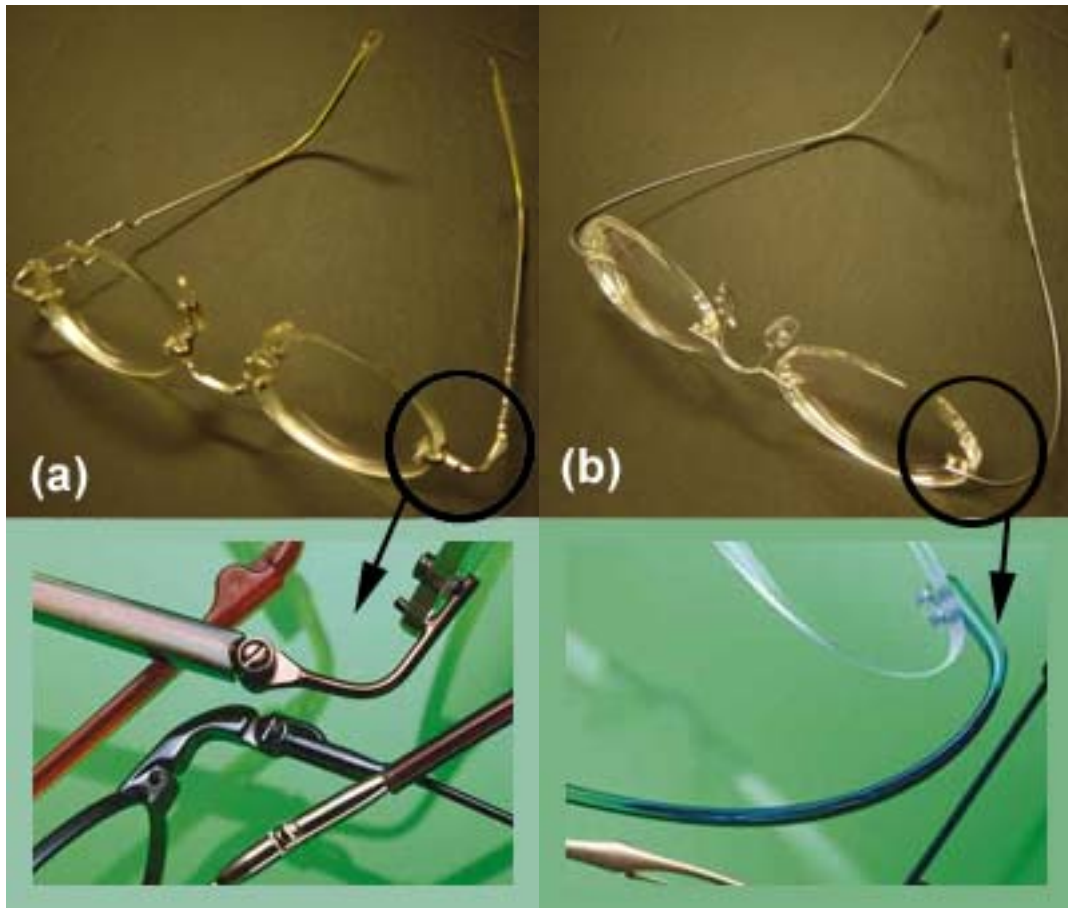
Figure 1-4: (a) Glasses with traditional kinematic hinges; (b) glasses with compliant temples (arms).

Actuator Tailoring

Smart actuators are compact and light-weight solid-state actuators made of materials such as shape memory alloys (SMA), piezoelectric materials, or magnetostrictive materials. The crystal structures of these materials change shape when subjected to external energy fields (heat source, electric field, or magnetic field). The crystal structure shape change results in bulk deformation of the material, which can be used for displacement or force actuation. Since the bulk displacement is the sum of the small deformation in crystal structure, the resulting output stroke is proportional to the

overall dimension of the actuator. The output stroke in these "compact" actuators is, therefore, often limited in range. Due to the absence of backlash and wear, compliant mechanism is particularly effective to work with such small displacements (1-100μm). The compliant mechanism can be seen as the transmission between the actuator and the desired output port. Using optimization techniques, it is possible to design a compliant mechanism with the desired input-output characteristics. Figure 1-5 shows a compliant mechanism that can efficiently amplify the displacements of electrostatic comb drives (commonly used in MEMS) by a factor of 20 without significant reduction in the output force (Kota et al., 2001; Kota, Rodgers, and Hetrick, 2001; Hetrick and Kota, 2003).
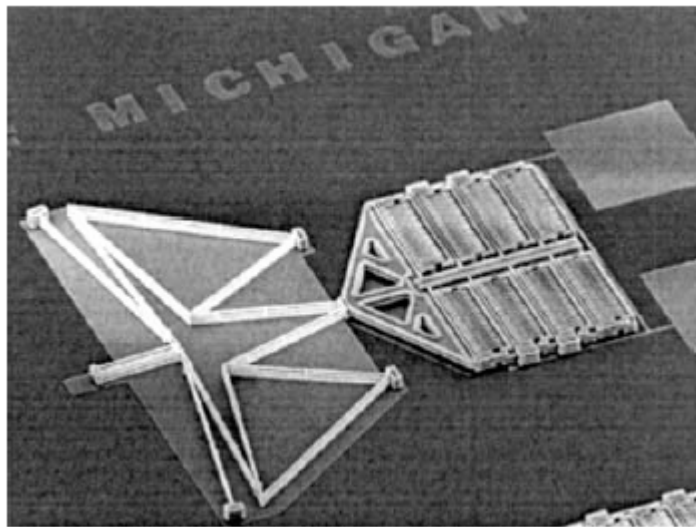
Figure 1-5: A MEMS displacement amplifier, when combined with the comb drive actuator, providing improved actuator (system) characteristics (Kota et al., 2001; Kota, Rodgers, and Hetrick, 2001; Hetrick and Kota, 2003).

Material Property Synthesis

Similar to the smart actuators that derive bulk deformation from shape change in crystal structure, bulk material property of any material can be "altered" by designing the topology of microstructure. The bulk material can be seen as an aggregation of many repeated microstructures. The micro structural behavior (deformation due to external load

or thermal expansion) can be designed to provide a desired bulk material property, such as negative thermal expansion coefficient or negative poisson's ratio. These micro structures are one-piece continuum with desired deformation, and can be regarded as micro compliant mechanisms. Figure 1-6 shows the microstructure of a material with a negative thermal expansion coefficient (Sigmund and Torquato, 1999).
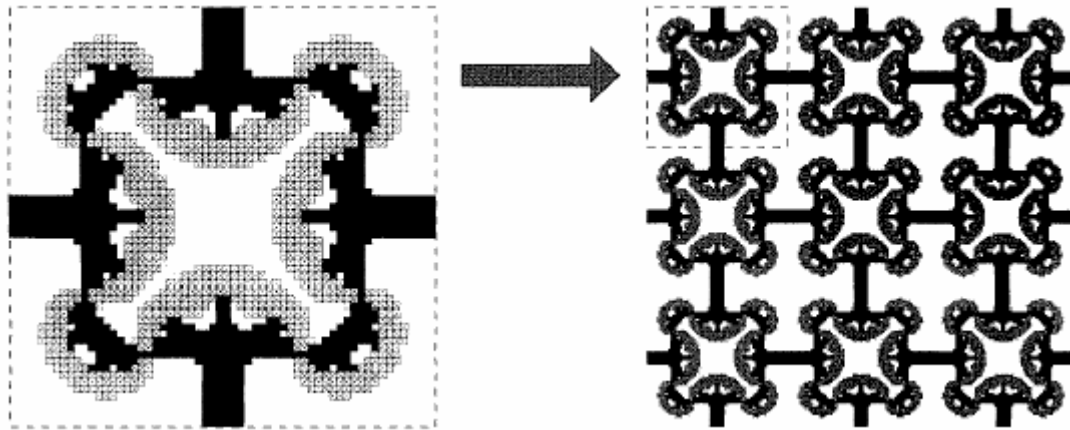
Figure 1-6: The optimized periodic microstructure of a material with a negative thermal expansion coefficient (macro-scale bulk behavior).

Micro- and Nano-electromechanical Systems (MEMS and NEMS)

In the MEMS or even NEMS field, the systems are operating at micro- or nano-meter range where the back lash and friction in conventional joints are no longer negligible. Assembling parts at such small scale is also difficult and undesirable. Compliant mechanism thus offers a superior paradigm for creating mechanisms working in such small scales. The monolithic nature allows compliant mechanisms to be easily created using photolithography, thus eliminating the need for micro assembling. Figure 1-7 shows a MEMS gripper for micro scale manipulation (Ananthasuresh, Kota, and Kikuchi, 1994). Other designs in MEMS include micro mirrors and suspensions.

8
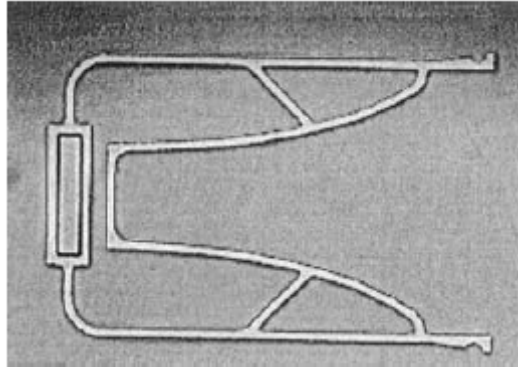
Figure 1-7: A MEMS gripper.

Precision Engineering

Flexures have been used in precision engineering for years before the term "compliant mechanism" was first defined in Her and Midha (1987). When the backlash in the kinematic joint is comparable to the required accuracy, flexures provide a simple yet high precision alternative. The absence of joint also eliminates the friction in conventional joints, which is difficult to model, control, and calibrate due to uncertainty in the contact region. Figure 1-8 shows a notch type double compound rectilinear spring used in ultraprecision mechanism (Smith and Chetwynd, 1992).
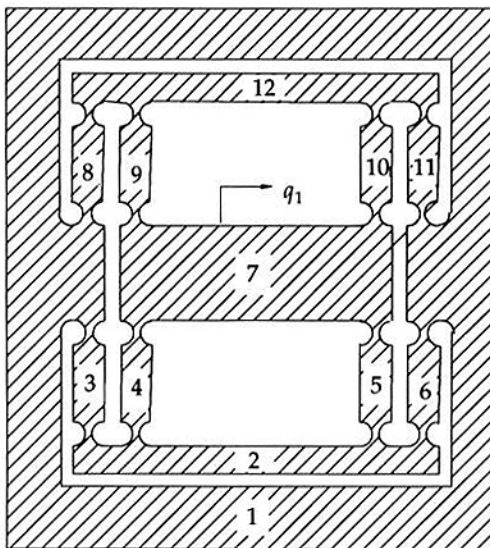
Figure 1-8: A notch type double compound rectilinear spring used in ultraprecision mechanism.

Bi-Stable Mechanisms

Compliant mechanisms can be seen as spring-loaded mechanisms, due to the storage of strain energy in the deformed structure. This property can be used to design bi-stable mechanisms such as switches and relays. Bi-stable mechanisms take advantage of the two stable configurations to generate binary on/off output that does not require continuous supply of energy to hold the mechanism in position. Figure 1-9(a) and (b) show the two stable positions of a lumped compliant mechanism that works as a thermally actuated micro-switch (Jensen et al., 2001), while Figure 1-10 shows another bi-stable partially compliant mechanism with one revolute joint (Jensen and Howell, 2000).
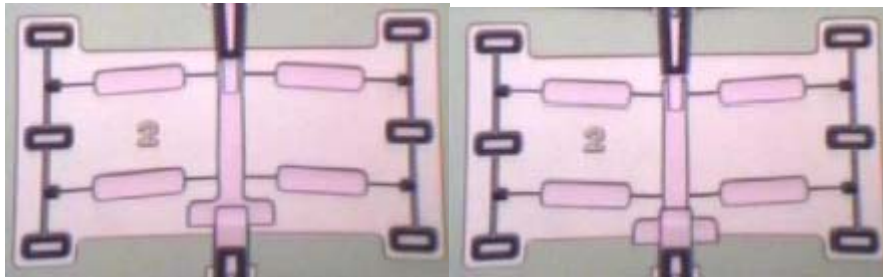
Figure 1-9: The two stable positions of a bi-stable compliant mechanism as a MEMS switch.
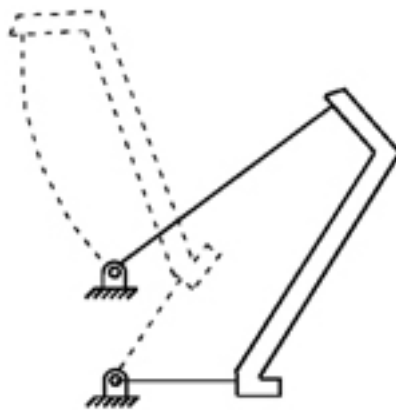
Figure 1-10: A partially compliant mechanism with bi-stable characteristics.

Adaptive Structures

In addition to the reducing stress concentration, a fully distributed compliant mechanism has a smooth deformation throughout the structure, which is particularly attractive to shape morphing applications (Kota, 1999, 2002). Morphing aircraft wings and flexible antenna reflectors are two examples where changing the wing or reflector shapes can increase system versatility and improve performance. In this dissertation, the compliant mechanism is tailored specifically for shape morphing applications. A more detailed discussion on shape morphing systems will be introduced in the following section.

1.2 Shape Morphing Systems

The performance of many mechanical/structural systems, such as aircraft wings and antenna reflectors, is directly related to the geometric shapes of their components. Such systems require different shapes under different tasks and operating conditions, but they are generally designed to have one fixed shape that constitutes a compromise with respect to all the operating conditions. For example, most aircraft wings are optimized to produce minimum drag under a particular flying speed, at which the largest proportion of fuel is expended. However, in reality, flying speed varies continuously throughout flight. Hence, morphing the wing shape in response to the change in flying speed can help maintain optimal fuel efficiency. The need for shape morphing in this example is *static*, because the wing shape may change in response to gust loads and assume the primary function of conventional control surfaces. Shape change can also be *active* in a system where the component morphs shape to perform various tasks. For example, the aircraft

wing shape can change actively to perform tasks ranging from high speed flight to long range loiter. A flexible antenna reflector is another example that changes its shape actively to vary the radiation signal pattern, while the external condition remains the same. This shape morphing concept can also be applied to many other engineering fields in various scales, such as lumbar support, fluid flow control devices, and biomimetic systems with embedded actuators/sensors to mimic the body shape change in fish or birds. A brief review of the development in shape morphing systems will be introduced in the following, focusing mainly on aircraft wings and antenna systems.

1.2.1 Conventional Rigid-Link Mechanisms

Shape change is conventionally achieved using rigid-link mechanisms, which involves push pins, lead screws, and all types of kinematic joints. Figure 1-11 shows an adjustable aircraft trailing edge by varying the angle at the joint. However, the hinge creates discontinuity over the wing surface, leading to early airflow separation (Kudva et al., 1997). This separation leads to reduced lift and increased drag. Moreover, the assembly of links and hinges are heavy and cumbersome. A smooth hingeless shape change, therefore, could potentially improve the aerodynamics and reduce weight, hence the fuel efficiency.

Figure 1-11: (a) A hinged flap that leads to earlier flow separation; (b) a smooth, continuous surface with improved aerodynamic characteristics.

Figure 1-12 shows a piecewise deformable antenna subreflector comprised of many discrete rigid panels that are hinged together (Lawson and Yen, 1988). Push rods are connected to the hinges to adjust the local curvature of the subreflector. Although the mechanism approach is simple and readily available, the hinges presented in the design may introduce backlash error, thus reducing the system accuracy. The friction at the joints also requires feed back control to maintain surface accuracy.
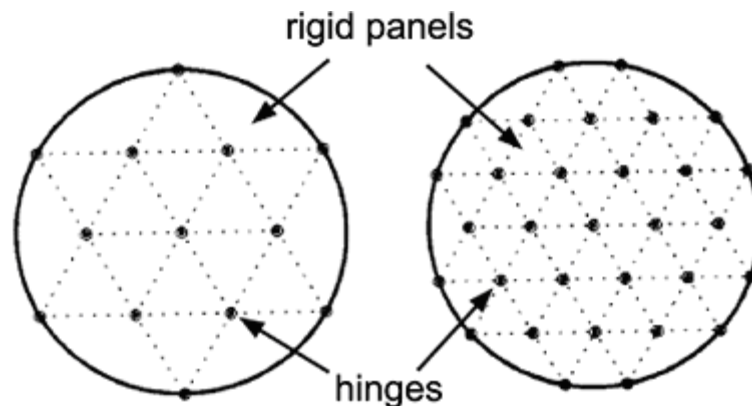
Figure 1-12: Piecewise deformable subreflector consisting of hinged panels.

1.2.2   Smart Material Actuators

Smart materials are light weight compact actuators that utilize the shape change of the material crystal structure to generate bulk force and displacement output. Some commonly seen smart actuators include piezoelectric actuators, magnetostrictive actuators, and shape memory alloy (SMA) wires. They are favorable choices for aerospace applications to reduce weight and increase payload. Majority of the previous research has proposed utilization of smart material actuators for aircraft wing morphing to reduce drag, improve fuel economy, and enhance performance (Austin and Van Nostrand, 1995; Austin et al., 1997; Martin et al., 1997; Webb, Lagoudas, and Kulkarini, 1999; Birkemeyer, Rosemann, and Stanewsky, 2000; Lutz, 2000; Wadehn et al., 2002). Figure 1-13 and Figure 1-14 are two shock control designs incorporating SMA wires and

piezoceramic actuators respectively. However, most of the studies have been focusing on

scaled down models, and the scalability of the smart actuators is still uncertain. In

addition, these materials suffer from hysteresis and creep which require a more

complicated control scheme. Readers interested in smart materials can refer to Chapter 3

in Saggere (1997) for a more detailed review in their applications in shape morphing

systems.
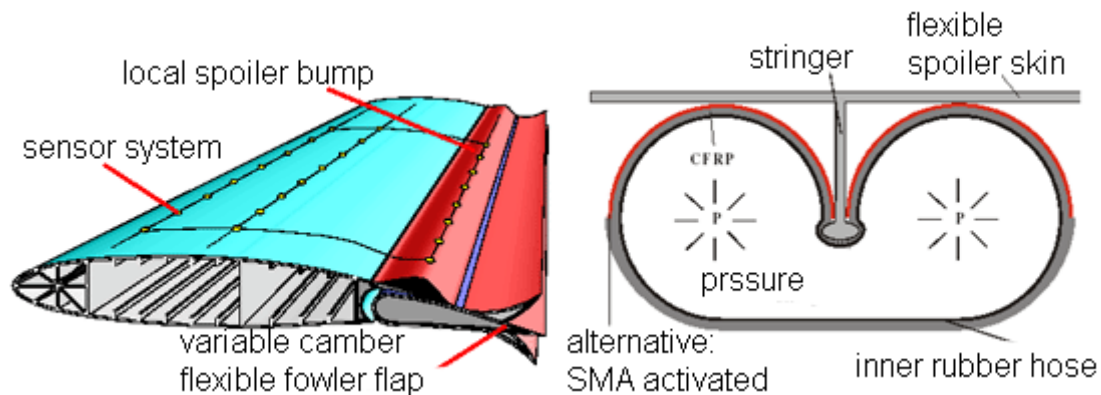
Figure 1-13: An adaptive spoil for transonic shock control using SMA wires (Bein, Hanselka, and Bereitbach, 2000).
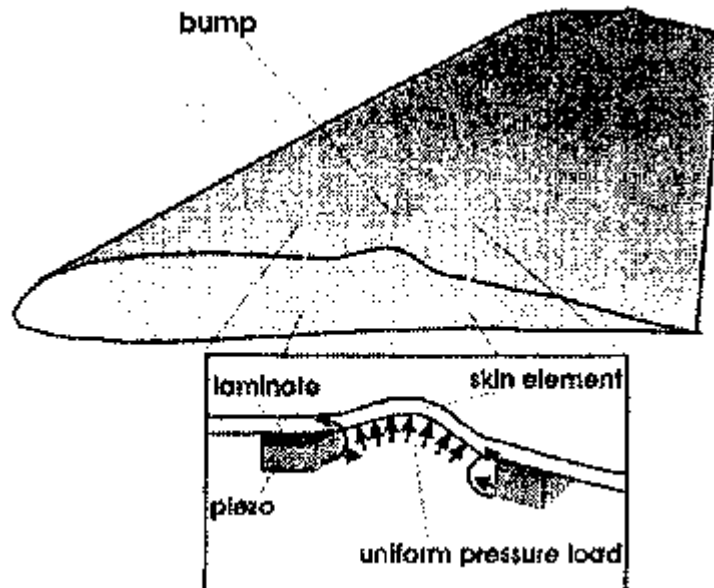
Figure 1-14: Airfoil shape control using piezoceramic actuators (Ameduri, Esposito, and Concilio, 2001).

Smart materials and actuators have also been incorporated in adjustable antenna reflectors. As seen in Figure 1-15 and Figure 1-16, Polyvinylidene fluoride (PVDF) thin films (Washington, 1996; Martin, Main, and Nelson, 1998; Martin et al., 2000) and piezoceramic (lead zirconate titanate, PZT) strips (Yoon and Washington, 1998; Yoon, Washington, and Theunissen, 2000) have been incorporated in antenna reflectors to vary signal pattern and change direction. However, both PVDF and PZT only provide a small displacement output and do not scale up proportionally for larger reflectors. Angelino and Washington (2001) then proposed an actuator system that combines a PZT stack and a screw-type mechanism. Although the lead-screw mechanism provides larger stroke and self-locking feature, the friction inconsistency in the driving mechanism complicates the required control system in order to take into account the nonlinearity and uncertainties.
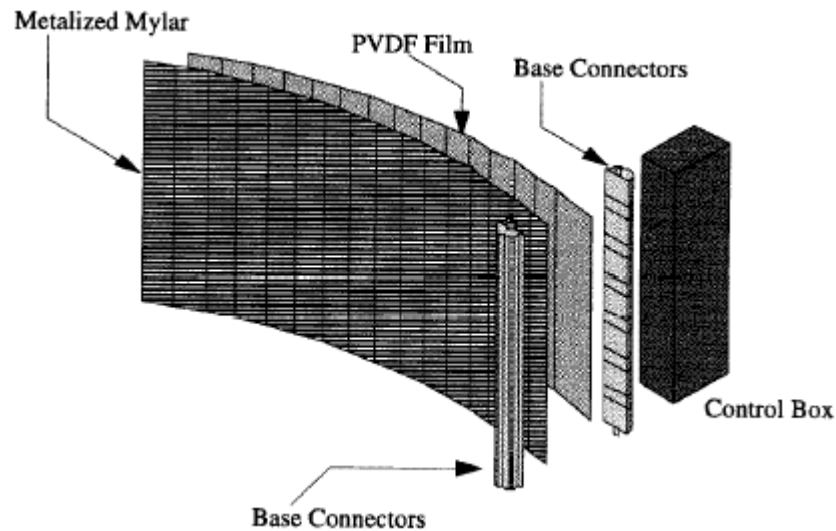
Figure 1-15: Adjustable cylindrical antenna reflector made of PVDF thin films.
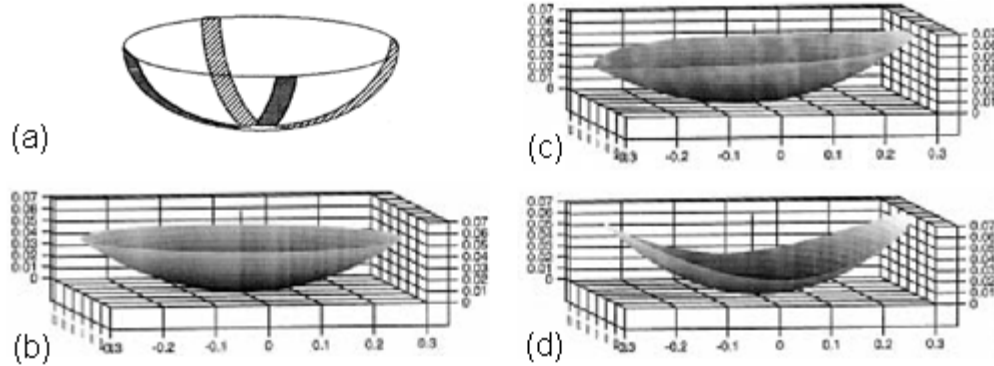
Figure 1-16: A doubly-curved adjustable antenna reflector incorporating PZT strips.

Most of the above systems involve using smart actuators in conjunction to a flexible structure (flexible airfoil and deformable reflector) to provide a smooth surface. Although the resulting shape morphing comes from the interaction between the actuator and the deformable surface, the deformation of the underlying structure that assists the shape change has been overlooked. The idea here is to design a more elaborated structure such that structural deformation can be seen as a functioning agent that controls the shape. However, no systematic design approaches have been developed particularly on how to design these structures. This research is, therefore, motivated to develop a systematic approach to synthesize such morphing compliant mechanisms.

1.2.3   Compliant Mechanisms

Unlike conventional rigid-link mechanisms, the hingeless nature of compliant mechanism provides a smooth morphing boundary (no discontinuity) with better fluid dynamic and aerodynamic characteristics. It changes shape through the structural deformation, which is independent of the scale of the problem, thus offering a scalable alternative for shape morphing. As opposed to the distributed actuation using smart actuators, compliant mechanisms utilize the distributed compliance to achieve the desired

shape change with fewer actuators (typically one) at a remote location, hence a simpler

control scheme. In addition, compliant mechanisms have low hysteresis, thus simplify the

control system.

Figure 1-17 illustrates the concept of a shape morphing compliant mechanism.

The actuator provides a displacement or force input to the system, and the compliant

mechanism deforms due to the structural flexibility, which, in turn, changes the boundary

from its initial state (initial curve profile) into a deformed state (deformed curve profile).

With a given input actuation, the shape of the deformed curve is determined by the

topology and dimensions of the compliant mechanism. By properly selecting the

topology and dimensions, the compliant mechanism can be designed to provide desired

shape morphing. However, systematic ways of designing such type of compliant

mechanism has been lacking in the literature. The goal of this research is, therefore, to

develop a systematic synthesis approach for shape morphing compliant mechanisms. A

brief overview of the development in typical compliant mechanism design will be given

in the next section.
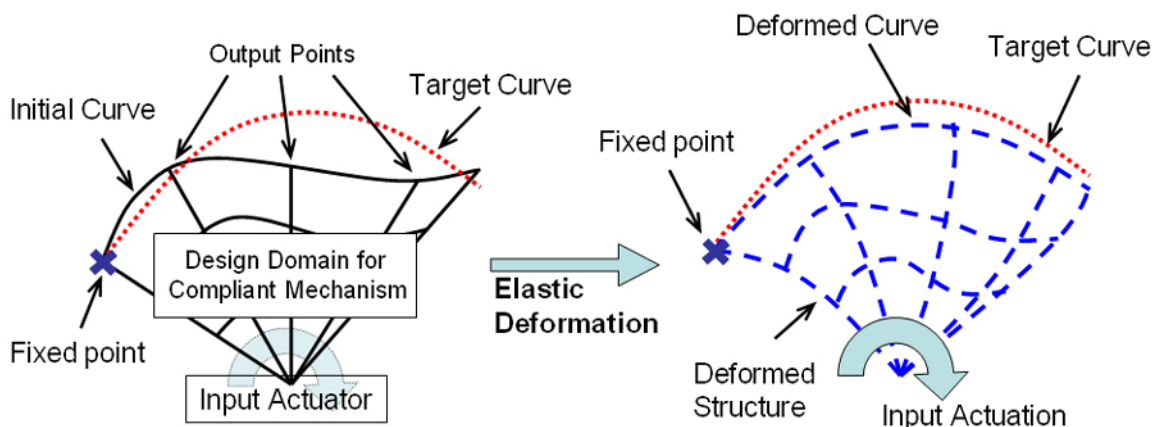
Figure 1-17: An illustration of the concept of a shape morphing compliant mechanism.

1.3 Compliant Mechanism Literature Review

Because of its shared features with mechanism and structure, the design of compliant mechanisms has mainly been approached from two different perspectives: kinematics approach and structural optimization approach. Both approaches have yielded successful designs, but the focus of each approach is different. The kinematic approach focuses on the modeling the structural deformation and strain energy storage of flexural pivots and flexible members in terms of torsional springs and kinematic joints, so the synthesis and analysis techniques from rigid-link kinematics can be used in designing compliant mechanisms. On the other hand, the structural optimization approach explores structural topologies that are non-intuitive to designers. Brief review of the development in these approaches will be introduced in the following.

1.3.1   Kinematics Approach

A compliant mechanism is different from a traditional mechanism in that compliance is presented in some or all of the links (flexible members) or joints (flexural pivots). The strain energy storage due to structural deformation in these flexible components has to be incorporated into the analysis to appropriately predict the mechanism behavior. However, solving a solid continuum problem, especially with non-linear large deflection, can be costly and does not incorporate insight from rigid-link kinematics. Modeling techniques based on rigid-body kinematics are, therefore, developed to include the effects from compliant components.

Flexural Pivots and Flexible Members

Flexural pivots (also termed as flexural hinges) and flexible members (leave springs) have been used in precision engineering as early as in the 18th century for precision instrumentations (Sobel, 1995). They are commonly seen nowadays ubiquitously from consumer products to precision machines. Possibly the main reason for their success is because flexures are easy to manufacture and provide smooth, friction free and wear free motion. They are designed to produce a geometrically well-defined motion upon application of a force. Various models can be found in (Slocum, 1992; Smith and Chetwynd, 1992; Smith, 2000) to aid in designing all types of flexure elements. However, flexures are only good for small range of motion, and they typically suffer from high stress concentration and have poor fatigue life.

Pseudo-Rigid-Body Model

With the abundant resources and foundation in rigid-link mechanism design, classical design and analysis techniques using kinematic chains can be modified to design compliant mechanisms if the compliance effects can be addressed. Howell and Midha (1994) introduced a *pseudo-rigid-body model* which models the behavior of flexible elements by combining rigid-body components (rigid links, kinematic joints, and springs) to give equivalent force-deflection characteristics. Pseudo-rigid-body models of various basic compliant configurations have been developed (Howell, 2001), including small-length flexural pivots, cantilever beam with end force, pinned-pinned segment, fixed-guided flexible segment, cantilever beam with end-moment loading, initially curved cantilever beam, and fixed-fixed segment. Two examples are shown in Figure 1-18 and

Figure 1-19 with their corresponding pseudo-rigid-body models, using torsional spring to

represent the member stiffness. As seen in Figure 1-19, the characteristic pivot is located

by γ (Howell and Midha, 1995) and the torsional spring constant can be determined based

on beam cross section geometry (Howell, Midha, and Norton, 1996). Using these pseudo-

rigid-body models, rigid-link mechanism theories can be employed to analyze compliant

mechanism behavior.
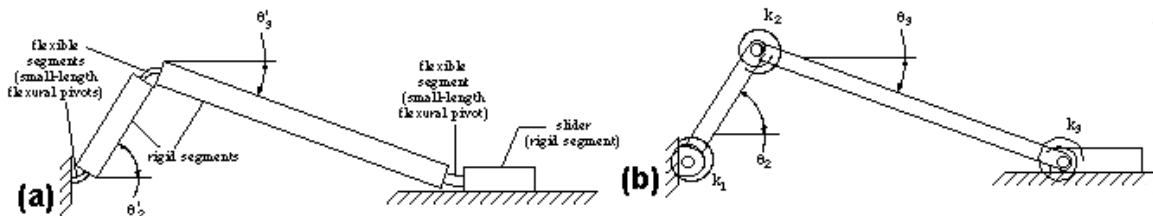
Figure 1-18: (a) A compliant slider mechanism and (b) its pseudo-rigid-body model.
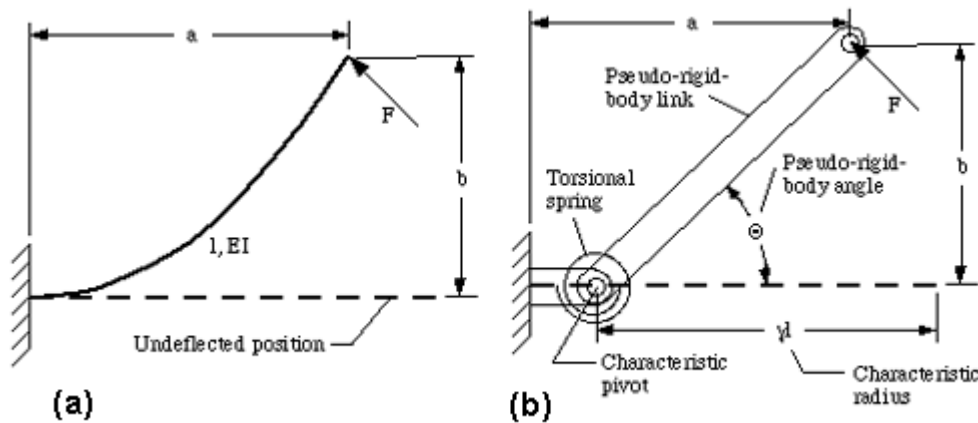
Figure 1-19: (a) A flexible segment and (b) its pseudo-rigid-body model.

For dimensional synthesis, Howell and Midha (1996) proposed a loop-closure

theory, based on analytical mechanism synthesis (Erdman and Sandor, 1991), to

synthesize compliant mechanism for traditional rigid-body mechanism tasks, such as path

or motion generation. Two classes of compliant mechanism synthesis have been

identified: (1) rigid-body replacement synthesis utilizes the rigid-link loop-closure

equations to determine kinematic geometry and replaces kinematic joints with flexural

pivots; (2) synthesis with compliance takes into account the energy storage in the compliant components, yielding additional equations and unknowns in loop-closure equations.

Type synthesis of compliant mechanisms can be accomplished with similar manner as designing rigid-link mechanisms with proper care of the flexible components. Murphy, Midha, and Howell (1996) investigated topology synthesis of compliant mechanisms by expanding graph theory and adjacency matrix to include flexible links and flexural pivots. This method provides a systematic technique for the enumeration of non-isomorphic compliant mechanisms.

Shape Morphing Designs

The majority of compliant mechanism synthesis using kinematics approach has been focusing on the three customary tasks in traditional kinematic synthesis: function, path, and motion generation. None of the previous research using this approach was found closely related to shape morphing applications. Shape morphing requires flexible links and no joints, rather than rigid links with flexible joints. The kinematic approach is, therefore, not a good candidate for designing shape morphing compliant mechanisms.

1.3.2 Structural Optimization Approaches

Since the introduction of the material distribution technique for computational implementations of topology design of continuum structures (the homogenization method) by Bendsoe and Kikuchi (1988), much research has been devoted to extend this approach to address other design problems in structural optimization as well as compliant

mechanism synthesis. This subsection gives a brief review of the development in

compliant mechanism synthesis using structural optimization techniques. In particular,

the review will focus on topology optimization. A more detailed review and the design

issues from shape morphing standpoint will be discussed in Chapter 2.

Continuous Optimization: Mathematical Programming

Ananthasuresh, Kota, and Kikuchi (1994) presented the first work to adopt

structural optimization techniques (homogenization) for compliant mechanism synthesis.

Since the deflection requirement in compliant mechanism render the problem much

different from traditional structural optimization problems, they formulated six different

objective functions to capture the compliant mechanism performance. Frecker et al.

(1997) and Nichiwaki et al. (1998) extended the weighted sum formulation in

Ananthasuresh, Kota, and Kikuchi (1994) and formulated a multi-criteria objective

function as a ratio of mutual potential energy over strain energy to address the problem

arising from scale differences between the two terms. The problem was implemented

using homogenization methods and truss ground structures, both giving similar results.

Larsen, Sigmund, and Bouwstra (1997) proposed a formulation using Geometric

Advantage (GeoA) and Mechanical Advantage (MA) to design compliant

micromechanisms. They suggested that GeoA times MA should be as close to one as

possible to ensure high efficiency in the compliant mechanism. The problem was

implemented using the SIMP approach (Solid Isotropic Material with Penalization)

(Bendsoe, 1989; Zhou and Rozvany, 1991; Mlejnek, 1992), which is very similar to the

homogenization approach but requires only 1/3 of number of design variables (Figure

1-20).
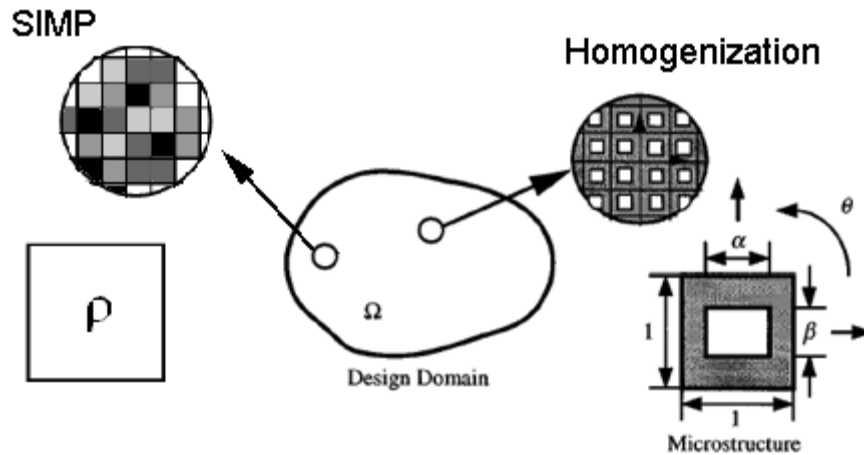
Figure 1-20: Two solid continua parameterizations. The SIMP approach uses the material density to describe each element; the homogenization approach uses the sizes and orientation of the micro void to describe each element.

Hetrick (1999) and Hetrick and Kota (1999) proposed an energy efficiency

formulation, which maximizes the transferred energy from input to the output port. The

problem was implemented using both truss and frame ground structures (Figure 1-21);

truss elements require less design variables, while frame (beam) elements eliminates the

structural singularity problem seen in truss structure. This work provides a well-posed

and robust objective formulation for topology, size, and shape optimization of compliant

mechanism. Joo (2001) extended the synthesis approach to address large deformation in

compliant mechanism by incorporating a non-linear finite element analysis (FEA).

Tapered beam elements were also included to render a smoother variation in compliant

segment cross sections.
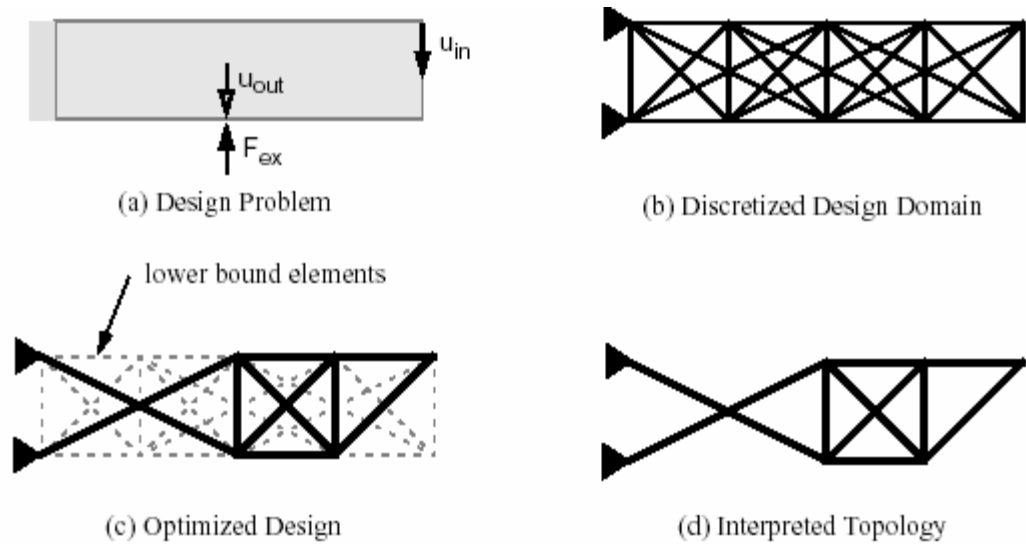
Figure 1-21: An illustration of the topology synthesis procedure using truss or beam ground structure parameterization (Hetrick, 1999).

The aforementioned works have been focusing on formulating new objective functions for compliant mechanism design in order to facilitate the use of traditional topology optimization methods, incorporating continuous optimization (based on mathematical programming techniques). However, the goal of topology design is to achieve a material and void structure (so called 0-1 or black and white structure) (Duysinx and Bendsoe, 1998), which is, in fact, a discrete problem by nature. Using continuous variables instead of discrete ones has led to the "gray area" problem, which generates ambiguity in the interpretation of the final topology. The generation of gray area also depends on the objective function; if strain energy term is considered in neither the objective function nor constraints, the resulting design may contain lots of gray areas and make the final interpretation even more difficult. The homogenization and SIMP approaches also create checkerboard patterns and hinge designs that are physically infeasible. Although the results can be interpreted using engineering intuition, the final designs generally have lumped compliances. This leads to various developments in

filtering schemes to remove these undesirable features. This is beyond the scope of this dissertation. Interested readers can refer to Bendsoe (1995) for more information.

One recent work by Sethian and Wiegmann (2000) has provided a new perspective to structural design problems. They adopted the level set method (Adalsteinsson and Sethian, 1995), originally used to track moving interfaces, for structural optimization. In a recent work, Wang, Wang, and Mei (2004) further adopted this method to design compliant mechanisms. The structural boundaries are represented using a level set model, and a 'speed function' is used to define the propagation speeds of boundaries, thus changing the design. Figure 1-20(a) shows a compliant gripper design example where the boundary merging process can be seen in (b)~(f). Unlike the previous research where structural topology is directly represented by the finite elements used in structural analysis, the structural representation (structural boundary in level set model) and the finite elements are now independent. The boundary is represented as a set of points on a three dimensional continuous surface, thus continuous optimization can be used. In addition, the material and void regions are clearly divided by the structural boundary, thus eliminating the gray area issue. However, the computer implementation of the algorithm is quite complex, and the approach has not yet been able to constrain maximum stress and minimum feature size. Furthermore, the results tend to have lumped compliance, which makes it unsuitable for shape morphing problems.
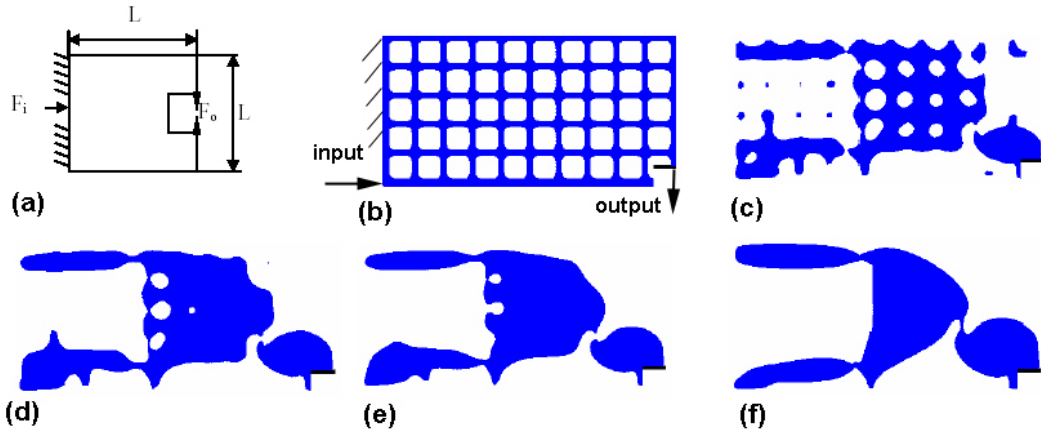
Figure 1-22: (a) Topology synthesis of a compliant gripper using level set method (Wang, Wang, and Mei, 2004); (b) the initial structural boundaries; (c)~(e) intermediate topologies; and (f) final design.

Discrete Optimization: Heuristic, Evolutionary, and Others

To address the discrete nature of topology optimization, discrete optimization techniques have been adopted to solve traditional structural topology optimization problems. The same objective functions are used as well as the design domain parameterization (solid continua and ground structures); however, the topology optimization problem is now addressed using discrete methods. Two most commonly used methods are the genetic algorithm (GA) (Holland, 1975; Goldberg, 1989) and simulated annealing (SA) (Metropolis et al., 1953). Chapman, Saitou, and Jakiela (1994) used a GA to optimize the topology of a cantilever beam with minimum deflection under end load. Shim and Manoochehri (1997) used SA to generate optimal configuration (topology and shape optimization) in structural design. GA and SA has also been used to search for the optimal topology (layout) in a truss ground structure (Hajela and Lee, 1995; Ohsaki, 1995; Rajan, 1995; Topping, Khan, and Leite, 1996; Rajeev and Kirishnamoorthy, 1997; Shrestha and Ghaboussi, 1998; Deb and Gulati, 2001; Kawamura, Ohmori, and Kito, 2002).

Similar to how structural optimization techniques could be adopted for compliant mechanism synthesis, discrete methods have also been used to design compliant mechanisms in recent years, especially with the improvement in computational capability. Saxena (2002) employed GA to find the optimal material distribution in a solid continuum and created compliant mechanisms with multiple materials. Parsons and Canfield (2002) used a frame-element ground structure and incorporated a multi-objective scheme in GA to search for the optimal compliant mechanism topology.

Using discrete optimization methods not only eliminates the gray area issue, it also has the flexibility to simultaneously optimize the structural dimensions during topology synthesis. However, previous research in both structure and compliant mechanism design has encountered singularity (disconnected structure) problems when discrete methods are used without connectivity constraints, as illustrated in Figure 1-23. They have, therefore, devised ways to identify or search for disconnected designs: Chapman, Saitou, and Jakiela (1994) used a connectivity analysis to ensure the structure is connected to the ground and loading point; Hajela and Lee (1995) used a singular value decomposition to assess the kinematic stability of truss structures; and Shim and Manoochehri (1997) used a connectivity checking algorithm to maintain connectivity between elements. Upon identification of a disconnected design, a penalty term was then used to penalize the design. However, searching and penalizing the disconnected design is computationally expensive, and, more importantly, this process was unable to effectively prevent the generation of disconnected structures.
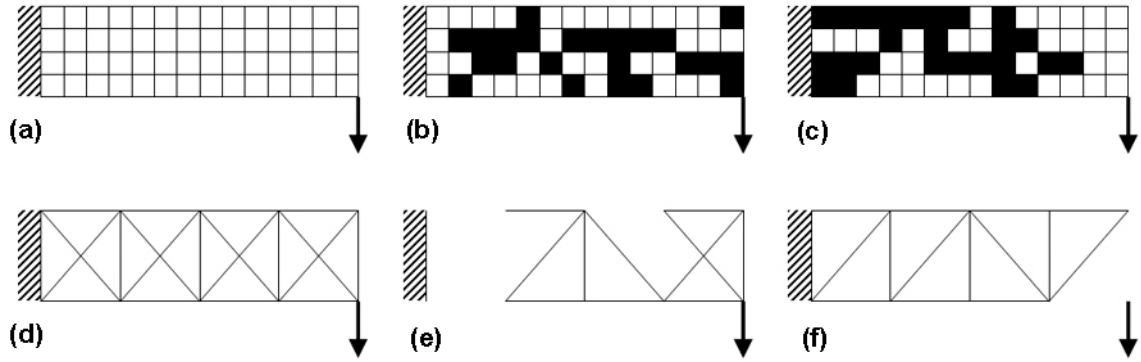
Figure 1-23: (a) Design domain discretization using solid continua parameterization and two potential disconnected structures in (b) and (c). (d) Ground structure parameterization and the potential disconnected structures in (e) and (f).

To overcome the disconnected structure issue, Tai and Chee (2000), Cui, Tai, and Wang (2002), and Akhtar, Tai, and Prasad (2002) introduced a morphological representation to represent structural topology and dimensions as a graph. The connectivity of the graph is predefined to ensure input, output, and ground supports are connected to each other. The represented structure is then mapped onto a finite element mesh for structural analysis in FEA. The graph representation (of the structure) is optimized using SA or GA to create structures as well as compliant mechanisms. This is approach is another example where the structural representation is independent of the finite element mesh (refer to (Wang, Wang, and Mei, 2004) in the continuous approaches). Although several examples have been reported to demonstrate the capability of this approach, the mapping from the graph representation to the finite element model is not easy to implement and may cause inefficiency in GA when large function evaluation is required. Figure 1-24 shows a path generation compliant mechanism example and the design reported in Tai, Cui, and Ray (2002).
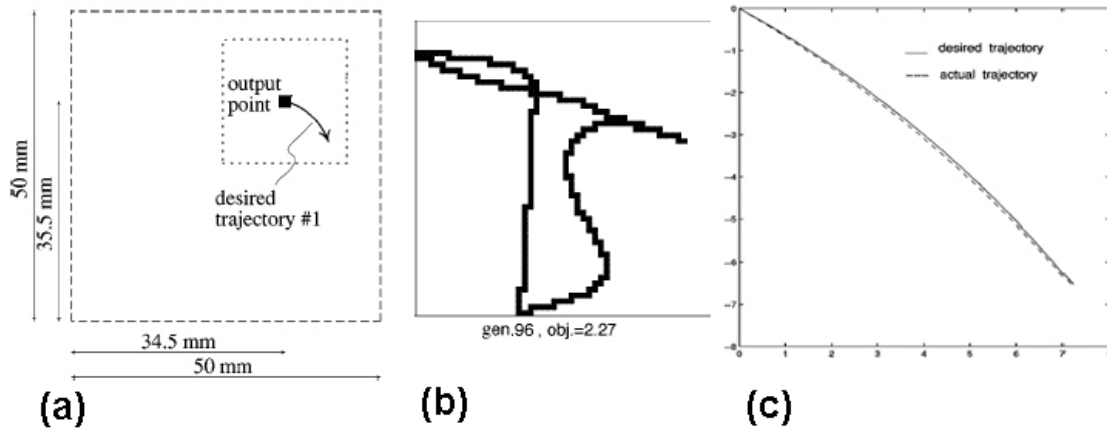
Figure 1-24: (a) A path generation compliant mechanism problem; (b) the design obtained from the morphological representation approach; (c) the desired and actual output point trajectories (Tai, Cui, and Ray, 2002).

Taking advantage of the development in optimization methods and the increase in computation speed, other iterative methods that are not based on mathematical programming have been developed to address structural design problems. Chu et al. (1996) introduced the evolutionary structural optimization (ESO) for topology optimization by iteratively removing materials from regions that are less sensitive to reducing the overall structural stiffness. Mattheck (1998) developed a computer aided optimization (CAO) that mimics the phenomena that have been observed in the mechanism of tree growth: self-optimization of living trees that follows the 'axiom of uniform stress.' Fourie and Groenwold (2002) applied the particle swarm optimization (PSO) to structural size and shape optimization. The algorithm, based on the simulation of a simplified social model, is closely tied to swarming theory introduced by Kennedy and Eberhart (1995). Although successful results have been reported in these works, these methods have only been applied to structural optimization problems. The applicability to compliant mechanism design is still uncertain, due to the kinematic requirement that renders the problem very different from structural design problem.

Shape Morphing Designs

Majority of the earlier literatures in compliant mechanism synthesis, using structural optimization techniques, have focused on formulating new objective functions to incorporate kinematic requirements into the traditional problem formulation in structure design. However, the kinematic requirement is generally defined by the performance at a single output point, while shape morphing can be seen as systems with multiple output points. Saggere and Kota (1999) was the only work focusing on shape morphing designs using compliant mechanisms. The design approach was separated into two steps: the topology is first determined by connecting the actuator to a prescribed number of output points whose locations (along the morphing boundary) are determined by an optimization routine; the structural dimensions are then optimized to obtain minimal difference between the morphed structure shape and the desired shape. The results have demonstrated the feasibility of the approach. However, the creation of topology was somewhat based on intuition; no systematic synthesis method was investigated. It is, therefore, essential to develop a systematic topology synthesis approach for shape morphing compliant mechanisms.

1.4 Scope of Investigation

The goal of this research is to develop a systematic approach to synthesize shape morphing compliant mechanisms. The synthesis approach will focus on fully compliant mechanisms for a smooth continuous boundary, which is generally desirable in shape morphing applications. The shape morphing considered in this dissertation will be limited to static shape change from a given initial shape to one desired target shape. This

provides the first step to potentially morph through as set of different shapes in the future. The compliant mechanism and its motion will be restricted to be planar, but the synthesis scheme should be general enough for future extensions to three dimensional compliant mechanisms. New objective functions will be formulated to evaluate the quality of the achieved shape morphing. For simplicity, linear finite element model will be used for structural analysis. Although non-linear analysis should be employed for more accurate results, it is not central to contribution in synthesis methods presented in this dissertation. Therefore, linear FEA is adopted here, while keeping the non-linear analysis optional.

Since a compliant mechanism derives its motion mainly from the bending of slender, beam-like segments, the design domain will be parameterized into a beam-based structure. Previous research has been using truss and frame ground structures, but the initial ground structure resolution and configuration are generally determined based on engineering intuition. In this dissertation, the frame ground structure approach will be investigated with guidelines on the selection of mesh resolution. To further address the disconnected structure problem seen in previous research, a load path representation will be introduced as a novel design domain parameterization method where the structure remains well-connected and the initial ground structure is no longer required.

To avoid the gray area issue, compliant mechanism topology should be addressed in its natural, discrete form. In this work, the synthesis approach will be implemented in a genetic algorithm, due to the simplicity of the algorithm and its ability to work with both discrete and continuous variables. In this way, the topology, size, and geometry aspects of compliant mechanism synthesis can be addressed simultaneously.

1.5 Organization of The Dissertation

The main purpose of this dissertation is to introduce two genetic algorithm based synthesis approaches for shape morphing compliant mechanisms; one uses a binary ground structure parameterization, and the other uses a load path representation method. Chapter 2 introduces the key components involved in the structural optimization based synthesis approach and identifies the need for a systematic synthesis approach tailored for shape morphing. Chapter 3 describes the problem formulation and assumptions, followed by a brief overview of the synthesis approach developed in this research. The key components in this synthesis approach will then be described separately from Chapter 4 to Chapter 6. Chapter 4 describes the design domain initialization which estimates the feasibility to morph between any two given shapes and identifies the minimum number of output points required in the shape morphing problem. Chapter 5 then introduces the *binary ground structure parameterization* and the *load path representation method* that have been developed in this research to represent various structural topologies (and dimensions) from two different perspectives. Chapter 6 describes the objective function quantifying the shape morphing effectiveness and the genetic algorithm (GA) used to search for the optimal design. Due to the distinct data structures in the two parameterization methods, reproduction strategies associated with either parameterization are also developed to ensure proper functioning of GA. Chapter 7 presents several design examples with results obtained from the two approaches. Insights to the shape morphing problem and the performance comparison of the two approaches are discussed following each example. Chapter 8 summarizes the contributions of this work and provides suggestions for future directions.

CHAPTER 2

SYNTHESIS OF COMPLIANT MECHANISMS

2.1 Topology, Size, and Geometry of Compliant Mechanisms

In the synthesis of compliant mechanisms, there are three design aspects that need to be addressed: the topology, size, and geometry of a compliant mechanism. Three different compliant mechanisms are shown in Figure 2-1 to illustrate different topologies and dimensions. The topology is the distribution of materials or *connectivity* within a given design domain. This material distribution creates holes and connections to form various topologies. The size and geometry of a compliant mechanism describe the dimensions of the remaining materials. The topology determines the 'qualitative' performance of the compliant mechanism and is typically characterized by the output 'direction' (a vector). The dimensions, on the other hand, control the 'quantitative' performance, which is based on the exact 'value' of an objective function, such as the output displacement or energy efficiency.
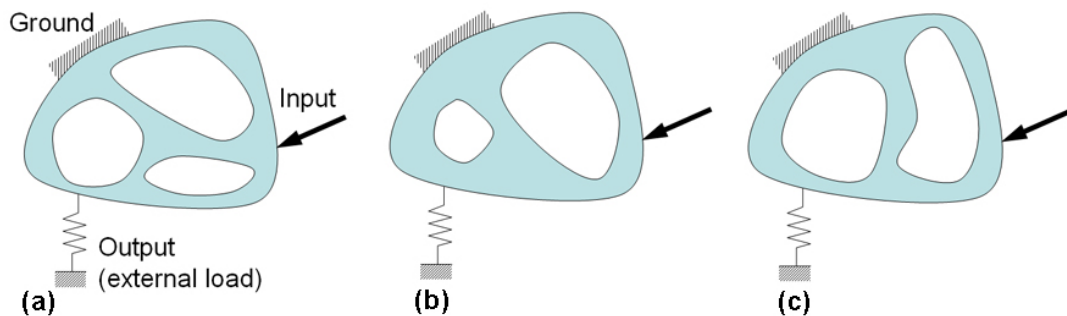
Figure 2-1: (a) A compliant mechanism design with three interior holes; (b) a design with two interior holes, hence a different topology from (a); (c) a design having the same topology as (b) but with different dimensions.

As illustrated in Figure 2-2, the synthesis of compliant mechanisms is typically accomplished through a two-step approach. The topology synthesis first determines the connectivity of the structure. The dimensional synthesis then optimizes the dimensions of a given topology to refine the design and enhance performance. Both steps rely on a structural optimization technique, which involves three key components: (1) the design domain parameterization, (2) the objective function, and (3) the optimization method. The design domain parameterization is the process of expressing various structural topologies in terms of a set of design variables. The parameterization should be able to describe all or as many as possible of the feasible topologies, while excluding infeasible ones from the solution space formed by the design variables. The objective function is a criterion that evaluates the performance of design in order to guide the optimization process towards optimum. An appropriate optimization method is then selected based on the parameterization to address discrete, continuous, or both types of design variables.
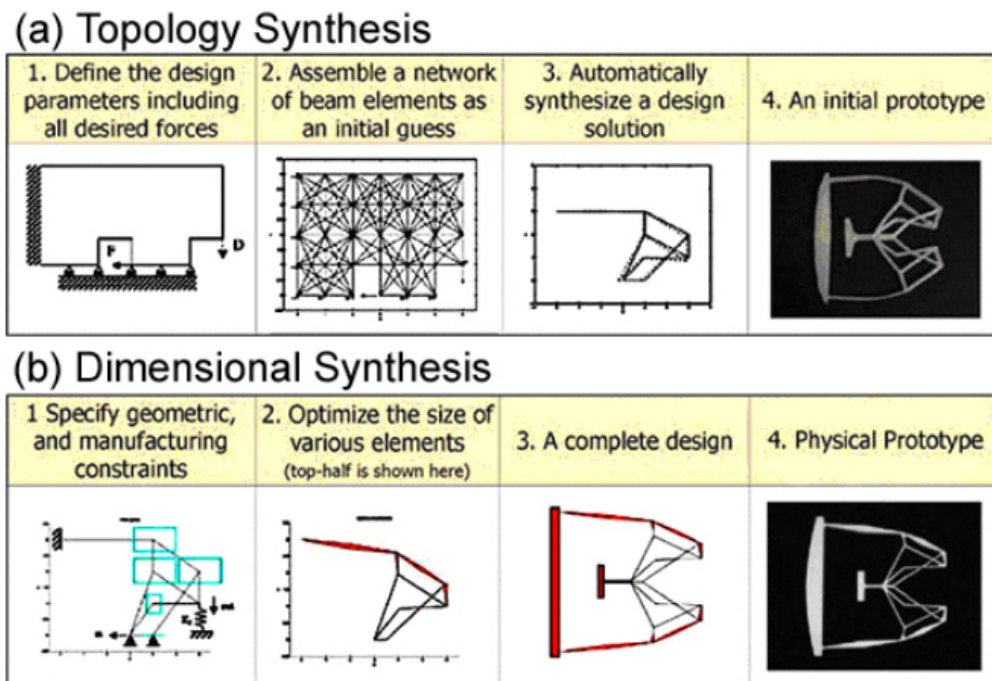
Figure 2-2: An illustration of the typical two-step approach for compliant mechanism synthesis: (a) topology synthesis, and (b) dimensional synthesis.

As seen in Figure 2-2(a-1), the topology synthesis starts with a given design domain and prescribed boundary conditions. Using a finite element (FE) discretization, the design domain is parameterized in terms of the element properties, such as beam cross section areas in Figure 2-2(a-2). The cross section areas are allowed to vary continuously between a lower and an upper bound, and the changes are directly reflected in the FE model, which, in turn, changes the compliant mechanism performance (eg. structural deformation and stress distribution). The optimal element cross sections are determined through an optimization based on the desired objective function, such as maximizing energy efficiency (Hetrick and Kota, 2000). The elements converging to the lower bound are eliminated from the initial mesh, and the remaining elements form the optimal 'topology' (Figure 2-2(a-3)~(a-4)). Ideally, the lower bound should be equal to zero to represent complete removal of an element, but a very small, non-zero value is used instead to prevent singularity of the FE stiffness matrix. This non-zero lower bound makes it difficult to apply stress constraint during the optimization, so the dimensional optimization is required as a second step to improve the design.

As shown in Figure 2-2(b-1), the dimensional synthesis starts with a given topology resulting from the previous step. The cross section dimensions and nodal locations are optimized in this step to improve the functional performance (eg. maximize mechanical advantage) while constraining stress and buckling. The objective function used in this second stage can be identical or different from the first stage, as long as the desired structural and kinematic performance can be captured. However, lower bound of the design variables is now set equal to the minimum manufacturable feature size, thus no elements are eliminated in this process. In other words, the dimensional synthesis

determines the optimal size and geometry of the design while keeping the topology

unchanged (Figure 2-2(b-2)~(b-4)).

The three key components in compliant mechanism synthesis – design domain

parameterization, objective function, and optimization method – will be introduced in

more detail in the following sections, leading to the discussion of specific research issues

encountered in designing shape morphing compliant mechanisms.

2.2 Design Domain Parameterization

In the majority of previous literature, two design domain parameterization

schemes were commonly incorporated in the topology synthesis step. One is a

continuum-based approach and the other is a ground structure approach. Both approaches

are based on the idea of discretizing the design domain with an initial finite element mesh

and using an optimization routine to remove unnecessary elements. Both linear and non-

linear FEA can be used to analyze the structural behavior within the optimization loop.

Linear analysis is more efficient, but may be inaccurate for larger deformation, while

non-linear analysis provides a more accurate result with higher computation cost.

2.2.1   Continuum-Based Approach

In the continuum-based approach, a predefined design domain is discretized with

an initial mesh of quadrilateral elements as shown in Figure 2-3(a). The structural

topology can be represented in terms of the element properties, so that by varying these

properties, the optimal material distribution (topology) as that in Figure 2-3(b) can be

found.
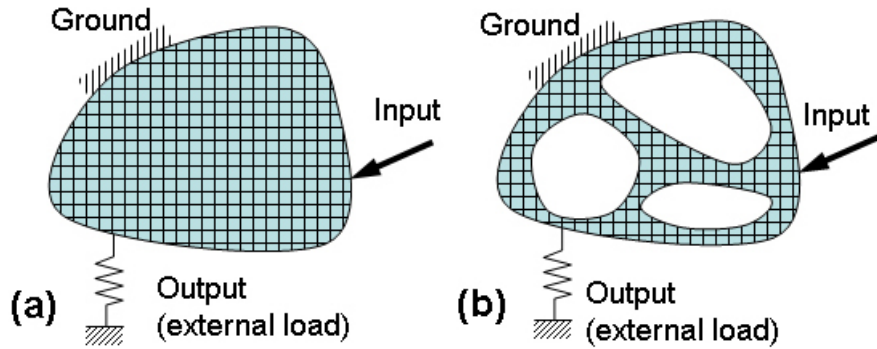
Figure 2-3: (a) A continuum-based design domain parameterization; (b) the optimized topology.

Two commonly used continuum-based methods are (1) the *homogenization method* (Bendsoe and Kikuchi, 1988) and (2) the *Solid Isotropic Material with Penalization* (SIMP) approach (Bendsoe, 1989; Zhou and Rozvany, 1991; Mlejnek, 1992). As seen in Figure 2-4, in the homogenization method, the design variables are the dimensions and orientation of the micro voids in the elements. For any given void size and orientation in an element, a homogenized element material property (elasticity tensor, E^H) can be calculated and reflected in the FEA. When the size of the void approaches the element size, this element has a very small E^H and can be considered an empty hole in the structure. Thus, the optimal material distribution (topology) can be found through optimizing the micro void arrangement in each element. Although this approach has provided bounds on the theoretical performance of structures (Sigmund, 2001), manufacturing such perforated structure is difficult. Therefore, the elements are interpreted as a solid material with the corresponding homogenized properties, E^H. This interpretation give rise to the gray area issue where removing intermediate E^H elements becomes ambiguous (see section 2.3.2).
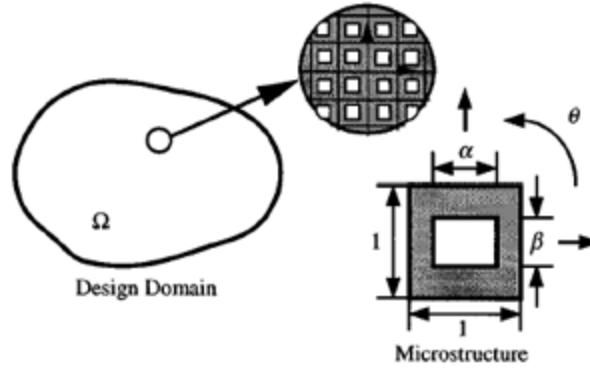
Figure 2-4: In the homogenization, the design variables are the dimensions and orientation of the void in the microstructure (Nishiwaki et al., 1998).

Alternatively, in the SIMP approach (or so-called "power-law" approach), the design variables are the element material density as shown in Figure 2-5(a). It is assumed that the material property of each element is the density raised to some power times the original material properties, shown in Eq.(2.1).

$$E_e = \rho_e^{\,p} E_0 \qquad (2.1)$$

where E_e: Young's Modulus of element e; ρ_e: material density of element e;
p: power-law constant (typically $p=3$); E_0: Young's Modulus of the solid material

(a)   (b)   (c)
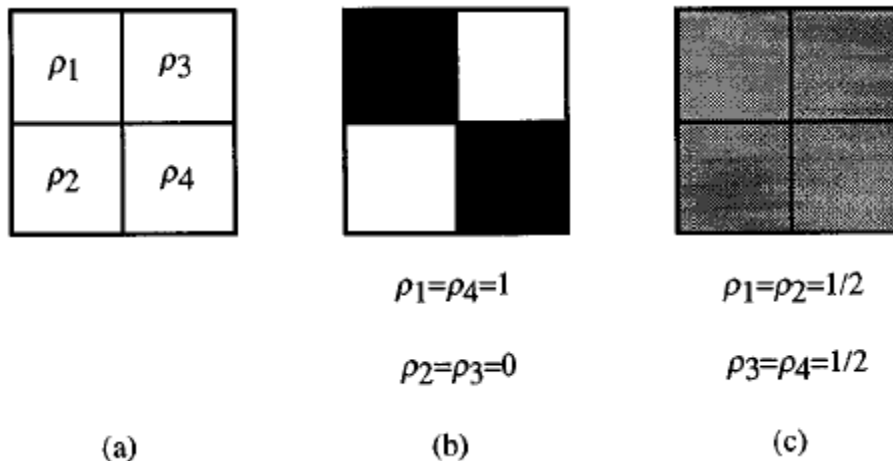
Figure 2-5: The checkerboard pattern commonly seen in structural optimization problems using continuum-based design domain parameterization (Nishiwaki et al., 1998).

When the density approaches 0, the element is seen as a void; when the density approaches 1, the element is treated as a solid. The power-low constant, p, is typically equal to 3 as suggested by Bendsoe and Sigmund (1999). In addition, the SIMP approach

must be combined with a perimeter constraint, a gradient constraint or with filtering techniques to ensure existence of solutions (Sigmund and Petersson, 1998).

One advantage of the continuum-based parameterization is that the size and geometry aspects of the structure can be addressed simultaneously in the topology optimization; the structure dimensions are defined by the solid material elements. However, stress constraint is generally not considered in the topology optimization, thus a second step dimensional optimization is still required to prevent failure. Duysinx and Bendsoe (1998) developed a constraint relaxation technique to constrain maximum stress in topology optimization, but the process adds more complexity to the algorithm. The technique was only applied to structural design; its applicability to compliant mechanism synthesis has not yet been demonstrated.

Although many successful designs have been created using these continuum-based approaches, the checkerboard pattern seen in Figure 2-5(b) is still an inherent problem associated with the continuum-based parameterization when using 4-node quadrilateral elements (Diaz and Sigmund, 1995). The hinge-like point contact in the checkerboard pattern is physically unrealizable, and it also creates singularity in FEA. A commonly used trick is to use a very small, non-zero value (eg. $\rho_{min}=10^{-9}$) instead of zero as the density lower bound to prevent singularity. However, the small $E(=\rho_{min}{}^{p}E_0)$ give rise to the checkerboard arrangement which has a seemingly larger stiffness than a homogenous material distribution in Figure 2-5(c). Various filtering or penalty schemes have been developed to suppress these undesirable features (see Saxena and Saxena (2003) for references), but these processes can further complicate the optimization algorithm, leading to inefficiency. As seen in Figure 2-6, although the checkerboard filter

reduces the checkerboard pattern in the design, gray area and hinge-like features still make the final design interpretation ambiguous. Typically, the checkerboard and gray area regions are interpreted as homogenous solid, and the hinge feature is replaced with a small-length flexural joint. But flexural joints may suffer from higher stress concentration and lead to earlier fatigue failure.
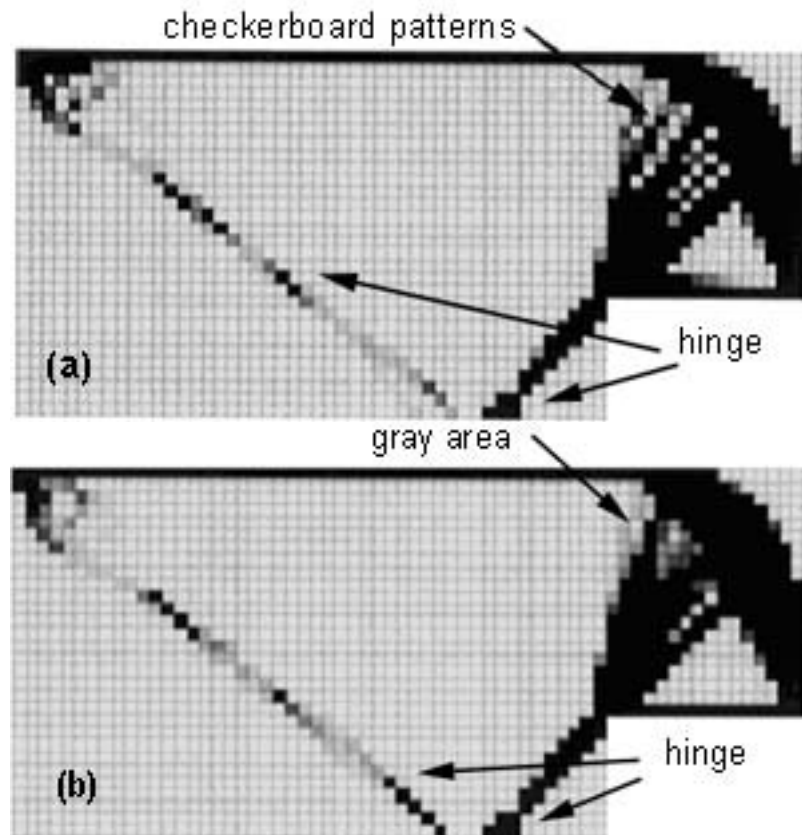
Figure 2-6: (a) The optimal topology for a compliant clamp without checkerboard filter; (b) the compliant clamp topology using checkerboard filter (Nishiwaki et al., 1998).

From the parameterization standpoint, the main reason why checkerboard pattern arises is because the quadrilateral elements parameterization allows point contact between diagonal elements. Saxena and Saxena (2003) recently proposed a honeycomb parameterization (Figure 2-7) to ensure line contact between elements. However, the element distortion can introduce error in FEA, and additional post processing is required to interpret the final structure with a smooth boundary.
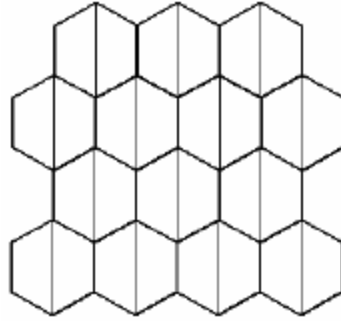
Figure 2-7: Each hexagonal cell in the honeycomb parameterization is represented by two 4-node quadrilateral elements controlled by one density variable (SIMP approach) to ensure line contact between two cells (Saxena and Saxena, 2003).
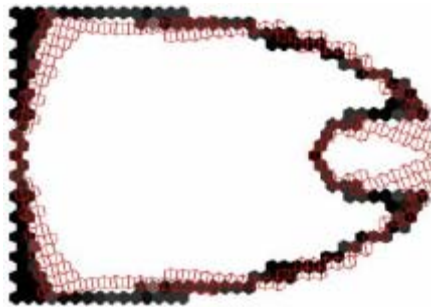
Figure 2-8: Optimal topology of a compliant pliers with stress constraints (Saxena and Saxena, 2003). Dark elements represent the final design, while light color elements show the deformed structure.

2.2.2 Ground Structure Approach

The ground structure approach has been used for optimal truss layout design (Prager, 1970, 1977). It has also been employed in optimal material distribution problems and compliant mechanism synthesis. Inspired by Bendsoe's work (1994) where the optimal microstructures have mechanism-type motion subject to loads differing from the design load, Sigmund (1994) parameterized the design domain using a truss ground structure to design material with prescribed constitutive parameters. The design domain is first discretized by a set of grid nodes. A fully grounded structure (Figure 2-9(a)) can then be created by connecting each grid node to every other node with truss or frame (beam) elements. A subset of the fully grounded structure is called a partially grounded structure, as shown in Figure 2-9(b). A 'ground structure' is typically used as a general term that

includes both fully and partially grounded structures, regardless of the mesh resolution

(grid size) and configuration (how the grid nodes are connected). Both truss and frame

(beam) ground structures have also been used in compliant mechanism topology

synthesis with the element cross sections as the design variables; an element is eliminated

when its cross-section dimension goes to zero in the optimization process. Figure 2-10(b)

shows an example topology derived from the initial ground structure in Figure 2-10(a).
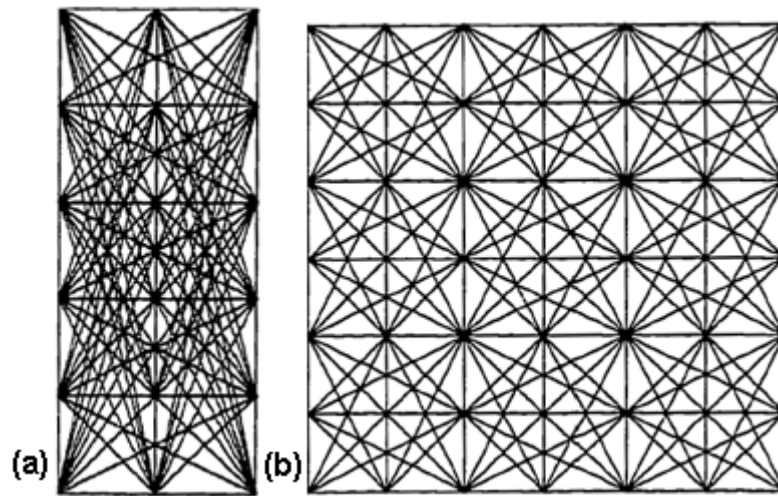
Figure 2-9: (a) A fully ground structure; (b) a partially ground structure.
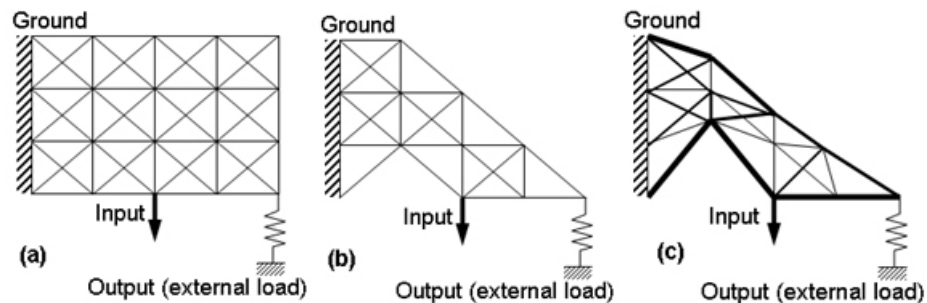
Figure 2-10: (a) An example initial partially ground structure; (b) a design obtained from the ground structure in (a); (c) the final design after size and geometry optimization.

Since the resolution of the final design directly depends on the grid size of the

initial mesh, a second step optimization can be applied to refine the resolution by

allowing the nodes to wander within the regions between the grid points. Additional

refinements, such as stress reduction, can also be included in this step. Figure 2-10(c)

shows how the structure geometry and element cross-section dimensions change after the size and geometry optimization with the topology in Figure 2-10(b).

Although both truss and frame ground structures have been used in compliant mechanism design, frame elements can capture the compliant mechanism behavior more accurately because the mobility is obtained mainly from bending of beam-like segments, not from lengthening and shortening of trusses. Earlier work (Frecker et al., 1997) adopted truss ground structure because of the simplicity, and suggested that bending can be interpreted as two trusses; one in tension and the other in compression. However, this kind of interpretation is more difficult to implement in an automated synthesis approach. The truss ground structures also suffer from singularity issue (Figure 2-11), because the hinges cannot take moment loads. From the shape morphing standpoint, the compliant mechanism should be modeled as beam elements because smooth shape morphing can only be achieved by bending of beam-like segments.
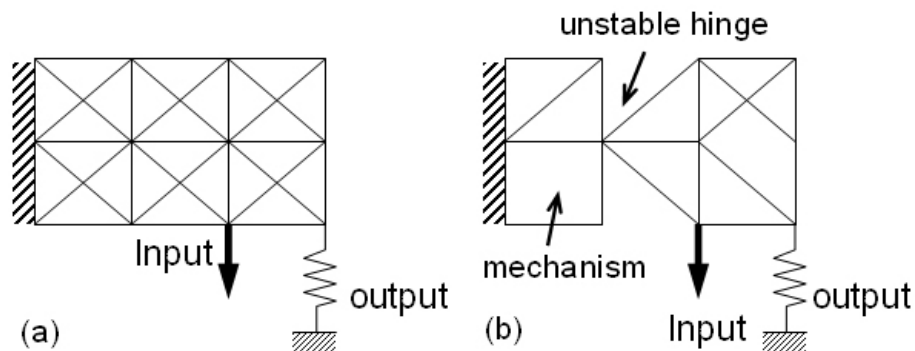
Figure 2-11: (a) The initial mesh using a partially ground structure of trusses; (b) mechanism-type designs (structural singularity) arise due to inappropriate element removal.

One major difference between the ground structure and continuum-based approach is that the former allows overlapping elements in the design to explore motions not possible from the strictly planar design (at the cost of manufacturing complexity). In fact, the solution spaces of the two parameterizations are not exactly identical. Ground

structures generally cover a larger solution space when many overlapping elements are included in the initial mesh. However, the selection of an initial mesh configuration and resolution is usually not intuitive. Since the final design is always a subset of all available element combinations in the initial mesh, the initial mesh selection is critical to the quality of the final solution as well as the size of the solution space. While the initial mesh was selected based on intuition in majority of the previous research, a novel parameterization scheme (load path representation) that does not require an initial mesh is developed in this research and will be introduced in Chapter 5.3.

2.3 Optimization Problem

Any optimization problem can be divided into three important parts: (1) the design variables, (2) the objective functions and constraints, and (3) the optimization method. In the structural optimization, the design variables are defined based on the design domain parameterization as discussed in section 2.2. While different parameterization defines a different solution space (continuum vs. ground structure), the formulation of objective function and the optimization method determine the search process within this solution space, hence the final solution.

2.3.1   Objective Functions

The major difference between structural and compliant mechanism topologies is stated in Ananthasuresh, Kota, and Kikuchi (1994):

> *"In the case of structures, topology is not crucial for functionality, although an optimal topology would help efficient use of material. In the case of compliant mechanisms, however, arbitrary topology cannot fulfill the functional requirements."*

A compliant mechanism derives its motion from the structural deformation, so one important design objective is to achieve the required deflection. At the same time, the compliant mechanism has to be stiff enough to bear external loads, similar to how a mechanism transmits the actuation force to the output point. Take a compliant gripper for example, the compliant mechanism should be flexible enough to deform and grip the object (kinematic requirement), yet stiff enough to withstand the external and reaction forces working against the intended motion (structural requirement). To properly address these two conflicting requirements, various objective functions have been formulated so that structural optimization techniques (homogenization, SIMP approach, or ground structure layout optimization) can be adopted for compliant mechanism synthesis. Table 2-1 shows several commonly used object functions for single input single output compliant mechanisms.

Table 2-1: Objective functions for compliant mechanism synthesis.

Weighted sum formulation (Ananthasuresh, Kota, and Kikuchi, 1994)	$\max\{\alpha d_{out} + (1-\alpha)\dfrac{1}{SE}\}$ prescribe F_{in} and F_{out}	(2.2)
Multi-criteria (ratio) formulation (Frecker et al., 1997)	$\max\dfrac{MPE}{SE}$ prescribe F_{in} and output direction	(2.3)
Force-displacement efficiency formulation (Hetrick and Kota, 1999)	$\max\dfrac{RW_{out}}{RW_{in} + C_{total}}$ prescribe u_{in} and F_{out}	(2.4)
Spring-efficiency formulation (Hetrick, 1999)	$\max\dfrac{E_{spring}}{E_{in}}$ prescribe F_{in} and K_s	(2.5)

The objective in traditional structural optimization problems is to minimize the strain energy (i.e. mean compliance) in order to create the stiffest yet lightest structure.

The strain energy (SE) can be used in compliant mechanism for the structural

requirement, but the required deformation at the output point needs another performance

criterion. In Ananthasuresh, Kikuchi, and Kota (1994), the kinematic requirement of a

compliant mechanism was captured by the output displacement, d_{out}, against a unit

dummy force. The SE and d_{out} were combined using a weighted sum shown in Eq.(2.2) in

Table 2-1 with a weighting factor, α, to give preferential bias to the two criteria. Frecker

(1997) then proposed a multi-criteria formulation where the SE and mutual potential

energy (MPE, essentially the output displacement) were posed in ratio form shown in

Eq.(2.3), thus eliminating the need of the weighting factor, α. As indicated in Hetrick

(1999), the multi-criteria formulations in Eq.(2.2) and Eq.(2.3) are prone to convergence

difficulty due to the fact that not all solutions on the Pareto optimum points represent

feasible compliant mechanism structures (either infinitely flexible or maximum stiffness

structures). Hetrick and Kota (1999) later proposed a force-displacement efficiency

formulations shown in Eq.(2.4) based on the reciprocal work theorem (Gere and

Timoshenko, 1984). Hetrick (1999) also formulated a spring-efficiency formulation,

Eq.(2.5), using a spring to capture the work done at the output port.

  The objective functions listed in Table 2-1 use the displacement or transferred

energy at the output point as the kinematic requirement measurement. But in the shape

morphing problem, the whole boundary deforms to match a desired target shape, and it

would necessitate choosing multiple output points along the morphing boundary. Kikuchi

et al. (1998) and Frecker, Kikuchi, and Kota (1999) have formulated objective functions

to address multiple output points, but the formulations have only been implemented on

problems with two output points. In addition, the formulation does not constraint output

displacement in the direction perpendicular to the desired direction. In the shape

morphing problem, the goal is to move all points along the boundary to match a desired

target shape, where the exact output direction and magnitude of each output point are

crucial to the final result. Therefore, the objective function should be able to measure the

difference between the achieved shape and the desired shape. Saggere (1999) used the

least square errors (LSE) to measure the shape differences. As shown in Eq.(2.6), the

objective function summarizes the point to point (location) differences along the achieved

curve (d_i) and the desired shape (d_i^*). This LSE formulation will be used in this research

with slight modification, while another new formulation using Fourier Transformation to

compare 'shape' differences will be introduced in Chapter 6.1.2.

$$\min LSE = \min \sum_{i=1}^{n} \frac{1}{2} w_i (d_i^* - d_i)^2 \qquad (2.6)$$

2.3.2 Optimization Methods

Continuous Optimization

Both continuous and discrete optimization methods have been employed in the

topology synthesis of compliant mechanisms. The selection of optimization method

typically depends on the nature of the problem. However, since gradient-based

continuous optimization methods are generally more efficient, problems with discrete

variables can sometimes be relaxed to facilitate the use of methods such as sequential

linear or quadratic programming (SLP or SQP). In the topology optimization, removing

unnecessary elements is a discrete decision, but the majority of the previous research

used a continuous approximation for the element removal. For each element, the material

density (continuum-based approach) or the member cross section area (ground structure

approach) is represented with a real variable that is allowed to vary continuously between 0 and 1 (or a maximum cross section). So, the result generally contains void regions (0: remove elements), solid regions (1: preserve elements), and gray areas (intermediate values between 0 and 1). Since the final physical structure only includes solid and void regions, elements with intermediate values should be interpreted either as a solid or a void. This is generally achieved using a filter, which the threshold value is specified by the designer. This is based on the assumption that elements with low density value ($<$ threshold) contribute only very little to the structural performance, thus can be removed without significant influence on the compliant mechanism behavior.

It is, however, difficult to define how small the elements should be before their effect can be neglected in the overall stiffness matrix, especially when the result has large portions of gray areas without obvious black/white feature (this may happen when strain energy is not considered in the problem formulation). The determination of the filtering threshold is often subjective, and if poorly selected, the functionality of the design could be destroyed. For example, when the design variables take on intermediate values that are non-trivial but substantially smaller than the upper bound, randomly selecting the filtering threshold will risk the elimination of important functional elements, and even lead to disconnected designs. When this happens, the designer has to use his intuition and engineering judgment to decide which elements are the critical ones that must remain to preserve structural integrity. But this may alter the original mechanism behavior of the design. From the perspective of a fully automated synthesis approach, this post-processing is somewhat ad hoc and difficult to implement systematically and objectively.

Therefore, discrete optimization methods are employed in this dissertation to address the topology optimization in its natural, discrete form to avoid the gray area issue.

On the other hand, in the size and geometry optimization, continuous optimization method provides an efficient and effective means to find the optimal dimensions. Filtering threshold is no longer required because the topology is fixed in this step. The issues encountered in topology optimization thus vanish because dimensions vary continuous within their prescribed range based on manufacturing constraints.

Discrete Optimization

Discrete optimization methods have also been employed in the topology optimization problem, using discrete (binary) variables to represent the presence/removal (1 or 0 respectively) of physical elements. Although this does require removing corresponding degrees of freedom in the stiffness matrix to prevent singularity in FEA, the final result is more accurate and free of gray areas. More importantly, the discrete optimization should be used because topology optimization problem is also discrete by nature.

One challenge discrete optimization faces is the high requirement of computation time. Since many discrete optimization methods, especially heuristic approaches, do not incorporate gradient information during the searching process, the search is guided only based on the objective function value and generally requires more function evaluations. However, with the development in computation technology, discrete optimization methods have been developed and successfully applied to various types of problems.

The structural connectivity is a bigger issue when discrete optimization methods are used in structural topology optimization problems. Since the design variables (element densities or cross-section areas) are now binary, the structure can be disconnected (contain floating substructure, or disconnected from input and ground supports) when a set of binary values are randomly assigned to the variables. These designs should be penalized during the optimization process using a connectivity constraint. However, the structural connectivity of a design cannot be *seen* directly from the design variables. Therefore, a verification algorithm is generally required to identify and penalize a disconnected design. Although previous research has demonstrated the feasibility of this approach, the verification algorithm can only penalize the *bad* design but it cannot completely avoid the generation of disconnected designs. As indicated in Hamda et al. (2002), when more design variables are involved, the algorithm was unable to identify a good solution, because it was difficult enough just to find a well connected structure. The origin of the disconnectivity issue comes from the parameterization. The structural connectivity is not considered when using the FE mesh to represent structural topology; the *global* (structural level) effect of removal of a single element cannot be seen from the *local* level (element-wise representation). In this research, a new parameterization scheme (load path representation) will be introduced to ensure structural connectivity (see Chapter 5).

2.4 Research Issues for Shape Morphing Compliant Mechanisms

Various systematic strategies introduced in this chapter have been developed in the past decade for compliant mechanism synthesis, using the structural optimization

approach. These synthesis approaches rely on a two-step design process such as that

shown in Figure 2-2. The two-step approach decomposes the interrelated topology and

dimensional synthesis into two separate stages: the topology synthesis ensures the motion

in the desired output direction, leading to a qualitative solution; the size and geometry

optimization refines the mechanism dimensions to achieve a desired objective, such as

desired displacement, leading to a quantitative solution. Research has suggested that the

decomposition can simplify the problem and yield successful results in single-input

single-output (SISO) applications (Ananthasuresh, Kota, and Kikuchi, 1994; Frecker,

1997; Hetrick, 1999; Joo, 2001). However, the quality of the solutions to the shape

morphing problems depends greatly on the precise deformation (direction and magnitude)

of *all or several* discrete output points along the shape-changing boundary. With multiple

output points in shape morphing problems, it is inappropriate to adapt the two-step

approach that focuses on the performance of only one particular output point. Since the

deformation of the shape-changing boundary is simultaneously influenced by the

topology and dimensions of the compliant mechanism, it is critical to unify the two

synthesis steps and address them simultaneously. New objective function has to be

formulated as well to evaluate the effectiveness of shape morphing. Furthermore, in order

to avoid the confusion associated with the gray area, the topology optimization problem

has to be formulated in the discrete form while preserving continuous design variables to

address the dimensions. In this dissertation, beam element-based compliant mechanisms

(ground structure approach) are chosen, because smooth curves can only be achieved by

deforming beam-like segments. In addition, the compliant mechanism gains its mobility

mainly through beam bending. Since the final design depends greatly on the initial

discretization mesh, resolution and configuration selection guidelines should be studied.

Moreover, new parameterization schemes should be developed to address the structural

connectivity issue. The research goals are, therefore, summarized as follow.

- New objective function: Formulate new objective functions, involving
  multiple output points, to evaluate shape morphing performance.

- New design paradigm: Develop a unified approach to simultaneously
  synthesize the topology and dimensions of compliant mechanisms.

- New optimization technique: Incorporate optimization methods that allow
  discrete and continuous variables to appropriately model the compliant
  mechanism topology and dimensions.

- New parameterization scheme: Develop initial mesh selection strategies or
  new design domain parameterization schemes to address the initial mesh
  dependency issue.

Integrating the above research goals provides a new synthesis approach to shape

morphing compliant mechanisms that can also be generalized to solve traditional

structural optimization and SISO compliant mechanism problems. The problem statement

and assumptions will be introduced in the next chapter, followed by the details on how

these research goals are achieved.

CHAPTER 3

PROBLEM STATEMENT

3.1 Design Objective

The objective of this dissertation is to develop a systematic approach to synthesize shape morphing compliant mechanisms. As illustrated in Figure 3-1, a compliant mechanism changes its shape through elastic deformation due to an input actuation. This structural deformation, hence the shape change on the boundary, can be utilized to achieve desired shape morphing. The goal is, therefore, to find the optimal compliant mechanism topology and dimensions, so that the deformed boundary profile matches the desired target curve with minimum error. The mechanism is subjected to space constraints to fit within the specified design domain, as well as the stress constraints to prevent structural failure. Although Figure 3-1 only illustrates the shape morphing between two curves using a two-dimensional planar compliant mechanism, it can be regarded as one cross-section of a shape morphing surface, such as an aircraft wing cross-section along the wingspan. More complicated three-dimensional surface shape change can be explored in the future by expanding the synthesis method developed in this research, but the scope of this research will be restricted to the design of planar compliant mechanisms. The morphing problem considered here will only include morphing between two shapes (initial and target curves) as the first step toward morphing through a set of prescribed shape profiles.
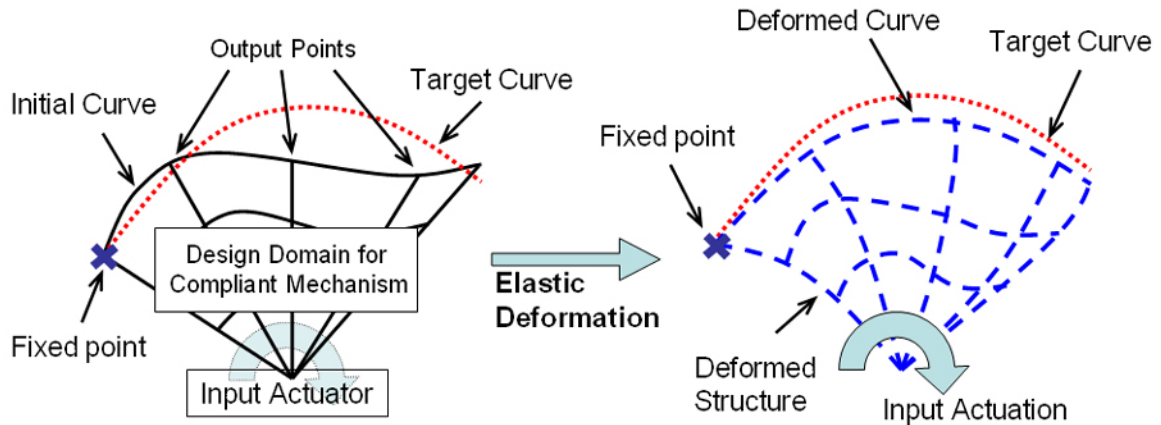
Figure 3-1: An illustration for a shape change compliant mechanism; (a) shows the problem specifications and how the input actuator is connected to the active points; (b) shows the deformed structure. The boundary profile after deformation is defined as the deformed curve.

3.2 Design Specifications and Assumptions

Some specifications are given as parameters by the designer and remain unchanged in the synthesis procedure. These specifications include the initial and target curve profiles, actuator type and location, support locations, external loads, available design domain, out-of-plane structural dimension, material properties, and minimum in-plane feature size based on manufacturing constraints. The compliant mechanism will be actuated by a prescribed input motion (translation or rotation). An actuator with matching motion and force requirements, such as electric motors or smart actuators, is then selected.

Several assumptions are made in this research to simplify the problem without losing its generality:

1) The morphing object will change from its specified initial profile to only one specified target profile,

2) The shape-changing object is integrally attached to the compliant mechanism,

3) The compliant mechanism has only a single actuator at a specified location,

4) The morphing compliant mechanism is comprised of frame-like elements because a smooth shape morphing can be better achieved by beam bending, and

5) The beam segments have rectangular cross section area; the in-plane beam dimensions can vary from segments to segments, while the out-of-plane dimensions are prescribed as a constant for all beams.

6) Axial strain is negligible in the elements, since the longitudinal stiffness is significantly larger than bending stiffness. Figure 3-2 shows a cantilever beam with a rectangular cross section under transverse and axial loading conditions. As can be seen from Eq.(3.1) to (3.3), the longitudinal stiffness is orders of magnitude larger than the bending stiffness (for L/h>10). For a typical beam of L=10 and h=1, k_{axial} is 400 times larger than k_{bend}. Thus, the mobility of the compliant mechanism comes mainly from beam bending with relatively small axial strain.

$$E, \ I = \frac{bh^3}{12}$$

$$d_L = \frac{FL^3}{3EI} \Rightarrow F = k_{bend} d_L$$

(a) Transverse loading

$$E, \ A = bh$$

$$\frac{F}{A} = \frac{Ed}{L} \Rightarrow F = k_{axial} d$$
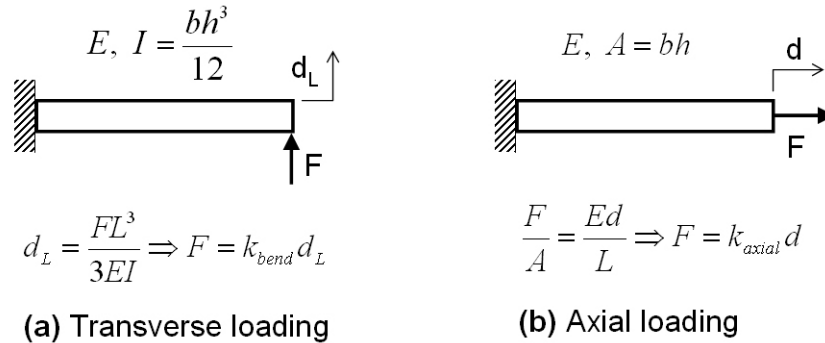
(b) Axial loading

Figure 3-2: (a) Transverse loading and (b) axial loading of a cantilever beam.

$$k_{bend} = \frac{3EI}{L^3} \tag{3.1}$$

$$k_{axial} = \frac{EA}{L} \tag{3.2}$$

$$\frac{k_{axial}}{k_{bend}} = \frac{4L^2}{h^2} \tag{3.3}$$

3.3 Synthesis Approach Overview

Figure 3-3 shows the overall flowchart of the proposed synthesis approach. It contains three major components: (1) the design domain initialization, (2) the design domain parameterization, and (3) the optimization routine. The design domain initialization starts with a feasibility analysis to ensure the shape change is attainable. A number of output points are then identified along the morphing boundary to facilitate the parameterization in the next step. Two design domain parameterization schemes are developed in this research to represent various compliant mechanism topologies in terms of design variables. The binary ground structure parameterization is mapped onto a fixed FE mesh, while the load path representation automatically generates an adaptive mesh to facilitate the use of FEA in the optimization procedure. Both parameterizations involve the use of binary and continuous design variables to simultaneously address the structural topology and dimensions. Due to the mixed variable types (discrete + continuous), a genetic algorithm (GA) is chosen in the optimization routine to search for the compliant mechanism that can best achieve the desired shape morphing. Within the optimization routine, an FEA is employed to solve for the structural deformation. The deformed structural boundary is then extracted to compare with the desired target shape. In the optimization, the objective is to minimize the shape deviation between the deformed and target curves. Upon termination of the optimization routine, the optimal topology and dimensions can be found, hence achieving the desired shape morphing.
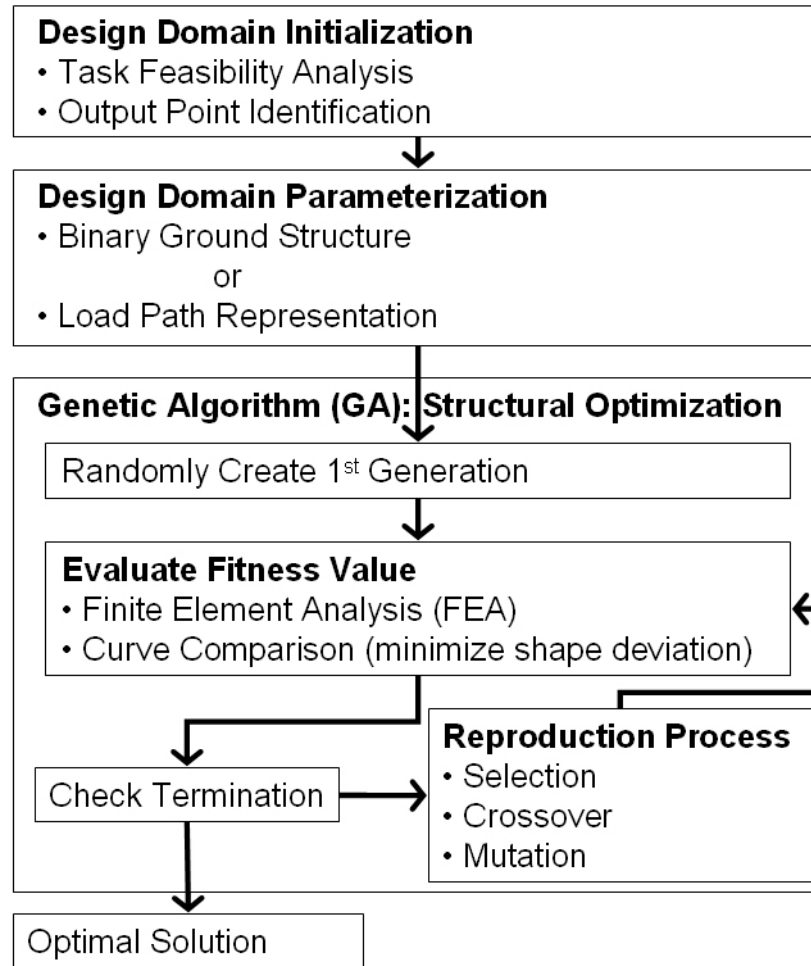
Figure 3-3: Flowchart for the compliant mechanism synthesis approach.

The three main components in this synthesis approach will be introduced in the following chapters in more details: Chapter 4 describes the design domain initialization, Chapter 5 introduces the two parameterization methods, and Chapter 6 discusses the optimization problem.

CHAPTER 4

DESIGN DOMAIN INITIALIZATION

4.1 Task Feasibility Analysis

The first step in the synthesis approach is the design domain initialization. It starts with a feasibility analysis that examines the given initial and target curves in order to evaluate if the shape change is attainable. The shape change is considered feasible if "the initial curve can be deformed into the desired target shape within the range of elastic deformation of constituent elements." The initial curve is assumed to be stress free before the shape change with a uniform rectangular cross-section. The stress distribution along the curve can be estimated by the change in total curve length and the change in curvature. The maximum stress along the curve is checked against yielding (linear elastic range) with two criteria: (1) the stress due to axial tension or compression must be smaller than yielding stress, and (2) the stress due to bending must be smaller than yielding stress. The main purpose of the stress evaluation is to provide an initial feasibility check of the problem. It is by no means an attempt to precisely evaluate the actual stress distribution in the final design.

For the axial stress criterion, the length of both curves (initial and target) are calculated in order to estimate the axial stress required to stretch or compress the curve from its initial length to the target one. Since each curve is generally represented as a set

of data points, the curve length is estimated as the sum of the linear segments connecting

the points, shown in Eq.(4.1),

$$L = \sum_{i=1}^{n-1} \sqrt{(x_{i+1} - x_i)^2 + (y_{i+1} - y_i)^2}$$

(4.1)

where the initial and target curves are assumed to have the same number of data points, n.

The axial stress can then be calculated from Eq.(4.2),

$$\sigma_{axial} = \frac{E(L_{TAR} - L_{INI})}{L_{INI}}$$

(4.2)

where L_{TAR} and L_{INI} are the curve lengths of the target and initial curves, and E is the

material Young's Modulus.

For the bending stress criterion, the bending stress based on the curvature change

from the initial shape to the target shape is estimated. As illustrated in Figure 4-1(a), this

is achieved by, first, calculating the angle change at each point ($\Delta\theta$ at P_i); a line dividing

$\Delta\theta$ is then drawn through P_i to be the tangent of the curve.
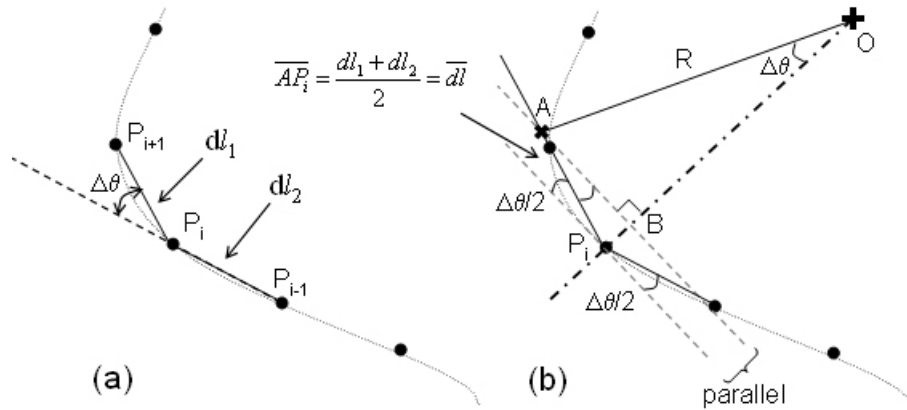
Figure 4-1: (a) The angle change at each point; (b) estimation of the curvature at point P_i, where O is the center of curvature, R is the radius of curvature, and distance between A and P_i is the average of dl_1 and dl_2.

As shown in Figure 4-1(b), the radius of curvature, R, can be calculated from

Eq.(4.3), thus the curvature at P_i can be expressed as Eq.(4.4).

$$\overline{AB} = R\sin(\Delta\theta) = \overline{dl}\cos\left(\frac{\Delta\theta}{2}\right) \tag{4.3}$$

$$\kappa = \frac{1}{R} = \frac{\sin(\Delta\theta)}{\overline{dl}\cos\left(\dfrac{\Delta\theta}{2}\right)} \tag{4.4}$$

The curvature difference function, $d\kappa(l)$, is then defined in Eq.(4.5),

$$d\kappa(l) = \kappa_{INI}(l) - \kappa_{TAR}(l) \tag{4.5}$$

where $\kappa_{INI}(l)$ and $\kappa_{TAR}(l)$ are the curvature functions of the initial and target curves and, l is the normalized arc length varying from 0 to 1. This can be considered the local curvature change along the curve for bending the initial curve into the target curve. Since the bending stress along a beam is proportional to its local curvature change, according to Euler-Bernoulli beam theory, the maximum bending stress can be calculated from the curvature difference function and is shown in Eq.(4.6),

$$\sigma_{max} = \frac{Eh}{2}\max(d\kappa(l)) \tag{4.6}$$

where E is the material Young's Modulus; h is the nominal in-plane beam height (minimum manufacturable feature size).

If both of the maximum stresses due to axial tension and bending stay within the yielding limit of the selected material, the shape change is considered feasible, and the algorithm proceeds to the next step.

4.1.1 Feasibility Check Example

A shape morphing example is shown in Figure 4-2 to illustrate feasibility check. The task here is to deform an initially straight beam into a cubic (target) curve. They are specified in terms of two sets of data points shown in Table 4-1. The curves are created by connecting adjacent data points with straight lines, thus the curve lengths are

approximated by the length of the piecewise linear curves. Using Eq.(4.1), the initial and

target curve lengths are 200mm and 200.015mm respectively, which gives an axial stress

of 12.58MPa $< \sigma_{yield}$(=34.45MPa). The corresponding $\kappa_{INI}(l)$, $\kappa_{TAR}(l)$, and $d\kappa(l)$ are shown

in Figure 4-3, where $\kappa_{TAR}(l)$ and $d\kappa(l)$ overlap each other because the straight initial curve

has zero curvature. As can be seen, the maximum curvature change ($d\kappa(l)$) occurs at

l=0.05 (and l=0.95), where $d\kappa$=0.0059mm^{-1}. With h=1mm and E=2480MPa, the

corresponding bending stress is σ_{max}=14.61MPa $< \sigma_{yield}$(=34.45MPa). Both axial and

maximum bending stresses are within the yielding limit. This shape change is, therefore,

considered feasible.
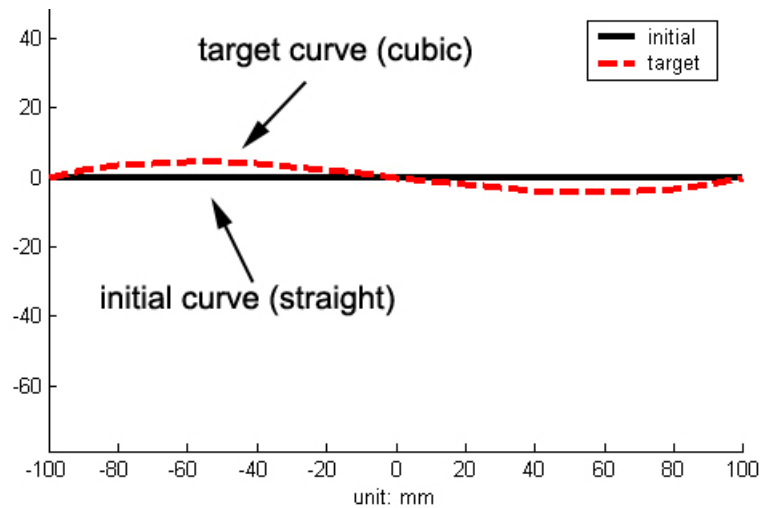
Figure 4-2: A shape morphing example that deforms a straight beam into a cubic profile.

Table 4-1: The x-y coordinates of the data points along the initial and target curves in Figure 4-2.

Data point #	Initial Curve Data Points		Target Curve Data Points	
	X (mm)	Y (mm)	X (mm)	Y (mm)
1	-100	0	-100	0
2	-90	0	-90	1.9432
3	-80	0	-80	3.2727
4	-70	0	-70	4.0568
5	-60	0	-60	4.3636
6	-50	0	-50	4.2614
7	-40	0	-40	3.8182
8	-30	0	-30	3.1023
9	-20	0	-20	2.1818

Data point #	Initial Curve Data Points		Target Curve Data Points	
	X (mm)	Y (mm)	X (mm)	Y (mm)
10	-10	0	-10	1.125
11	0	0	0	0
12	10	0	10	-1.125
13	20	0	20	-2.1818
14	30	0	30	-3.1023
15	40	0	40	-3.8182
16	50	0	50	-4.2614
17	60	0	60	-4.3636
18	70	0	70	-4.0568
19	80	0	80	-3.2727
20	90	0	90	-1.9432
21	100	0	100	0
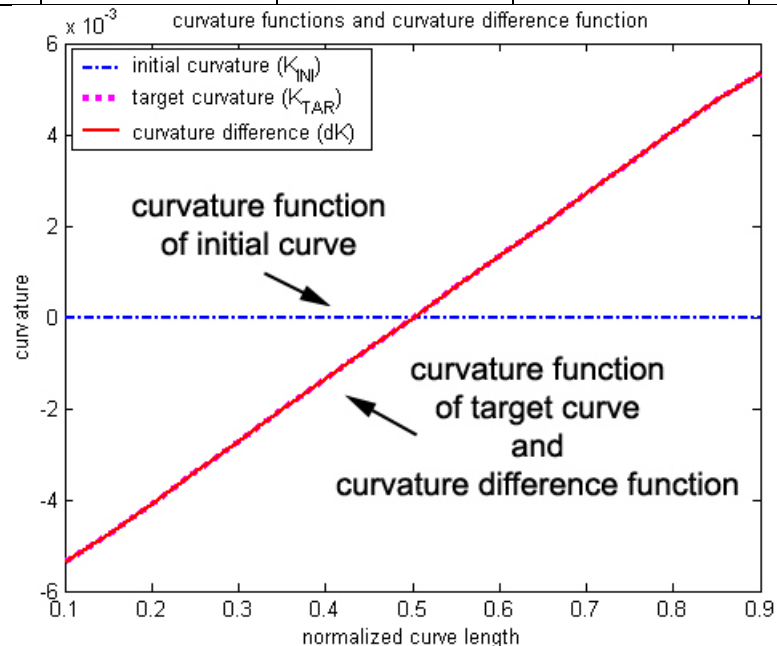
Figure 4-3: The curvature functions of the initial and target curves shown in Figure 4-2, and the curvature difference function between them.

4.2 Output Point Identification

Shape morphing is a multiple output problem, since the goal is to move every point along the initial curve toward the target curve. Designing a morphing compliant mechanism involves finding the topology that connects the (single) input to multiple output points. It is assumed that the compliant mechanism is connected to the morphing boundary at several discrete points, such as P_1, P_2, and P_n in Figure 4-4. The mechanism

can then transmit the input actuation motion through these output points to control the shape of the boundary (the adaptive surface). The shape change can be achieved with minimum error if we have full control over every point along the curve, but designing a compliant mechanism with so many output points might require very large number of design variables and is nonrealistic. It is, thus, important to identify a minimum number of required output points, such that, when input actuation is transmitted to the boundary through these points, the desired shape change can be achieved with acceptable error.
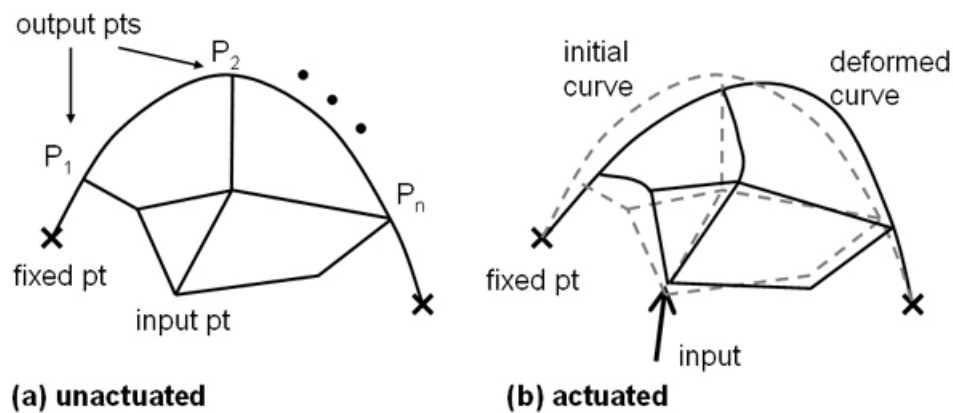
Figure 4-4: (a) Output points along the compliant mechanism boundary; (b) the motion at the input is delivered to the output points to control the shape of the morphing boundary.

To determine the number and locations of the output points, a piecewise linear function is used to approximate the curvature difference function, $d\kappa(l)$, and the output points are defined as the end points of each linear section. The curve fitting function is piecewise linear because the curvature distribution is linear for a straight beam with constant cross-section, subjected to end loads (Figure 4-5(a)). As seen in Figure 4-5(b), the morphing boundary can be regarded as several beam segments connected in series; the input actuation transmitted to the boundary through the output points can be seen as end loads on each segment.
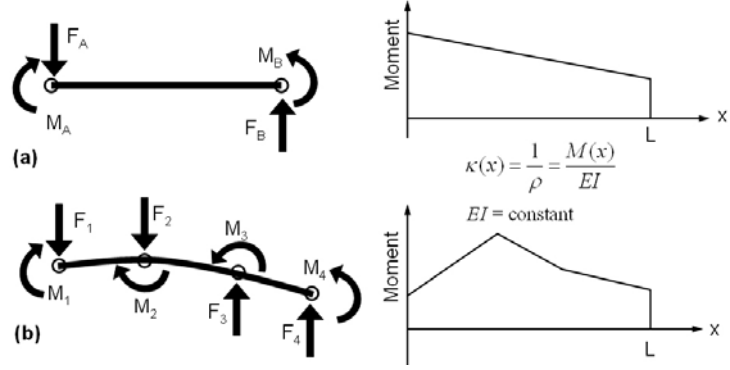
Figure 4-5: (a) A beam segment with end loads has a linear moment distribution along its length; (b) the morphing boundary can be seen as a series of beam segments with loads on the output points. The moment distribution is piecewise linear along the length.

An optimization process is then used to determine the minimum number of output points while ensuring that the curve fitting error is below an acceptable tolerance, ε. The design variables, objective function, and constraint are shown in Eq.(4.7) ~ Eq.(4.9). The design variable, $outputPt_i$, is a row vector representing potential output points. Binary variables are used to switch each data point on and off in $outputPt_i$. When $outputPt_i=1$, the ith data point is considered an output point. A genetic algorithm (GA) (Goldberg, 1989) is employed to find the optimal 0 and 1 combination in $outputPt$. Details regarding GA will be introduced in Chapter 6.

Design variable:
$$outputPt = [outputPt_1, \quad outputPt_2, \quad \cdots \quad outputPt_{n-1}, \quad outputPt_n] \tag{4.7}$$

Objective: $\min_{outputPt_i} \left(\sum_{i=1}^{n} outputPt_i \right)$ Minimize number of active points   (4.8)

Subject to
$$g1 : |d\kappa(l_i) - d\kappa^*(l_i)| \leq \varepsilon \qquad \text{Curve fitting error constraint} \tag{4.9}$$

where n is the number of data points along the morphing boundary; $outputPt_i \in \{0,1\}$; $d\kappa(l)$ is the curvature difference function; $d\kappa^*(l)$ is the piecewise linear function connecting $(l_j, d\kappa(l_j)) \in \{j|outputPt_j = 1\}$; and ε is the acceptable fitting error.

The piecewise linear curve fitting is based on the assumption that no external loads are applied on the morphing boundary. When external loads such as uniform

pressure is applied, a piecewise quadratic curve should be used instead of a piecewise

linear curve because the moment distribution is quadratic along a beam subject to

uniform pressure. For other types of external load distribution, the curve fitting principle

is the same except using a different order of piecewise function. Because using higher

order curve fitting will result in fewer number of output points, the piecewise linear curve

fitting should be sufficient to identify all the required output points (including those

resulting from higher order curve fitting). In this research, piecewise linear curves are

used throughout the examples for simplicity.

4.2.1   Output Point Identification Example

Continuing from section 4.1.1, piecewise linear curve fitting is applied to the

curvature difference function to identify the required output point for the shape change in

Figure 4-2. Following the procedure described in 4.2, the output points are identified to

be the two end points, thus only one linear segment is shown in Figure 4-6. This suggests

that the desired shape morphing can be achieved by applying forces or moments to the

two end points, as illustrated in Figure 4-7.
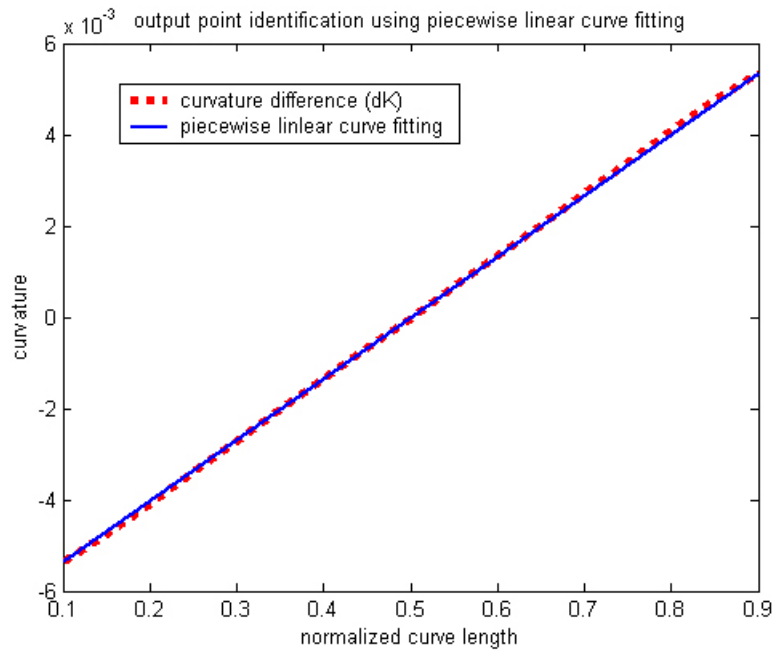
Figure 4-6: Piecewise linear curve fitting of the curvature difference function for the example shown in Figure 4-2.
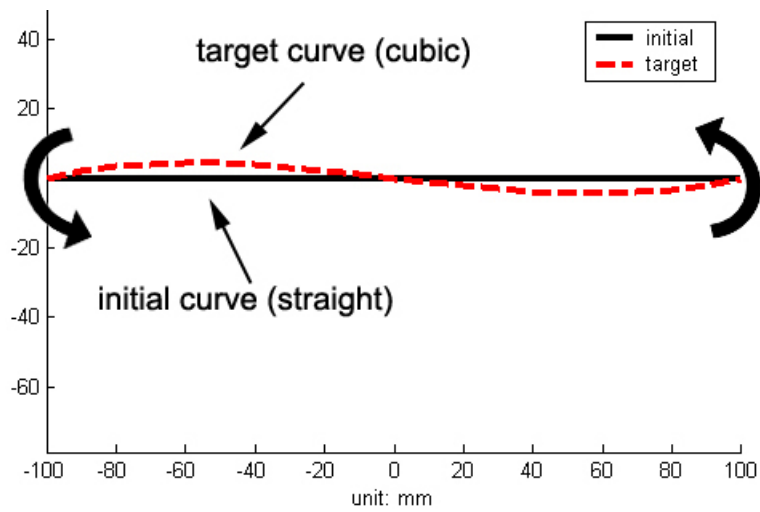
Figure 4-7: The curve fitting result in Figure 4-6 suggests that the desired shape morphing can be achieved by applying force or moment to the two end points.

CHAPTER 5

DESIGN DOMAIN PARAMETERIZATION

5.1 Defining the Design Domain

The design domain is the region specified by the user within which the mechanism must fit. In the shape morphing problem, the design domain is defined by the area enclosed within the initial curve, the input location, and support locations, as shown in Figure 5-1. However, it can be reduced or relaxed depending on space constraints.
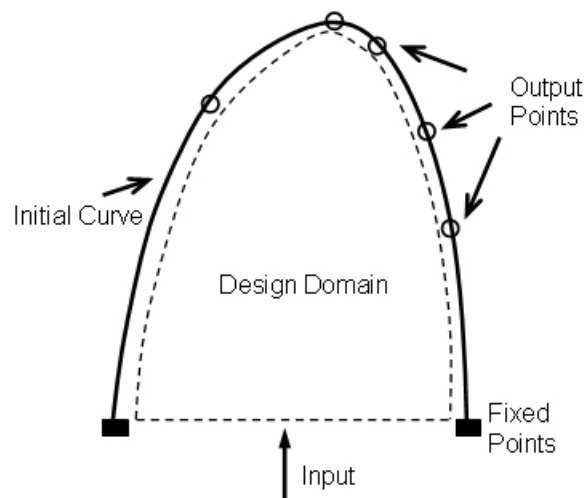
Figure 5-1: The design domain is defined by the initial curve, input, and support locations.

To facilitate the use of an optimization procedure, the design domain is parameterized so that various compliant mechanism designs can be represented with a number of variables. We have developed two parameterization methods in this research: (1) the binary ground structure parameterization, which is the discrete form of the ground structure approach seen in previous research; (2) the load path representation, which is

developed to address the structural connectivity issue encountered in the former

parameterization scheme.

5.2 Binary Ground Structure Parameterization

In the binary ground structure parameterization, the design domain is discretized

by an initial mesh to form a ground structure. The mesh connects the input, ground

supports, and the output points that are determined in the design domain initialization

step (section 4.2). Figure 5-2 shows an example of the discretization network, but various

network configurations can also be investigated to explore different design space. With a

given initial mesh, the element network provides many possible topologies for the final

solution simply by removing or including different elements within this network. The

best topology among them is later determined using an optimization routine. This

parameterization is similar to the grounded structure approach seen in previous research,

but, rather than arbitrarily selecting the initial mesh resolution, the resolution is now

partly determined by the output points. Although the resolution in the other direction

(parallel to initial curve) and the mesh configuration are still selected based on

engineering intuition, the output points do provide a good starting point in constructing

the ground structure. The binary ground structure parameterization is also different from

typical ground structure approach in that the structural topology is now represented by

binary (discrete) variables as opposed to continuous variables in the latter approach. By

incorporating additional continuous variables, the topology and dimensions of the

compliant mechanism can be addressed simultaneously in this approach.
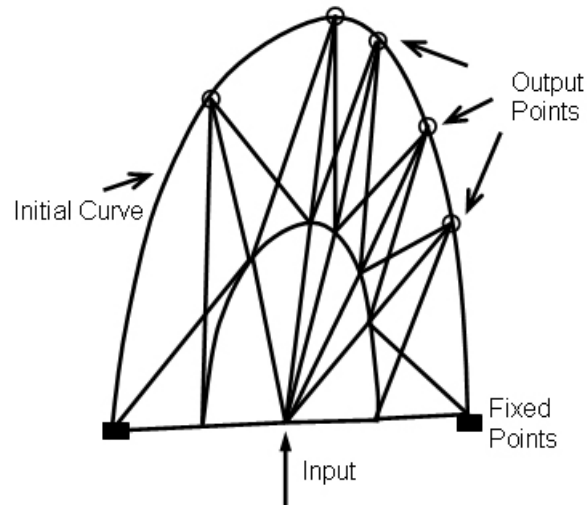
Figure 5-2: An example of design domain discretization using a binary ground structure of beams.

It should be noted that the selection of the initial mesh is critical to the final solution. Since the initial mesh defines all the available topologies, the mesh configuration directly affects the complexity of the final solution. Moreover, the initial mesh resolution also controls how detail the structure can be. However, the required topology (mesh configuration) for a particular shape morphing is generally unknown at the outset. Therefore, several different initial meshes should be tested before concluding on a final design. Although a fully grounded structure with fine resolution can include what can be represented with a coarse mesh, the computation time will increase dramatically as the solution space gets larger. Partially grounded structures (or modular ground structures) are, therefore, preferred in many previous studies, as well as in the binary ground structure parameterization, to take into account the trade-off between the mesh and the available computation time. A novel parameterization using load paths will be introduced in section 5.3 to address the initial mesh selection issues.

5.2.1 Design Variables

Two design variables are assigned to each beam element to describe the topology and dimensions of the compliant mechanism. A binary variable ($hTop$) is used to describe the presence ($hTop = 1$) or absence ($hTop = 0$) of a beam element. Various topologies can, thus, be created when different elements are eliminated from the initial mesh. On the other hand, a real value continuous variable ($hDim$) is assigned to each beam to describe its cross-section dimension. It is assumed that each beam element connecting any two grid nodes has a constant rectangular cross-section; the in-plane beam dimensions (beam heights) are considered the dimensional design variables, while the out-of-plane dimensions (beam widths) are prescribed to be constant for all elements. The beam height of the morphing boundary can also vary. Although the boundary curve is comprised of several beam elements, their beam heights are assumed to be constant and are described by one continuous variable ($hBoundary$). Each compliant mechanism is, therefore, represented by the data structure shown in Eq.(5.1), where n is the total number of elements in a design.

$$design = \left[\underbrace{hTop_1, \quad hTop_2, \quad \cdots \quad hTop_n}_{Topo\log y}, \underbrace{hDim_1, \quad \cdots \quad hDim_n}_{Dimensions}, hBoundary \right] \quad (5.1)$$

The resulting beam dimensions used in the finite element analysis (FEA) is obtained from multiplying $hTop$ and $hDim$, shown in Eq.(5.2)~(5.4). When $hTop_i$ is zero, the ith element is removed from the FE mesh; when $hTop_i$ is one, the beam height of the ith element is $hDim_i$. With this representation, the topology and dimensions of a compliant mechanism can be optimized simultaneously. Due to the presence of both discrete and continuous design variables, a genetic algorithm (GA) is adopted in this research to

address both types of variables. The optimization using GA will be introduced in Chapter 6.

$hTop_i \in$ binary (1: element on, 0: element off) $\hspace{3cm}$ (5.2)
$hDim_i$, $hBoundary \in$ positive real numbers $\hspace{3cm}$ (5.3)
$h_i = hTop_i \times hDim_i$, where $i = 1, 2, \dots$, number of elements $\hspace{1cm}$ (5.4)

Parameters

The variables that remained fixed throughout an optimization process are defined as parameters. In the ground structure parameterization, the number of cross members (layers parallel to the boundary) in Figure 5-2 is considered a parameter that controls the mesh resolution. The value is prescribed by the designer and remains constant in the problem. The mesh configuration is also selected by the designer, typically based on intuition.

Number of Design Variables

In the binary ground structure parameterization, the number of design variables is directly related to the initial discretization mesh configuration. For instance, in Figure 5-2, each straight line connecting any two grid points is considered one beam element. Each element has two design variables, the *hTop* and *hDim*. Thus, the number of design variables is twice the total number of elements.

Since the initial mesh is chosen partly depending on the number of output points, the number of design variables also depends on the output points. Figure 5-3 shows two fully grounded structures with 3 and 5 output points respectively. Larger number of output points leads to an increase in number of design variables, hence mesh complexity. For N output points with M horizontal layers of grid points, the number of elements in a

fully grounded structure is shown in Eq.(5.5). For fixed M (let M=4 as in Figure 5-3), the number of elements is $8N^2$-2N, thus the number of design variables are $16N^2$-4N. The number of design variables, therefore, increases quadratically with N. Similar trend can be seen when N is held fixed while M increases to give higher resolution in vertical direction.
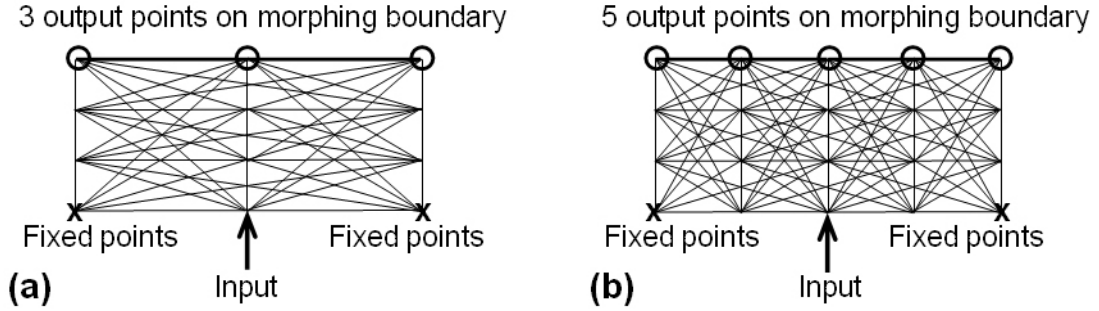
Figure 5-3: (a) A fully grounded structure for 3 output points (132 design variables); (b) a fully grounded structure for 5 output points (380 design variables).

$$C_2^{NM} = \frac{NM(NM-1)}{2} = \frac{N^2M^2 - NM}{2} \tag{5.5}$$

Finite Element Mesh Mapping

The FE mesh is created by looping through all the beam elements, but only elements with hTop=1 are assembled into the global stiffness matrix. Two-dimensional frame elements (6 degrees of freedom beam elements) are used to model the compliant mechanism. By assuming linear elasticity, the element stiffness matrix, k_e, is shown in Eq.(5.6), where E is the Young's Modulus of the material, A_e is the cross section area of the eth element, l_e is the element length, and I_e is the area moment of inertia. Although non-linear analysis can be employed in order to capture the deformed shape in a more realistic manner, only linear analysis is incorporated in this research for simplicity. Non-linear analysis can be performed in a post-processing stage after the synthesis approach to verify the performance of the design.

$$
[k_e] = \begin{bmatrix}
\dfrac{EA_e}{l_e} & 0 & 0 & \dfrac{-EA_e}{l_e} & 0 & 0 \\[2ex]
0 & \dfrac{12EI_e}{l_e^3} & \dfrac{6EI_e}{l_e^2} & 0 & \dfrac{-12EI_e}{l_e^3} & \dfrac{6EI_e}{l_e^2} \\[2ex]
0 & \dfrac{6EI_e}{l_e^2} & \dfrac{4EI_e}{l_e} & 0 & \dfrac{-6EI_e}{l_e^2} & \dfrac{2EI_e}{l_e} \\[2ex]
\dfrac{-EA_e}{l_e} & 0 & 0 & \dfrac{EA_e}{l_e} & 0 & 0 \\[2ex]
0 & \dfrac{-12EI_e}{l_e^3} & \dfrac{-6EI_e}{l_e^2} & 0 & \dfrac{12EI_e}{l_e^3} & \dfrac{-6EI_e}{l_e^2} \\[2ex]
0 & \dfrac{6EI_e}{l_e^2} & \dfrac{2EI_e}{l_e} & 0 & \dfrac{-6EI_e}{l_e^2} & \dfrac{4EI_e}{l_e}
\end{bmatrix}
\tag{5.6}
$$

5.2.2 Structural Connectivity

Although Eq.(5.4) provides a convenient way to combine the topology and dimensional aspects in compliant mechanism synthesis, this representation has an inherent issue regarding structural connectivity. Since the binary topology variables are defined in the element level, they do not explicitly contain any information about the overall connectivity, which is in the structural level. When certain elements are eliminated at the same time, the GA can produce invalid designs such as those shown in Figure 5-4 that includes disconnected substructures or is disconnected from the input or ground. In general, the structural connectivity is unknown when simply looking at the design variables in the form of Eq.(5.1). An additional checking algorithm has to be applied *after* a topology is created to detect the structural connectivity and penalize invalid designs. However, these additional processes may lead to inefficiency in GA. To tackle this problem from its root, we have developed another parameterization scheme, using the load paths in a structure as the design variables to facilitate the detection of structural connectivity.
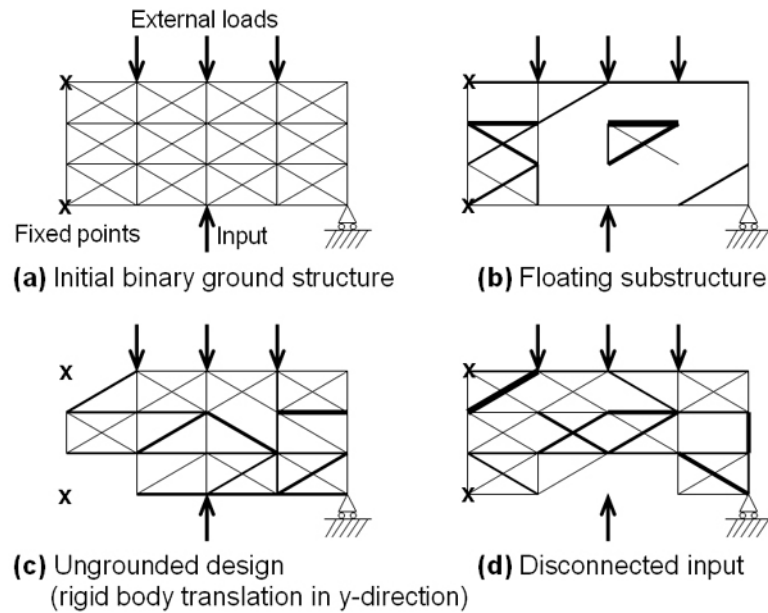
Figure 5-4: (a) The binary ground structure used to discretize the design domain; (b) an invalid design with disconnected substructure; (c) an invalid design that is disconnected from the ground; (d) an invalid design where the input is disconnected.

5.3 Load Path Representation

The development of the load path representation is largely inspired by Tai and Chee's (2000) work on morphological representation. They raised an important point stating that the input and output regions must be connected to one another either directly or indirectly for a valid structural design. In the morphological representation, the connections between input, output, and ground supports are represented using Bezier curves, and the structural topology is created by mapping the curves onto a fixed finite element mesh. Various topologies can be created using only several control points of the Bezier curves, and the mapping onto the FE mesh produces black-and-white designs that are free of gray areas. However, the approach has only been applied to structure design and SISO compliant mechanisms; the applicability to multiple output problems is uncertain. The approach is also computationally very costly, possibly due to the inefficiency in mapping the Bezier curves to the FE mesh; 26~60 hours of computation

time has been reported (Tai and Chee, 2000; Akhtar, Tai, and Prasad, 2002; Cui, Tai, and Wang, 2002; Tai, Cui, and Ray, 2002). Nonetheless, the morphological representation has provided the inspiration essential to the load path representation developed in this research to address multiple output points in shape morphing problems. The load path representation ensures structural connectivity and is capable of creating various topologies. The representation also allows simple meshing to facilitate structural analysis in FEA, thus increasing the efficiency. The load path representation is detailed in the rest of this chapter.

In any compliant mechanism, there always exist three types of points (defined as *essential ports*): input, output, and fixed points (ground supports). These *essential ports* are always connected directly or indirectly to each other to form a well connected structure. Several paths are highlighted in the compliant gripper example in Figure 5-5 to illustrate direct (path 1) and indirect (path 2 and 3) connections between the *essential ports*. These connections are called the 'load paths' in a structure. They can be seen as paths that transmit the energy from the input to the ground supports and output points. Most importantly, they represent the connectivity in a structure. We, therefore, developed a novel design domain parameterization method that takes advantage of these load paths to represent various compliant mechanism designs. The load path representation not only allows easy detection of invalid designs, it also provides variable mesh resolution and configuration. This parameterization can be generalized to design structures and single output compliant mechanisms.
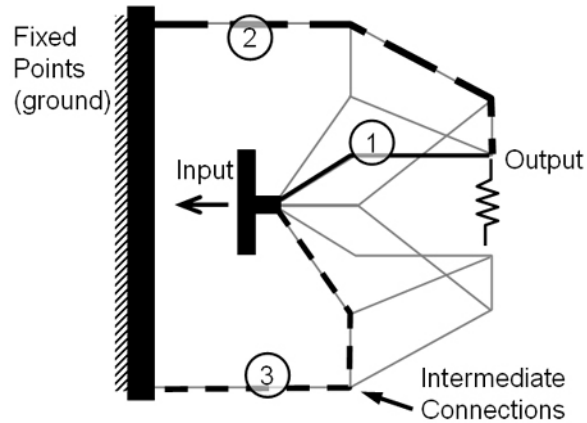
Figure 5-5: A compliant gripper example to illustrate the different load paths in a structure.

5.3.1 Design Variables

Topology Design Variables: *pathSeq* and *pTop*

The load path representation is based on the connection between the three types of *essential ports*. Figure 5-6 illustrates the direct and indirect load paths in a structure. The load paths can be categorized into three types: (1) paths connecting input to output points, (2) paths connecting input to fixed points, and (3) paths connecting fixed points to output points. They will be referred to as *pathInOut*, *pathInFix*, and *pathFixOut* respectively. The structural topology can, therefore, be represented as a graph by expanding Figure 5-6.
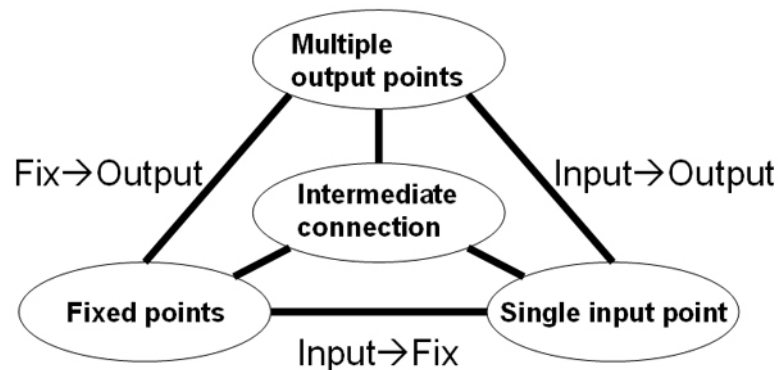
Figure 5-6: Direct and indirect load paths between the essential ports.

Figure 5-7(a) is an example topology for a shape morphing compliant mechanism. Although it is the physical representation of the structure, it can also be regarded as a graph, having the same basic structure as in Figure 5-6. As can be seen, the input, output,

and fixed points are the vertices in the graph. The number of output points is determined in the design domain initialization, while the number of fixed points is specified by the designer. It is assumed that there is one input and two fixed points in this example. In addition to the essential ports, additional vertices (7~10) are introduced to allow intermediate connections between different paths. They are termed as the *intermediate connection ports* or *interconnect ports*. The number of interconnect ports is specified by the designer; generally, less than 10 is sufficient.
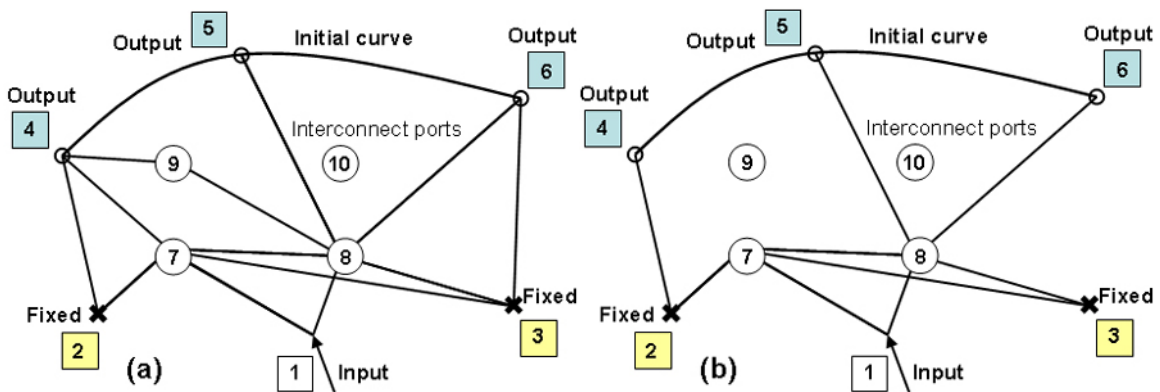
Figure 5-7: (a) A fully connected graph of a shape morphing compliant mechanism; (b) a partially connected graph derived from (a) by changing some pTop to zeros. Their corresponding topology information is shown in Table 5-1.

Table 5-1: Topology information for the shape morphing compliant mechanisms in Figure 5-7.

Path type	Path number	Start vertex	End vertex	Path sequence	pTop Figure 5-7(a)	pTop Figure 5-7(b)
In→Out	1	1	4	{1,7,4}	1	0
	2	1	5	{1,8,5}	1	1
	3	1	6	{1,7,8,6}	1	0
In→Fix	4	1	2	{1,7,2}	1	0
	5	1	3	{1,7,3}	1	1
Fix→Out	6	2	4	{2,4}	1	1
	7	2	5	{2,7,8,5}	1	1
	8	2	6	{2,7,8,6}	1	1
	9	3	4	{3,8,9,4}	1	0
	10	3	5	{3,8,5}	1	1
	11	3	6	{3,6}	1	0

To form a common data structure for all designs, it is assumed that "*every essential port is connected to every other essential port of a different type with one path*." For example, a fixed point has one load path to describe its connection to the input and every output point, but it does not have a load path to describe its connection to any other fixed point. Therefore, the total number of load paths for each design can be determined by the number of points in each category. As shown in Table 5-1, a total of 11 paths are used to describe the topology in Figure 5-7(a). Each load path is comprised of a sequence of edges in the graph, and it is represented by a sequence of vertex numbers, termed as the *path sequence* (*pathSeq*) in the data structure. The path sequences contain the vertex numbers the paths go through in the order according to the path types, from input→output, input→fixed point, or fixed point→output. Each path in the graph is then assigned a binary topology variable (*pTop*) to indicate the presence or absence of the path. Figure 5-7(a) is termed a fully connected graph because *pTop* = 1 for all paths. When some of the *pTop* are switched to 0, the associated paths are eliminated from the graph, thus creating a different topology. Figure 5-7(b) shows a partially connected topology with several *pTop*=0. Note that the two designs have exactly the same *pathSeq*, but different *pTop*'s lead to different topologies.

The fully connected graph functions similarly to a ground structure; different 0/1 combination in *pTop* creates different topologies. However, the binary variable now represents the presence of an entire path, rather than just an element as in the binary ground structure parameterization. Moreover, since *pathSeq* is also a variable, various fully connected graphs can be explored simultaneously in the optimization process. Furthermore, the load path representation allows overlapping elements, such as elements

between segment 1-8 and 3-7 in Figure 5-7, which makes this parameterization applicable to three-dimensional problems.

Geometry Design Variables: *portLocation*

As opposed to the ground structure approach where the final design depends on the initial mesh resolution and configuration, load path representation allows variable resolution and configuration by varying the locations of the intermediate connection ports (*portLocation*). All the connection ports are allowed to move within the design domain. They control the lengths and orientations of the edge in the graph, hence the geometry (shape) of the compliant mechanism. They are, thus, regarded as the geometry (shape) variables. Figure 5-8 shows two designs with identical topologies as that in Figure 5-7(b); however, the structural geometries are different due to different interconnect port locations.
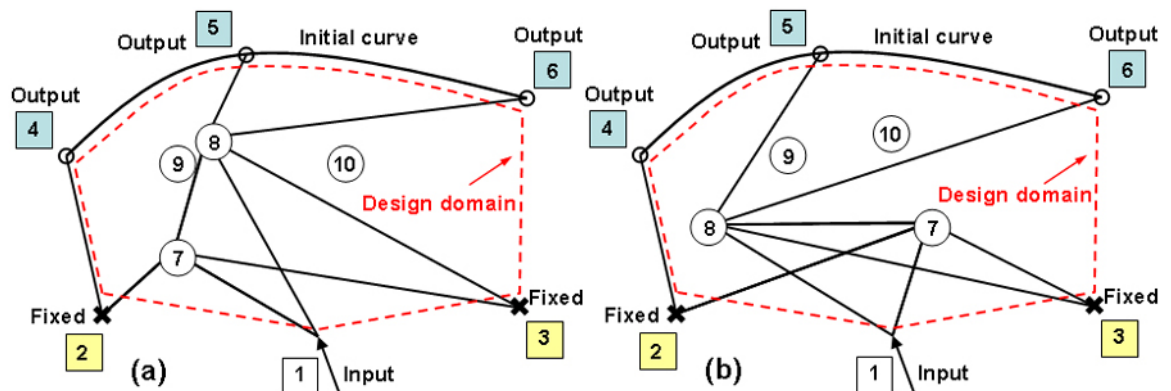
Figure 5-8: Different *portLocation***s render different geometries in the compliant mechanisms (a) and (b), although their topologies are identical.**

Size Design Variables: *pDim* **and** *hBoundary*

For each path in the load path representation, a size variable, *pDim*, is used to describe the path dimension. It is assumed that every edge in the graph represents a beam segment with uniform rectangular cross-section area. Since each path consists of several

79

edges, *pDim* contains a sequence of continuous values that represent the dimension of each edge in the order corresponding to *pathSeq*. The out-of-plane beam thickness is prescribed as a constant, thus *pDim* only describes the in-plane beam heights. Figure 5-9 shows two designs with different segment dimensions while their topologies and geometries are identical to that in Figure 5-8(a). The *pDim* information is listed in Table 5-2. Some path dimensions are not shown because the corresponding *pTop* value is zero. Note that there may be more than one *pDim* value describing the same beam segment, such as that between fixed point 2 and interconnect port 7 in paths #7 and #8 (bold values). Since only one value is required to describe the section dimension, one *pDim* value is randomly selected from the potential values (5 and 3 in design (a) and 3 and 1 in design (b)) with uniform probability. This can be seen as one value dominating the other one. The non-dominating values are then be replaced by the dominating values.
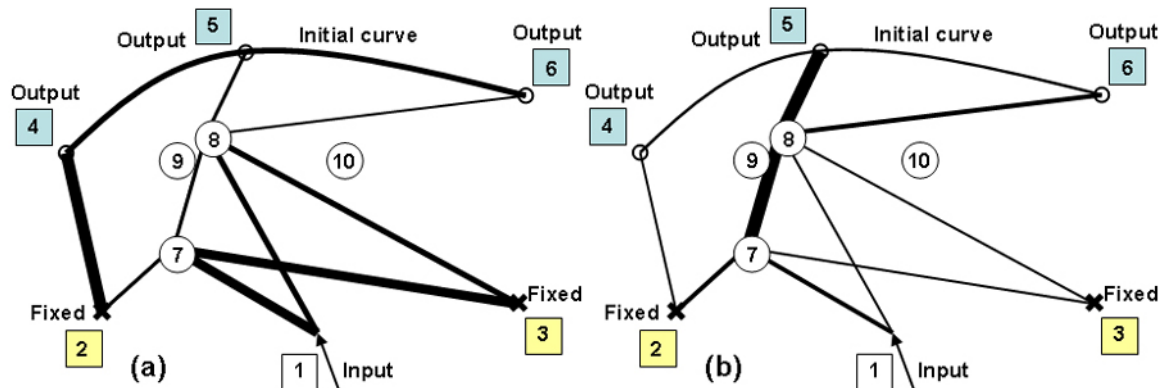
Figure 5-9: Two variations of the design in Figure 5-8(a) with different in-plane beam dimensions.

Table 5-2: Topology and size information for the compliant mechanisms in Figure 5-9.

Path type	Path number	Path sequence	pTop Figure 5-9	pDim Figure 5-9(a)	pDim Figure 5-9(b)
In→Out	1	{1,7,4}	0	{2,5}	{4,2}
	2	{1,8,5}	1	{5,3}	{2,11}
	3	{1,7,8,6}	0	{5,2.5,1}	{3,5.2,4}
In→Fix	4	{1,7,2}	0	{6,1.8}	{3.75,3.2}
	5	{1,7,3}	1	{8,8}	{3,2}
Fix→Out	6	{2,4}	1	{10}	{2}
	7	{2,7,8,5}	1	{**5**,3,3}→{**3**,3,3}	{**3**,11,11}

Path type	Path number	Path sequence	pTop Figure 5-9	pDim Figure 5-9(a)	pDim Figure 5-9(b)
	8	{2,7,8,6}	1	{**3**,3,2}	{**1**,11,4}➔{**3**,11,4}
	9	{3,8,9,4}	0	{4,7,2}	{1.2,5,3}
	10	{3,8,5}	1	{5,3}	{2,11}
	11	{3,6}	0	{8.5}	{9.3}
hBoundary		{4,5,6}	**1**	{5}	{2.5}

In addition to *pDim*, another continuous variable, *hBoundary*, is used to represent the beam height of the boundary. It is assumed that the shape morphing boundary always exists in every design, and the boundary has a uniform rectangular cross-section. The *hBoundary*s for the designs in Figure 5-9 are shown in Table 5-2. Since the boundary always exists, the path sequence and *pTop* are only listed here for reference. Only *hBoundary* is recorded in the data structure.

Parameters

Several parameters are associated with this parameterization. The first one is an upper bound on the path length (*maxPathLength*), which is defined by the number of vertices in a path sequence. The *maxPathLength* is prescribed by the user and is considered a constant. All paths should be less than or equal to the maximum length. For the examples shown in Table 5-2, the *maxPathLength* = 4. The larger the maximum length is, the more likely for a path to intersect with another path at interconnect ports.

Another parameter is the number of interconnect ports, which indirectly controls the complexity of the design. As shown in Figure 5-8, not all interconnect ports are used in every design, thus the number of interconnect ports only gives an upper bound of the mesh complexity. The smaller the port number is, the more likely for a path to intersect

with another path. As a rule of thumb, up to 10 ports are generally sufficient for shape

morphing problems addressed in this research (see Chapter 7).

Number of Design Variables

In the load path representation, the number of design variables depends on the

number of essential ports, the number of intermediate connection ports, and the

parameters. The number of essential nodes determines the total number of paths. For

instance, in Figure 5-10, there will be a total of 5+2+2×5 =17 load paths, thus 17 *pTop*

binary variables. Assuming *maxPathLength*=4, the maximum number of *pDim* variables

will be 4×17=68 (neglecting *hBoundary*). The number of interconnect ports (nPort) also

add more design variables; in this example, 10 the interconnect ports are used, thus

nPort=10. The total number of design variables, therefore, sums up to 17+68+10 = 95.

Compared to 380 design variables required in the binary ground structure for a similar

complexity design in Figure 5-10(b), the load path representation requires only 95 design

variables, which is a significant reduction.

For a more general problem with N output points and 2 layers of interconnect

ports (N ports in each layer), the total number of design variables are shown in

Eq.(5.7)~(5.10) as 17N+10, assuming one input, two fixed points, and *maxPathLength*=4.

As can be seen, the number of design variables increases linearly as the number of output

point increases (as opposed to the quadratic increase in the binary ground structure

parameterization). In fact, the increase could be less than predicted, because

maxPathLength is an upper bound, the actual path lengths can be less than 4 as shown in

Figure 5-10. In addition, the number of interconnect ports does not need to increase with

the number of output points. As a rule of thumb, 10 interconnect ports are sufficient for

problems encountered in this research, regardless of the output point numbers.
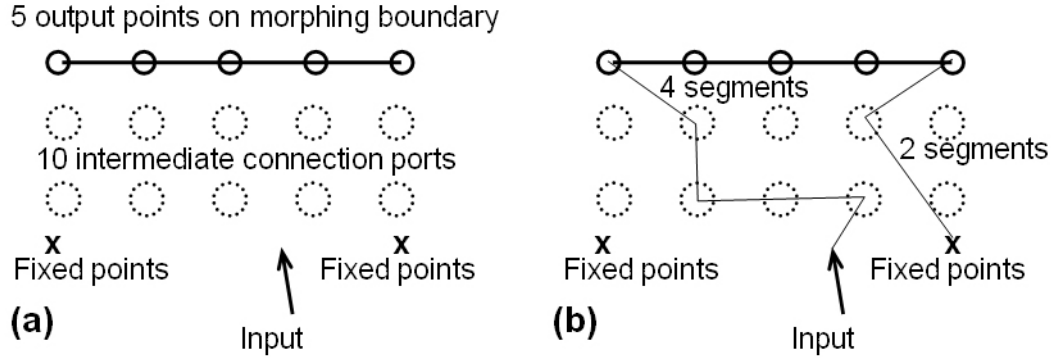
Figure 5-10: (a) A hypothetical problem with 5 output points, 10 interconnect ports, one input, and two ground supports; (b) the *maxPathLenth*(=4) imposes an upper bound on the length of *pathSeq*.

# of load paths (pTop)	$N + 2 + 2N = 3N + 2$	(5.7)
# of dimensions (pDim)	$maxLength(3N + 2) = 4(3N + 2) = 12N + 8$	(5.8)
# of interconnect ports (nPort)	$nLayer \times N = 2N$	(5.9)
Total # of design variables	$3N + 2 + 12N + 8 + 2N = 17N + 10$	(5.10)

In the binary ground structure, the mesh resolution can only be increased at the

expense of increasing the number of design variables. As opposed to the fixed mesh in

the binary ground structure, load path representation utilizes the interconnect ports to

create variable mesh resolution and configurations. In other words, the design resolution

is independent of the number of design variables. This makes load path representation

particularly powerful compared to the ground structure parameterizations.

Finite Element Mesh Mapping

It is important to connect the structural representation to the finite element mesh

so as to facilitate the use of FEA for structural analysis. In the load path representation,

the FE model for a design can be created simply by replacing the vertices and edges in

the graph with nodes and beam elements (Eq.(5.6)). The nodes can be created based on

the locations of the essential ports (remain fixed in one design) and the interconnect ports (geometry design variables). The element connection can be constructed based on the *pathSeq*. Although the change in *portLocation* requires re-meshing for each design, it can be done efficiently with the readily available connectivity information in *pathSeq*.

5.3.2   Structural Connectivity

By observing various structures and compliant mechanisms, we found that there are two important requirements to avoid invalid designs: (1) input must be connected to one or more output points, and (2) the structure must be grounded at one or more fixed points. In the shape morphing problem, since the morphing boundary always exists, the structural connectivity can be ensured with at least one path in both *pathInOut* and *pathFixOut* categories. This information can be easily obtained from the *pTop* values associated with each path type. As long as the sum of *pTop's* in both categories are greater than zero, the two connectivity requirements can be satisfied. This is a major advantage over the binary ground structure approach, where structural connectivity information has to be 'searched for' using additional routines. The load path representation describes the structural topology in terms of the presence of individual paths, thus making the connectivity information readily available and thereby improving the optimization performance.

An additional advantage over ground structure type approach is that the number of design variables is now independent of the FE mesh resolution. Most of the ground structure type approaches involve the use of an initial discretization mesh, which directly determines the final design resolution. In general, when higher resolution features are

desired, finer discretization mesh should be used. Since the number of design variables depends on the number of elements, when higher resolution is required, the number of design variables will increase accordingly. In the load path representation, fine structural features can be achieved without using many design variables, since the locations of the intermediate connection ports can vary continuously inside the design domain. In other words, multiple gradations of structural resolution and a variety of configurations can be generated without increasing the number of design variables.

CHAPTER 6

OPTIMIZATION PROBLEM

6.1 Objective Function for Curve Comparison

Shape morphing compliant mechanism utilizes the structural deformation to morph shapes. Upon input actuation, the structural boundary morphs from its initial shape into the deformed shape. The goal is to design the structural topology and dimensions so that the deformed boundary profile can match the desired target shape. Since every point along the structural boundary is displaced in a different direction and magnitude, an objective function involving multiple output points should be used in the optimization procedure to allow quantitative comparison between different designs.

In this work, the structural deformation due to input actuation is solved for using a finite element analysis (FEA). The deformed boundary profile is extracted from the FEA, and a curve comparison objective function then evaluates the deviation between the deformed shape and the desired target shape. In the following, two curve comparison schemes will be introduced, including a Least Square Error (LSE) deviation that captures the point-to-point deviation between the two curves, and a modified Fourier Transformation (FT) deviation that captures the pure difference in shape regardless of their scales and orientations.

6.1.1   Least Square Error Deviation

To compare the deformed and target curves, the two curves are first expressed in terms of two sets of sampling points that are evenly distributed along the curve lengths, as shown in Figure 6-1. In general, the number of sampling points is identical to the number of data points in the initial curve specification. The sampling points on the deformed curve are simply the nodes on the boundary in FEA. However, if more sampling points are desired, additional points can be interpolated using the shape functions defined in FEA.
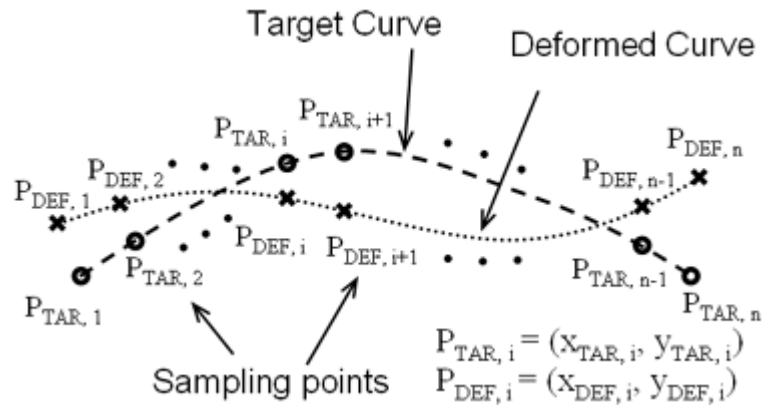
Figure 6-1: Sampling points on the deformed and target curves.

The least square error (LSE) deviation is defined as the sum of Euclidian distance between each pair of sampling points (x and o in Figure 6-1) on the two curves. This is shown in Eq.(6.1), where n is the total number of sampling points; (x_{DEF}, y_{DEF}) and (x_{TAR}, y_{TAR}) are the coordinates of the sampling points along the deformed and target curves respectively. Since every point-to-point deviation is included in the formulation, the LSE deviation can capture the difference in scale (curve lengths), shape, and orientation, leading to a solution that matches the target curve exactly.

$$LSE_{dev} = \sum_{i=1}^{n} \sqrt{(x_{DEF,i} - x_{TAR,i})^2 + (y_{DEF,i} - y_{TAR,i})^2} \qquad (6.1)$$

For situations where symmetry is presented in the problem, however, LSE deviation cannot identify the symmetric solution because the 'location' is measured in addition to the 'shape' difference. Figure 6-2(a) shows an example that changes a symmetric curve (about y-axis) into a curve that bends towards the right. Assuming that Figure 6-2(b) is a solution to this problem, it can be seen that Figure 6-2(c) can also be a valid solution simply by mirroring the solution about y-axis, but this solution will be discarded using LSE deviation. Figure 6-3 shows another situation where LSE deviation is inappropriate to describe the 'shape' difference. The goal is to deform a circle into an ellipse, but the ellipse can be in any orientation because the circle is axisymmetric. Using LSE deviation will prevent the optimization algorithm from finding the design in Figure 6-3(c). Although the orientation of the deformed ellipse is at an angle to the target, this implies that an alternate design can be obtained by changing the actuator orientation. Since the input actuator is specified based on intuition, if the chosen direction is unable to produce the desired shape change, it would be difficult for LSE deviation to identify an acceptable solution, while a simple change of actuator orientation can lead to a good solution.
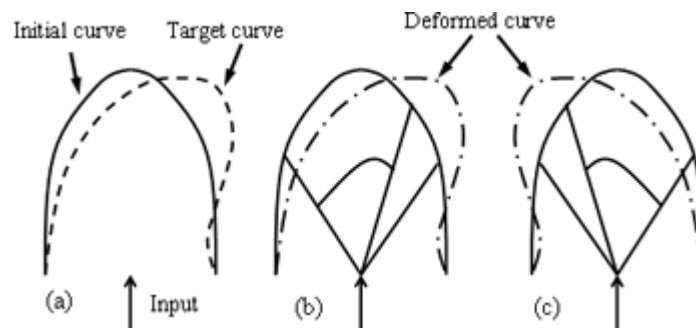
Figure 6-2: (a) A shape change example where initial curve is symmetric with respect to the vertical axis; (b) an example solution (not the actual solution) to this problem; (c) a mirror image solution which could be discarded during the optimization process using LSE.
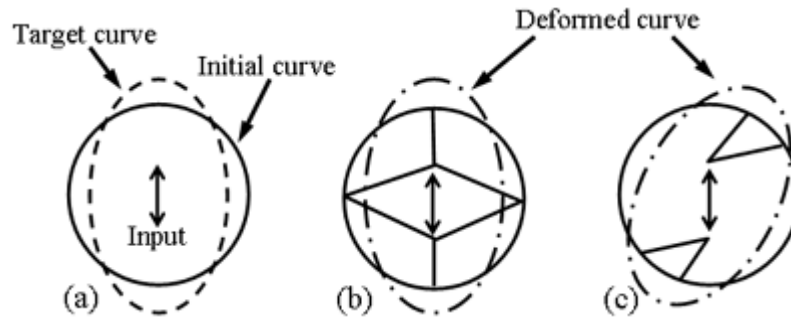
Figure 6-3: (a) A shape change example that changes a circle into an ellipse; (b) a design with deformed curve that matches the target curve exactly (shape and locations); (c) a design that can achieve shape change from a circle to an ellipse at an angle.

An alternative objective function focusing on the 'shape' difference is, therefore, formulated to include all potential designs in problems with symmetry. The shape information is extracted using Fourier Transformation, and this will be introduced in the next section.

6.1.2   Modified Fourier Transformation (FT) Deviation

To emphasize the difference in 'shape' rather than the 'point-to-point' difference, a modified Fourier Transformation (FT) deviation is used to characterize and compare the deformed and target curves. Standard Fourier Transformation is shown in Eq.(6.2), where f(t) is a periodic function in time-domain. It transforms the periodic function into its frequency content in terms of harmonic amplitudes and their corresponding frequencies, as shown in Figure 6-4. Lower frequency information dominates the overall signal shape, while higher frequency information usually contributes to finer features. This is especially useful for the curve comparison task not only because the information is purely about the shape, but it also provides shape information of varying levels of significances.

$$F(\omega) = \text{F}\{f(t)\} = \int_{-\infty}^{\infty} f(t)e^{-jwt}dt \qquad (6.2)$$
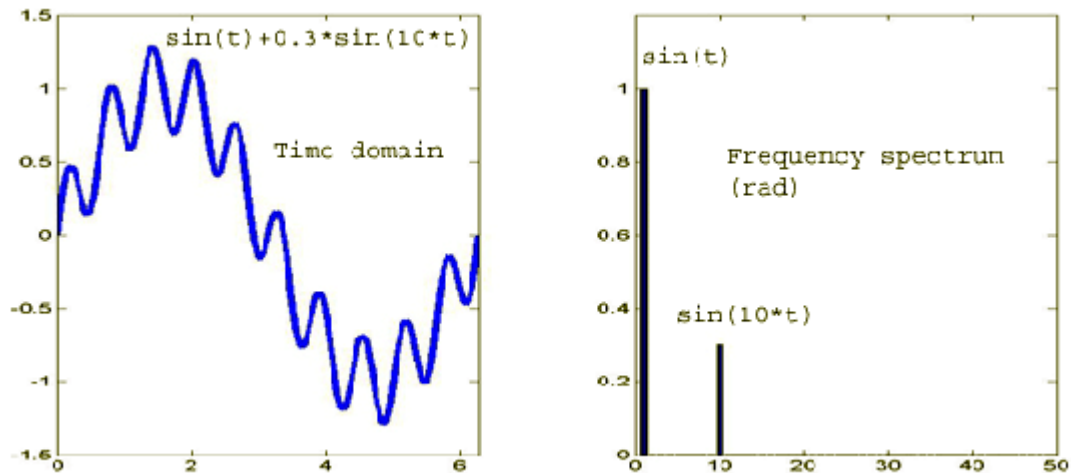
Figure 6-4: A one-dimensional periodic signal and its frequency spectrum. Lower frequencies dictate the overall shape, while higher ones describe the finer details.

To utilize FT, the curve has to be represented as a one-dimensional periodic signal. One way to achieve this setting is to express the curve shape in terms of its location in Y-direction as a function of its arc length. Since the start and end points of the curve do not necessarily have the same value in global Y-direction, the sampling points on the curve are transformed from the original global X-Y coordinates to the x'-y' coordinates, where the x'-axis is determined by connecting the start and end points of the curve, as shown in Figure 6-5. The curve is then expressed as a function of the arc length, hence, a one-dimensional periodic signal. Because the curve is expressed in terms of the sampling points (exact curve function is generally unknown), Discrete Fourier Transformation (DFT) is used in place of standard FT. The DFT transforms discrete sampling information on the curve into discrete frequencies and their corresponding harmonic amplitudes, termed as the Fourier Descriptors (FDs). In this work, Fast Fourier Transformation (FFT) is used to further accelerate the calculation speed by re-sampling the modified curve (arc length vs. y'-direction value) with 2^N points, where N is an integer.
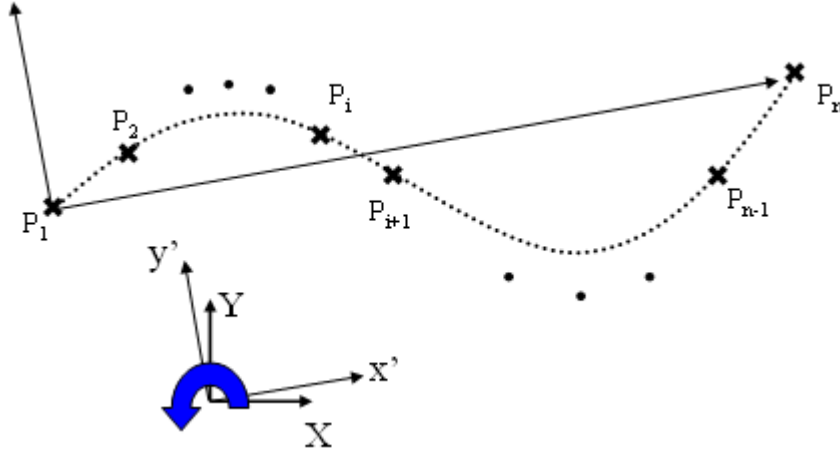
Figure 6-5: The coordinate transformation used in the modified FT method, so that the deformed and target curves can have the same y value (in the y'-direction) at the starting and end points.

To evaluate the deviation between the deformed and target curves, the modified

FT (coordinate transformation + FFT) is used to characterize each curve separately,

resulting in two sets of FDs. As shown in Eq.(6.3) and Figure 6-6, the sum of amplitude

differences at corresponding frequencies is then defined as the FT deviation between the

two curves, where $AmpTAR_k$ and $AmpDEF_k$ are the kth harmonic amplitudes for the target

and deformed curves respectively, and nAmp is number of amplitudes taken into account.

Since the lower frequency terms dominate the overall shape, only first few terms are

considered in the modified FT deviation. Furthermore, the shapes involved in the

morphing applications are generally smooth without many high frequency noises, thus

nAmp $\leq$ 5 is sufficient in general. Note that the zero frequency term is removed from the

FDs because it represents the mean signal value (average location) of the curve rathern

than the 'shape.'

$$FT_{dev} = \sum_{k=1}^{nAmp} | AmpTAR_k - AmpDEF_k | \tag{6.3}$$
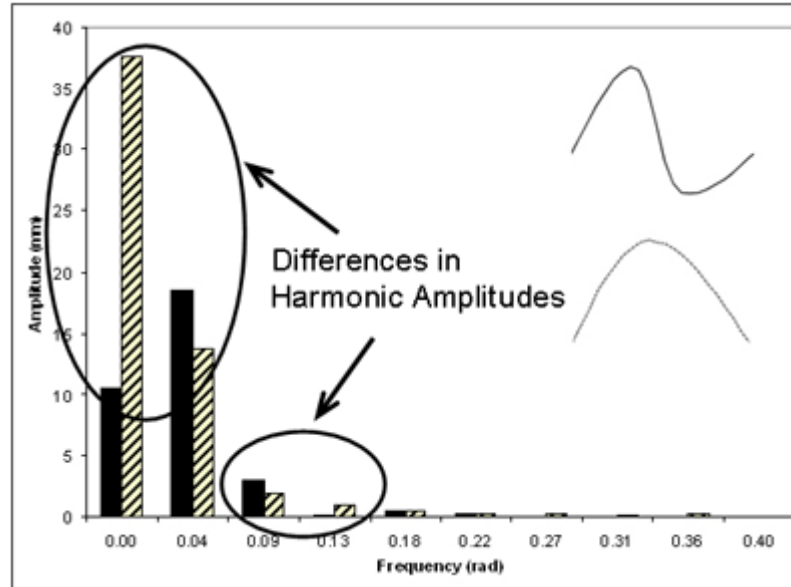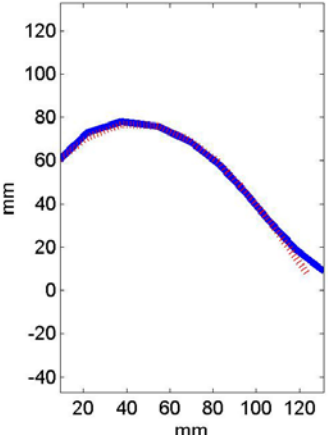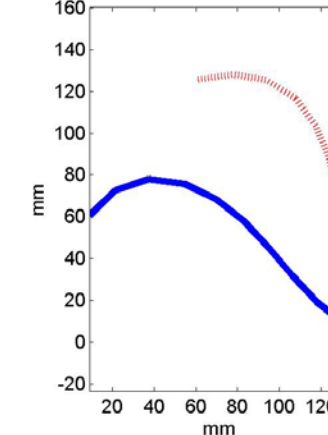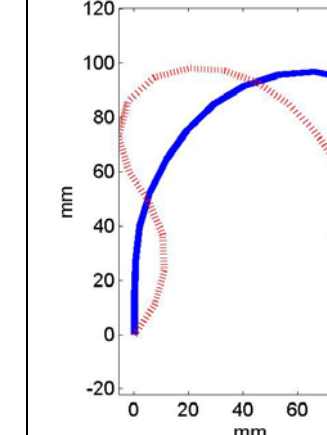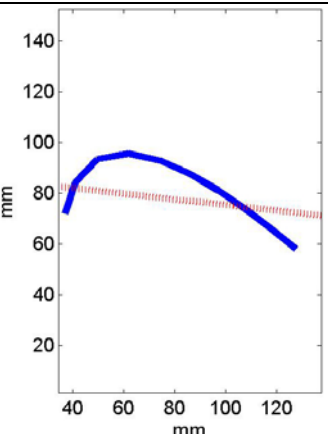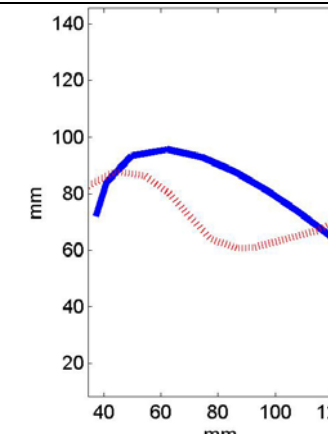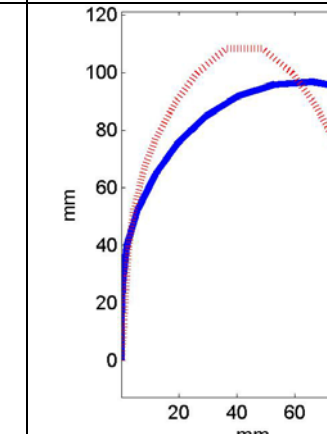
Figure 6-6: An example of the differences in harmonic amplitudes for two curves.

6.1.3   Objective Function Verification

To examine how the LSE and FT deviations explore different aspects of shapes, the deviation measures defined in Eq.(6.1) and Eq.(6.3) are applied to several test shapes. The curves and associated LSE and FT deviations are shown in Table 6-1. The LSE deviation used here is the mean value rather than the sum of all errors in Eq.(6.1), since the average error is easier to interpret visually. In the FT deviation, only the first three frequencies are considered (nAmp = 3). Test 1 shows two curves with slight difference on the lower right end. The LSE and FT deviations are both small. The deviation values in all other tests will be normalized with respect to the values in Test 1 and listed after the arrows. Test 1 and 2 evaluates the same two curves, but in Test 2, the dash curve (lighter color) is translated and rotated with respect to the solid curve. Thus, FT deviations are the same in both cases (same shape), but LSE gives a large deviation value in test 2 due to the difference in location and orientation. Test 3 shows two curves that are almost mirror images of each other, so the FT deviation is small while LSE deviation gives a large

92

value. Test 4 shows that when two curves have very different shapes, both LSE and FT have large deviation values; however, the normalized values suggest that FT captures the shape difference better than the LSE deviation. Finally, Test 5 and 6 are two general cases where both objective functions perform equally well.

Table 6-1: Test shapes and their corresponding LSE and FT deviation values.

Test 1	Test 2	Test 3
LSE: 2.2999mm→1 FT: 1.0593mm→1	LSE: 52.612mm→22.8758 FT: 1.0593mm→1	LSE: 16.8667mm→7.3337 FT: 1.3732mm→1.2963
Test 4	Test 5	Test 6
LSE: 12.218mm→5.3124 FT: 17.9417mm→16.9373	LSE: 14.4634mm→6.2887 FT: 5.3164mm→5.0188	LSE: 9.3483mm→4.0647 FT: 9.865mm→9.3128

Although both LSE and FT can be used in any given shape morphing problem, the choice of objective function generally depends on the symmetry of the curves. FT deviation is used when symmetry is presented in either the initial or target curve. FT

deviation is also useful when matching the 'exact' shape is not critical; for example, if the target curve is not clearly defined, one can use the lower frequency information in the FT deviation to 'roughly' match the target curve. On the other hand, LSE deviation is used when no symmetry is presented in the problem. As will be shown later in the examples in Chapter 7, LSE is more versatile and used more often in general cases due to its simple yet effective measure. FT deviation is indeed capable of identifying the mirror images and suggesting improvements on actuator orientation. However, the implementation requires more computational cost, and care must be taken to avoid convergence to undesirable mirror image.

6.2 Optimization Using Genetic Algorithm

As indicated in section 1.3.2, various heuristic optimization methods have been applied to structural optimization and compliant mechanism synthesis. Among those methods, genetic algorithm (GA) (Holland, 1975; Goldberg, 1989) is one most commonly used method that can be applied to a wide variety of problems and is very easy to implement. It also has the flexibility to work with both discrete and continuous variables. It can be implemented with various types of data structures in different problems, as long as the fundamental working principle is followed. GA is, therefore, used in this research due to its many advantages.

The working principle in GA is based on the selection scheme, *survival of the fittest*, seen in nature to optimize *a group of designs* through evolution. Figure 6-7 is a flowchart of a typical GA, starting with an initial population of designs where the characteristics of each individual are encoded in its chromosome string. Each individual

also has an associated fitness value indicating the reproduction capability of the

individual. A selection scheme based on the fitness value is incorporated in GA to

simulate the selection seen in nature; healthier individuals have higher chance to

reproduce while inferior ones are less likely to generate healthy offspring. The

"chromosomes" of the selected parent designs go through genetic operations (crossover

and mutation) to create new designs while preserving part of the parents' characteristics.

When the number of new designs is equal to that in the parent design, the offspring

generation becomes the new parent generation, and the reproduction process starts over

again. As the number of generation increases, the overall fitness value of the population

will improve. This evolution process can, therefore, be adopted for optimization problems.
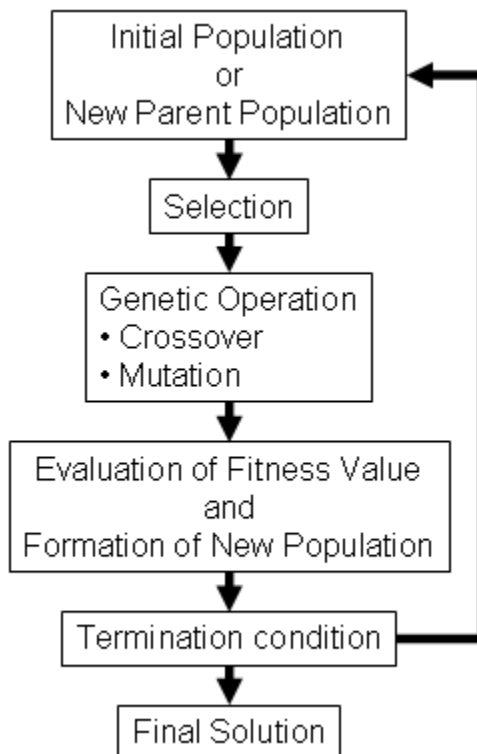
Figure 6-7: The flowchart of a typical GA.

Through the evolution of *a population of designs*, GA can simultaneously explore

various regions in the solution space; whereas, in continuous gradient-based optimization

methods, the algorithm iterates from *a single initial design* and searches within a localized region in the solution space. Since GA does not require any gradient information, the search jumps between different regions and is more likely to locate the global optimum, while the solutions from gradient-based methods are usually local optima that are starting point dependent. In the compliant mechanism synthesis, the solution space is non-convex, noisy, and multi-modal. From this perspective, GA is a particularly good choice, because distinct designs that perform equally well can potentially be included in the final population. This offers a useful tool for designers to identify various design alternatives. Although GA is efficient in exploring different regions in the solution space, converging to a local optimum is quite difficult, due to its heuristic nature and the fact that it does not require gradient information. Therefore, it is beneficiary to perform a local search following GA to accelerate the convergence to the nearby local optimum.

To utilize GA as an optimization tool, three important components must be defined: (1) the design variables consisting of the chromosomes, (2) the objective function which the selection scheme based on, and (3) and the genetic operations concerning how new designs are generated from parent chromosomes. In the shape morphing problem, two curve comparison objective functions have been introduced in section 6.1. Two parameterization schemes have also been introduced in Chapter 5 to describe various compliant mechanism topologies and dimensions. Due to the different data structures used in the binary ground structure parameterization and the load path representation, two sets of reproduction rules are developed to allow proper genetic operations in either chromosome structure. The reproduction process creates diversity

within each generation, which, in fact, provides the power behind GA to improve designs

as generations evolve. The crossover and mutation strategies are, therefore, essential to

the performance of GA. The following sections will introduce the optimization problem

formulations and the reproduction schemes corresponding to the two parameterizations

introduced in Chapter 5. Interested readers can refer to Goldberg and Holland (1975;

Goldberg, 1989) for more detailed discussion on GA.

6.2.1 Binary Ground Structure Parameterization

Problem Formulations and Constraints

The objective of the shape morphing problem is to minimize the deviation

between the deformed and target curves. Using the binary ground structure

parameterization, the optimization problem is summarized in Eq.(6.4) ~ Eq.(6.10).

Objective Function
$$\min_{\substack{hTop, hDim, \\ hBoundary}} \left(LSE_{dev}\right) \text{ or } \min_{\substack{hTop, hDim, \\ hBoundary}} \left(FT_{dev}\right) \tag{6.4}$$

Subject to

g1: $hDim_{min} < hDim_i \leq hDim_{max}$	size constraint	(6.5)
g2: $hDim_{min} < hBoundary_i \leq hDim_{max}$	size constraint	(6.6)
g3: $h_i = hTop_i \times hDim_i$	mixed variables	(6.7)
g4: $\mathbf{d} = \mathbf{K}^{-1}\mathbf{F}$	FEA equilibrium	(6.8)
g5: $\max(d_{unactuated}) \leq d_{allowable}$	stiffness constraint	(6.9)
g6: $\sigma_i \leq \sigma_{allowable}$	stress constraint	(6.10)

$hTop_i \in \{0,1\}$, $hDim_i \in \mathbb{R}^+$, and i $\in$ all beam elements

$d_{unactuated} \in$ displacement of nodes on the morphing boundary when input is held fixed

As shown in Eq.(6.4), either of the two deviation measures (LSE or FT) can be

used, depending on the symmetry in the problem. The design variables include the binary

topology variables ($hTop_i$), and positive dimensional variables ($hDim_i$ and hBoundary).

All the beam elements, including the morphing boundary, are allowed to vary continuous within the size constraints, shown in Eq.(6.5) and Eq.(6.6). The allowable range is generally based on the manufacturing constraints. The topology and dimensions of the compliant mechanism is defined by the mixed variables in Eq.(6.7). Structural equilibrium and deformation are then obtained from FEA in Eq.(6.8). The stiffness constraint shown in Eq.(6.9) limits the maximum deformation on the morphing boundary when the actuator is held fix (resisting external loads). A stress constraint, Eq.(6.10), is also applied to all elements to prevent structural failure.

Reproduction Schemes: Selection, Crossover, and Mutation Strategies

The GA starts with an initial population that is randomly created. Every chromosome string in the population has the same data structure shown in Eq.(6.11), where the subscript k represents the kth design in the population, n is the total number of elements in the binary ground structure, $hTop_i$ and $hDim_i$ are the topology and dimensional values for the ith beam element, and $hBoundary$ is the dimension of the elements along the morphing boundary. Successive generations are reproduced from selection, crossover, and mutation.

$$design_k = \left[\underbrace{h_kTop_1, \quad h_kTop_2, \quad \cdots \quad h_kTop_n,}_{Topo\log y} \underbrace{h_kDim_1, \quad \cdots \quad h_kDim_n, \quad}_{Dimensions} h_kBoundary \right] \quad (6.11)$$

A roulette wheel selection scheme is used in this research; designs with smaller deviation values have higher probability of being selected, while those with larger deviation values have less chance of being selected. This is analogous to the reproduction situation seen in nature, where healthier individual has higher chance to reproduce, but

the fitness evaluation is now based on the shape deviation objective function in Eq.(6.1) or Eq.(6.3). In order to translate the 'smaller' deviation into 'higher' fitness value, the fitness value is defined using Eq.(6.12). The coefficient *a* controls the slope of the curve when deviation approaches zero; the peak is smoother with smaller *a* as shown in Figure 6-8. Equation (6.13) defines the reproduction probability of the kth design in the roulette wheel selection scheme as the fitness value of the kth design over the total fitness value of the whole population.

$$fitness = \exp(-a \times deviation) \tag{6.12}$$
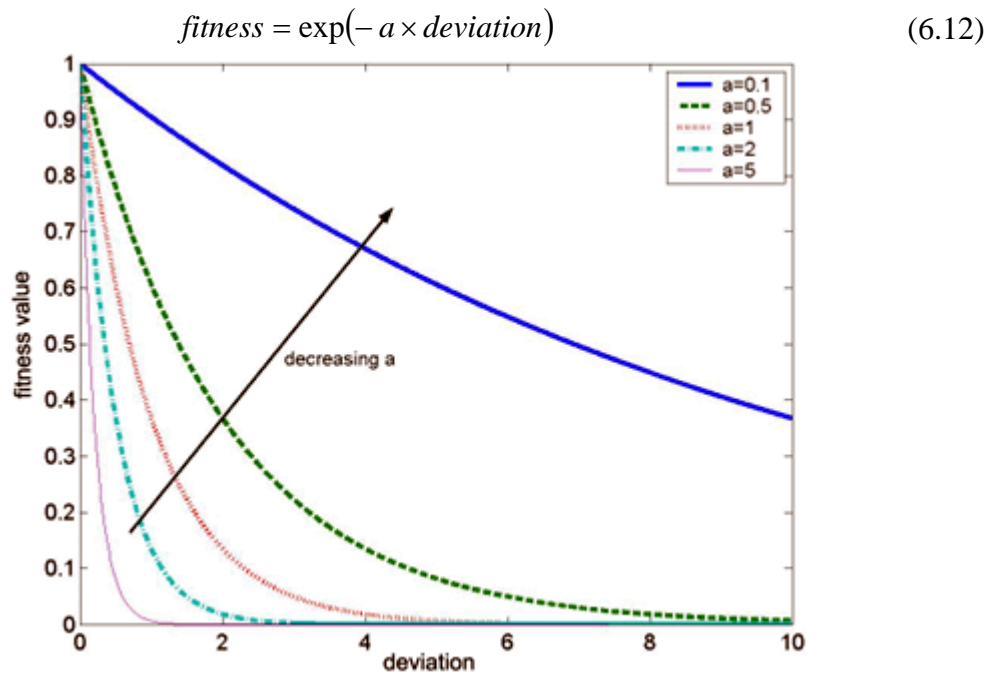
Figure 6-8: Mapping between the deviation and fitness value with different coefficient, *a*.

$$pr(design_k) = \frac{fitness_k}{\sum\limits_{i=1}^{nPop} fitness_i} \tag{6.13}$$

The crossover operation is shown in Eq.(6.14) ~ Eq.(6.17). Using the roulette wheel selection scheme, two parent chromosomes (p1 and p2) are selected from the first generation, and two new chromosomes (k1 and k2) can be created through crossover of

the parent chromosomes, p1 and p2. The crossover is achieved by exchanging portions of the parents' chromosome strings; the vertical lines in Eq.(6.14) and Eq.(6.15) indicate the point of crossover, while the underline portions in Eq.(6.16) and Eq.(6.17) show the segments of chromosome strings coming from the other parent. Note that the crossover point can be anywhere within the chromosome code, including the topology and dimensional variables.

$$p1 = \left[h_1 Top_1, \cdots, h_1 Top_n, h_1 Dim_1, \cdots, h_1 Dim_k, | \; h_1 Dim_{k+1}, \cdots, h_1 Dim_n, h_1 Boundary \right] \qquad (6.14)$$

$$p2 = \left[h_2 Top_1, \cdots, h_2 Top_n, h_2 Dim_1, \cdots, h_2 Dim_k, | \; h_2 Dim_{k+1}, \cdots, h_2 Dim_n, h_2 Boundary \right] \qquad (6.15)$$

$$k1 = \left[h_1 Top_1, \cdots, h_1 Top_n, h_1 Dim_1, \cdots, h_1 Dim_k, \; \underline{h_2 Dim_{k+1}, \cdots, h_2 Dim_n, h_2 Boundary} \right] \qquad (6.16)$$

$$k2 = \left[h_2 Top_1, \cdots, h_2 Top_n, h_2 Dim_1, \cdots, h_2 Dim_k, \; \underline{h_1 Dim_{k+1}, \cdots, h_1 Dim_n, h_1 Boundary} \right] \qquad (6.17)$$

Equations (6.18) and (6.19) illustrate the mutation in the reproduction process. A randomly selected 'bit' on the chromosome string changes value while the rest of the values remain unchanged. When the selected bit is part of the binary topology variables, the value is changed from 1→0 or 0→1. When a dimensional variable is selected, a new dimension within the bounds is generated to replace the original value. Although multiple mutation points can be implemented, in this work, the mutation occurs only at one location for each design. The two mutation locations (underlined) shown in Eq.(6.18) and Eq.(6.19) are shown to help illustrate the mutation of different variable types.

$$design_k = \left[1,0,\underline{1},1,0,1, \quad 0.6,1.4,\underline{0.8},0.5,1,1.5, \quad 0.96 \right] \qquad \text{original chromosome} \qquad (6.18)$$

$$design_k^{mutate} = \left[1,0,\underline{0},1,0,1, \quad 0.6,1.4,\underline{1.2},0.5,1,1.5, \quad 0.96 \right] \qquad \text{mutated chromosome} \qquad (6.19)$$

During reproduction, parent designs are selected from the parent generation to create new designs for the offspring generation until the new generation has the same number of designs as the parent generation. This new generation then becomes the parent

generation for yet another new generation. This reproduction process repeats until the termination condition is met. Here, the reproduction terminates upon reaching the maximum number of generations, and the fittest design in the final generation is considered the 'optimal' solution. In each offspring generation, two copies identical to the top two designs in the parent generation are generated automatically to guarantee the next generation will be at least as good as its parent generation, while the rest of the individuals are new designs generated from reproduction.

6.2.2 Load Path Representation

Problem Formulation and Constraints

The optimization problem formulation using load path representation is summarized in Eq.(6.20) ~ Eq.(6.29).

Objective Function

$$\min_{\substack{pTop, pDim, \\ hBoundary, \\ portLocation}} \left(LSE_{dev}\right) \text{ or } \min_{\substack{pTop, pDim, \\ hBoundary, \\ portLocation}} \left(FT_{dev}\right) \tag{6.20}$$

Subject to

g1: $pDim_{\min} < pDim_{i,j} \leq pDim_{\max}$	size constraint	(6.21)
g2: $pDim_{\min} < hBoundary \leq pDim_{\max}$	size constraint	(6.22)
g3: $h_e = pTop_i \times pDim_{i,j}$	mixed variables	(6.23)
g4: $(x_{\min}, y_{\min}) \leq portLocation \leq (x_{\max}, y_{\max})$	variable mesh geometry	(6.24)
g5: $\sum\limits_{i \in pathInOut} pTop_i \geq 1$	connectivity constraint for *pathInOut*	(6.25)
g6: $\sum\limits_{i \in pathFixOut} pTop_i \geq 1$	connectivity constraint for *pathFixOut*	(6.26)
g7: $\mathbf{d} = \mathbf{K}^{-1}\mathbf{F}$	FEA equilibrium	(6.27)
g8: $\max(d_{unactuated}) \leq d_{allowable}$	stiffness constraint	(6.28)
g9: $\sigma_e \leq \sigma_{allowable}$	stress constraint	(6.29)

where pTop $\in \{0,1\}$; pDim, hBoundary, portLocation $\in \mathbb{R}^+$;

    i: path number;

    j: section number in the ith path;

    e: number of elements;

$d_{unactuated}$: displacement of nodes on the morphing boundary when input is held fixed.

The objective is to minimize the LSE or FT deviation between the deformed and target boundary profiles. The beam element dimensions (in-plane) are constrained between a minimum and a maximum values, typically based on the manufacturing constraints, shown in Eq.(6.21) and Eq.(6.22). The resulting compliant mechanism topology and dimensions are simultaneously determined by the *pTop* and *pDim* variables as in Eq.(6.23). As seen in Eq.(6.24), the locations of the interconnect ports are allowed to wander within a specified range, typically the design domain. Equations (6.25) and (6.26) are the connectivity requirements discussed in chapter 5.3.2 to ensure all designs are properly connected. The structural deformation and equilibrium is obtained through the use of FEA, shown in Eq.(6.27). As seen in Eq.(6.28), the stiffness is achieved by constraining the maximum nodal displacement to stay within an acceptable value, when the actuator is held fixed. A stress constraint in Eq.(6.29) is imposed on all the elements to prevent failure.

Note that the structural connectivity is now guaranteed through the constraints in Eq.(6.25) and Eq.(6.26). If a design violates these constraints, indicating all *pTop* are zero, the design can also be fixed quickly by randomly switching a *pTop* from 0 to 1. For example, if a design has no path from input to output, violating Eq.(6.25), the algorithm will automatically make *pTop*=1 for a randomly selected path in the *pathInOut* category. This can be seen as a mutation in the evolution process and can help the algorithm search for useful designs efficiently. This is another advantage over the binary ground structure approach where disconnected designs are simply penalized (assigned a large deviation value or low fitness value) but not really removed from the population.

Another feature that is different from the binary ground structure approach lies in the finite element mesh. As opposed to having a fixed initial mesh, the mesh resolution and configuration in the load path representation are controlled by the connection port locations Eq.(6.24). That is, every design may have a different mesh configuration and re-meshing is required in every FEA. With the load path representation, an adaptive mesh using beam elements can actually be implemented quite easily; locations of the basic points and interconnect ports define the nodes, the pathSeq describes the element connectivity, and pDim controls the element dimensions (beam cross-section properties).

Reproduction Schemes: Selection, Crossover, and Mutation Strategies

In the load path representation, the selection scheme is identical to that used in the binary ground structure approach (see section 6.2.1). However, since the chromosomes are no longer in 'string' format, more sophisticated strategies have to be developed to make crossover and mutation possible in the load path representation.

The crossover strategy in this approach is to 'exchange' randomly selected paths between two parent designs. More than one path can be selected for crossover. The *pathSeq* and *pTop* of the parent designs are exchanged during this process while preserving the original *pDim* and *portLocation*. Since new *pathSeq* leads to new connectivity in the offspring design, the number of segments (length of *pDim*) along each path may be different from that in the parent design. The *pDim* must be modified by inserting additional values or removing extra ones to maintain compatibility with the *pathSeq*. In addition, the boundary dimension (hBoundary) of the two parent designs can be exchanged according to the crossover probability.

Figure 6-9 shows two example designs (P1 and P2) with their load path information listed in Table 6-2. Path #1 and #5 are selected, for example, to illustrate the crossover operation. The two new designs are shown in Figure 6-10 and Table 6-3 as K1 and K2. As shown in Table 6-3, the original *pathSeq* and *pTop* of Path #1 and #5 in P1 and P2 are replaced with the values from the other parent, while *pDim* and interconnect port locations remain the same. However, the length of *pDim* changes after the crossover. Therefore, a random value (within the *pDim* bounds) is inserted into $pDim_1$ of K1 and $pDim_5$ of K2, and a randomly selected 'bit' is removed from $pDim_5$ of K1 and $pDim_1$ of K2. In addition, the boundary information is exchanged during crossover; since the connectivity of the morphing boundary is invariant, only the cross-section dimension is changed (*hBoundary*).
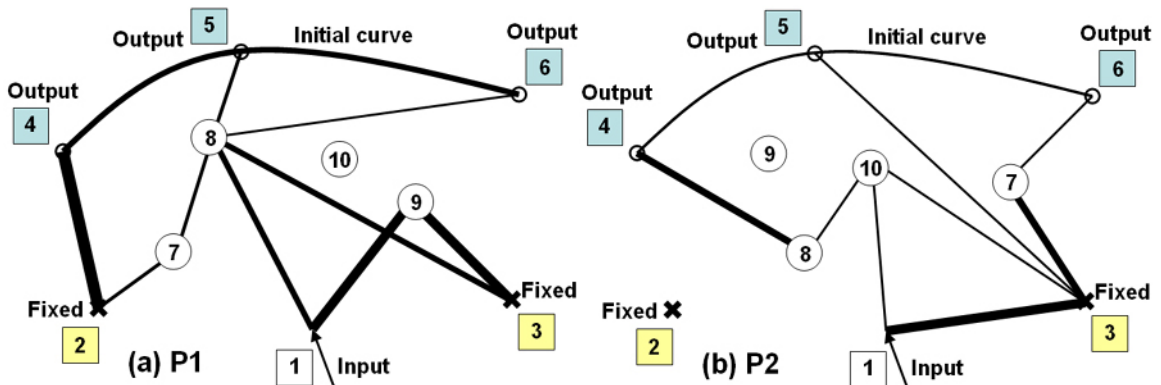
Figure 6-9: Two example parent designs with load path information listed in Table 6-2.

Table 6-2: The load path information for the parent designs shown in Figure 6-9.

Path type	Path #	Figure 6-9(a) P1			Figure 6-9(b) P2		
		PathSeq	*pTop*	*pDim*	*PathSeq*	*pTop*	*pDim*
In→Out	1	{1,7,4}	0	{2,5}	{1,10,8,4}	1	{2,2,6}
	2	{1,8,5}	1	{5,3}	{1,7,8,5}	0	{3,2.5,3}
	3	{1,7,8,6}	0	{5,2.5,1}	{1,8,6}	0	{5,1}
In→Fix	4	{1,7,2}	0	{6,1.8}	{1,9,2}	0	{6,1.8}
	5	{1,9,3}	1	{8,8}	{1,3}	1	{8}
Fix→Out	6	{2,4}	1	{10}	{2,10,4}	0	{10,7}
	7	{2,7,8,5}	1	{3,3,3}	{2,9,5}	0	{2,3}
	8	{2,7,8,6}	1	{3,3,2}	{2,9,7,6}	0	{3,4,5}
	9	{3,8,9,4}	0	{4,7,2}	{3,10,8,4}	1	{2,2,6}

	10	{3,8,5}	1	{5,3}	{3,5}	1	{2}
	11	{3,6}	0	{8.5}	{3,7,6}	1	{6,2}
hBoundary		{4,5,6}	1	{5}	{4,5,6}	1	{2.5}
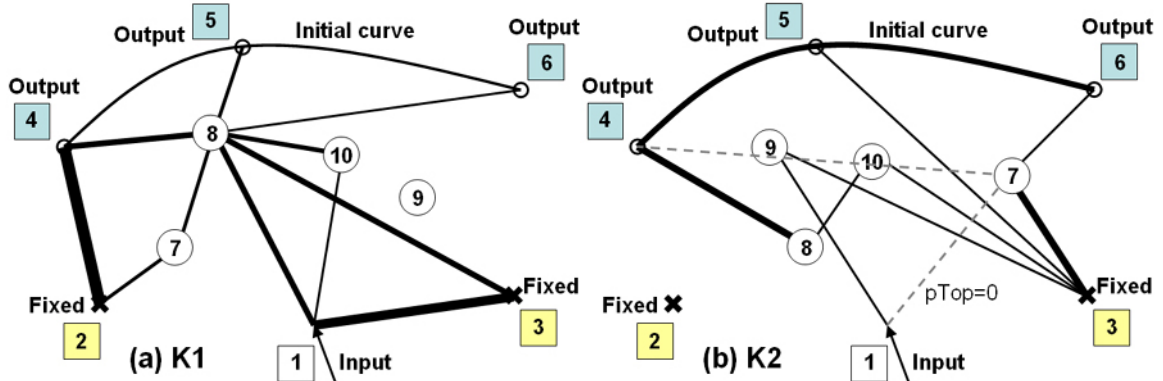
Figure 6-10: Two offspring designs obtained from the parent designs in Figure 6-9 by exchanging path #1 and #5. Their load path information is listed in Table 6-3.

Table 6-3: The load path information of the offspring designs shown in Figure 6-10.

Path type	Path #	Figure 6-10(a) K1			Figure 6-10(b) K2		
		PathSeq	*pTop*	*pDim*	*PathSeq*	*pTop*	*pDim*
In→Out	1*	**{1,10,8,4}**	**1**	**→{2,4,5}**	**{1,7,4}**	**0**	**→{2,2}**
	2	{1,8,5}	1	{5,3}	{1,7,8,5}	0	{3,2.5,3}
	3	{1,7,8,6}	0	{5,2.5,1}	{1,8,6}	0	{5,1}
In→Fix	4	{1,7,2}	0	{6,1.8}	{1,9,2}	0	{6,1.8}
	5*	**{1,3}**	**1**	**→{8}**	**{1,9,3}**	**1**	**→{2,8}**
Fix→Out	6	{2,4}	1	{10}	{2,10,4}	0	{10,7}
	7	{2,7,8,5}	1	{3,3,3}	{2,9,5}	0	{2,3}
	8	{2,7,8,6}	1	{3,3,2}	{2,9,7,6}	0	{3,4,5}
	9	{3,8,9,4}	0	{4,7,2}	{3,10,8,4}	1	{2,2,6}
	10	{3,8,5}	1	{5,3}	{3,5}	1	{2}
	11	{3,6}	0	{8.5}	{3,7,6}	1	{6,2}
hBoundary		{4,5,6}	1	**{2.5}**	{4,5,6}	1	**{5}**

Note that Path #1 in Figure 6-10(b) does not appear in the design because

$pTop_1$=0. By examine *pTop* in Table 6-3, it is observed that K2 now violates the

connectivity constraint in Eq.(6.25); the input is not connected to the output. Although

the input is still connected to the fixed point through Path #5, it does not transmit any

force to the output points. To fix K2, a randomly selected path from Path #1~#3 is then

switched back on by making its *pTop*=1. Figure 6-11 shows an example where $pTop_3$ is set equal to one. It is possible in other examples that the input is connected to the outputs indirectly through interconnect ports even though all *pTop*'s are zero for *pathInOut*. This type of *implicit connections* can be 'searched for' just like that in the binary ground structure parameterization. However, the purpose of load path representation is to eliminate the need of additional searching algorithm for structural connectivity identification. Therefore, the connectivity modification (flipping one *pTop* in *pathInOut* from 0 to 1) will be applied to all designs violating the constraints in Eq.(6.25) and Eq.(6.26) regardless of the existence of implicit paths. Since the load path representation is non-unique for one design, it is believed that the design with implicit paths can be expressed explicitly using different *pathSeq*.
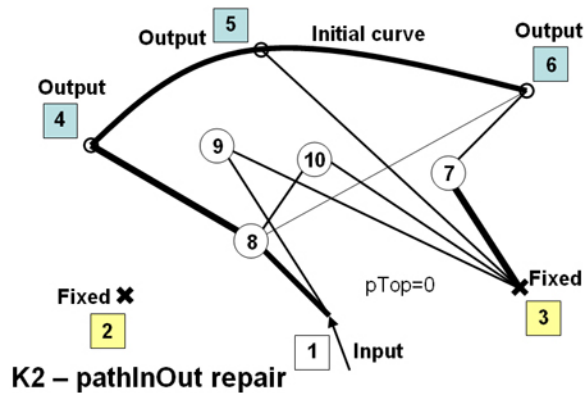
Figure 6-11: The new K2 (Figure 6-10(b)) after fixing the *pathInOut* (setting $pTop_3$=1).

Four options are offered in the mutation process: (1) mutation of *hBoundary*, (2) mutation of path destination, (3) mutation of *pTop*, and (4) mutation of *portLocations*. In *hBoundary* mutation, the boundary dimension is replaced by a randomly generated value within the upper and lower bounds. To mutate the path destination, the end vertices of some randomly selected paths can mutate to a different one within the same category. For example, a path originally connecting the input to one of the output points can be mutated

into a path connecting the input to another output point, simply by changing the last vertex in the *pathSeq*. The binary topology variable ($pTop_i$) is also allowed to mutate from 0 to 1 and vice versa for one randomly selected load path, thus changing the topology. The connection port location can also be mutated to a different location within the design domain. Figure 6-12 shows an example design mutated from K1 in Figure 6-10(a). The mutation in *hBoundary*, the destination change in Path #5, and mutation of $pTop_8$ and $pTop_{11}$ are shown in Table 6-4, while the location change of interconnect port 8 can be seen in Figure 6-12.
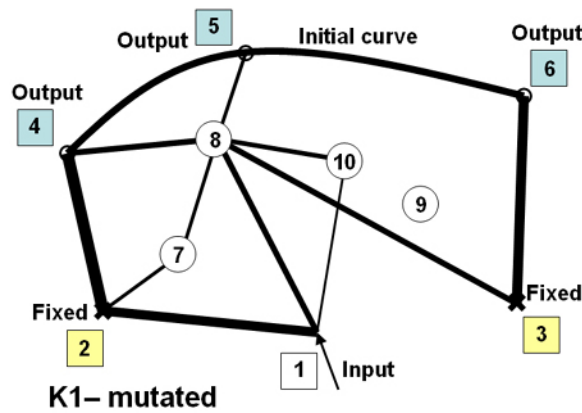
Figure 6-12: The new K1 (Figure 6-10(a)) after mutation shown in Table 6-4. Note that interconnect port 8 is also mutated to a different location.

Table 6-4: The load paths for the original K1 in Figure 6-10 and its mutated version in Figure 6-12.

Path type	Path #	Figure 6-10(a) K1 – original			Figure 6-12 K1 – mutated		
		PathSeq	pTop	pDim	PathSeq	pTop	pDim
In→Out	1	{1,10,8,4}	1	{2,4,5}	{1,10,8,4}	1	{2,4,5}
	2	{1,8,5}	1	{5,3}	{1,8,5}	1	{5,3}
	3	{1,7,8,6}	0	{5,2.5,1}	{1,7,8,6}	0	{5,2.5,1}
In→Fix	4	{1,7,2}	0	{6,1.8}	{1,7,2}	0	{6,1.8}
	5	{1,3}	1	{8}	{1,**2**}	1	{8}
Fix→Out	6	{2,4}	1	{10}	{2,4}	1	{10}
	7	{2,7,8,5}	1	{3,3,3}	{2,7,8,5}	1	{3,3,3}
	8	{2,7,8,6}	1	{3,3,2}	{2,7,8,6}	**0**	{3,3,2}
	9	{3,8,9,4}	0	{4,7,2}	{3,8,9,4}	0	{4,7,2}
	10	{3,8,5}	1	{5,3}	{3,8,5}	1	{5,3}
	11	{3,6}	0	{8.5}	{3,6}	**1**	{8.5}
hBoundary		{4,5,6}	1	{2.5}	{4,5,6}	1	**{6}**

It is noted that when the two parent designs are identical, the 'exchanging paths' (crossover) strategy fails to produce any new design. In fact, the offspring designs will be identical to the parent designs. The mutation probability is, therefore, higher in this approach to enhance diversity in each generation. Higher mutation also helps improve the crossover performance, because the more diverse a generation is, the less likely it is to select two identical parent designs.

Local Search

Due to the heuristic nature of GA, the algorithm is capable of searching the whole solution space extensively without being trapped in a local region. Although GA is more efficient in locating a region *close to* a local optimum, finding the *exact location* may be quite difficult. If GA can indeed explore the entire solution space thoroughly, performing a local search following GA can accelerate the convergence to the nearest local optimum, which is very likely to be the global optimum. However, there is no guarantee that GA can explore or *sample* the solution space evenly, so adding a local search after GA can only lead to a local optimum. In order to enhance the chance of finding the global optimum, a global search, DIRECT optimization algorithm (Jones, Perttunen, and Stuckman, 1993), is adopted to help investigate the global optimality. DIRECT optimization algorithm is a sampling algorithm that requires no knowledge of the objective function gradient. The algorithm samples points in the solution space and uses the information it has obtained to decide where to search next. It operates at both the global and local level. Once the global part of the algorithm finds the basin of

convergence of the optimum, the local part of the algorithm quickly and automatically

exploits it (Jones, Perttunen, and Stuckman, 1993).

In this work, the optimal connectivity obtained from GA is used as the input to the

DIRECT algorithm to perform additional iterations on the connection port locations and

beam section dimensions. As shown later in the results, the DIRECT algorithm can

effectively improve the design performance with the same structural connectivity.

However, the sampling nature of DIRECT algorithm implies that the obtained solution

depends greatly on the number of iterations (sampling points). Therefore, a local search

algorithm is utilized to accelerate the convergence to the nearby local optimum, after a

prescribed number of iterations are carried out using the DIRECT algorithm. In this

research, the local search is implemented using the optimization toolbox in Matlab. The

overall optimization procedure using GA, global search, and local search, is shown in

Figure 6-13.
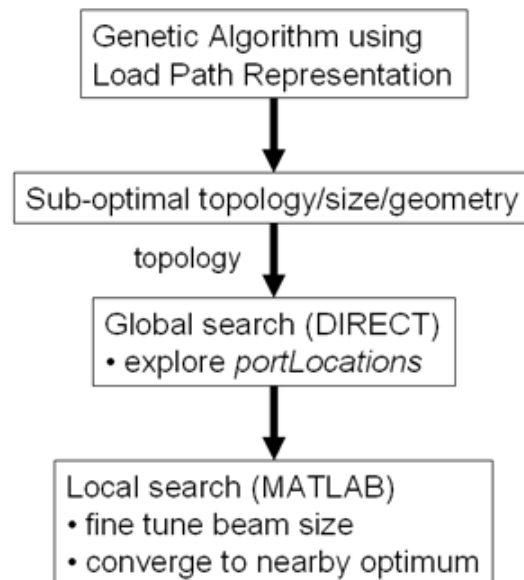
Figure 6-13: The load path representation incorporated in GA followed by a global search and a local search to improve the convergence to a local optimum.

Using GA alone can simultaneously search for the structural topology and dimensions. However, the subsequent global and local searches can greatly increase the efficiency of the overall optimization process. The main contribution of GA in this setting (Figure 6-13) is to identify structural connectivity (topology) that can potentially lead to the optimal shape morphing compliant mechanism. Although size and geometry design variables are included in both global and local search (DIRECT and Matlab), the effect of geometry change is more significant in the global search while the element size is optimized mainly in the local search stage. Therefore, the arrangement in Figure 6-13 can be interpreted as follow: GA is used to identify the optimal structural connectivity; the DIRECT algorithm helps identify the best *portLocations*; and the local search in Matlab makes final adjustment in element dimensions and geometries and accelerates the convergence to the nearest local optimum.

CHAPTER 7

DESIGN EXAMPLES

7.1 Design Approach Implementation

The synthesis approach for shape morphing compliant mechanism introduced in the proceeding chapters can be illustrated in the flowchart in Figure 7-1, starting with the design domain initialization, the design domain parameterization, and, finally, the structural optimization using GA. Two different parameterization methods can be incorporated in this synthesis approach, one using the binary ground structure parameterization, and the other using the load path representation. They are termed as "binary ground structure approach" and "load path approach" respectively in the following. In this research, all the algorithms are programmed in Matlab, including linear finite element analysis and genetic algorithms, except the local search algorithms (Jones, Perttunen, and Stuckman, 1993) described at the end of section 6.2.2. This chapter presents several design examples, including morphing aircraft wings, flexible antenna reflectors, and a compliant lumbar support. Results from both binary ground structure and load path approaches will be presented in each example, followed by a brief discussion. Single input single output problems are also investigated at the end of this chapter, using only the load path approach, to demonstrate the capability of the synthesis approach in addressing other types of problems. The CPU time shown in the results is based on the implementation on a 2.26GHz Pentium IV CPU desk top personal computer.
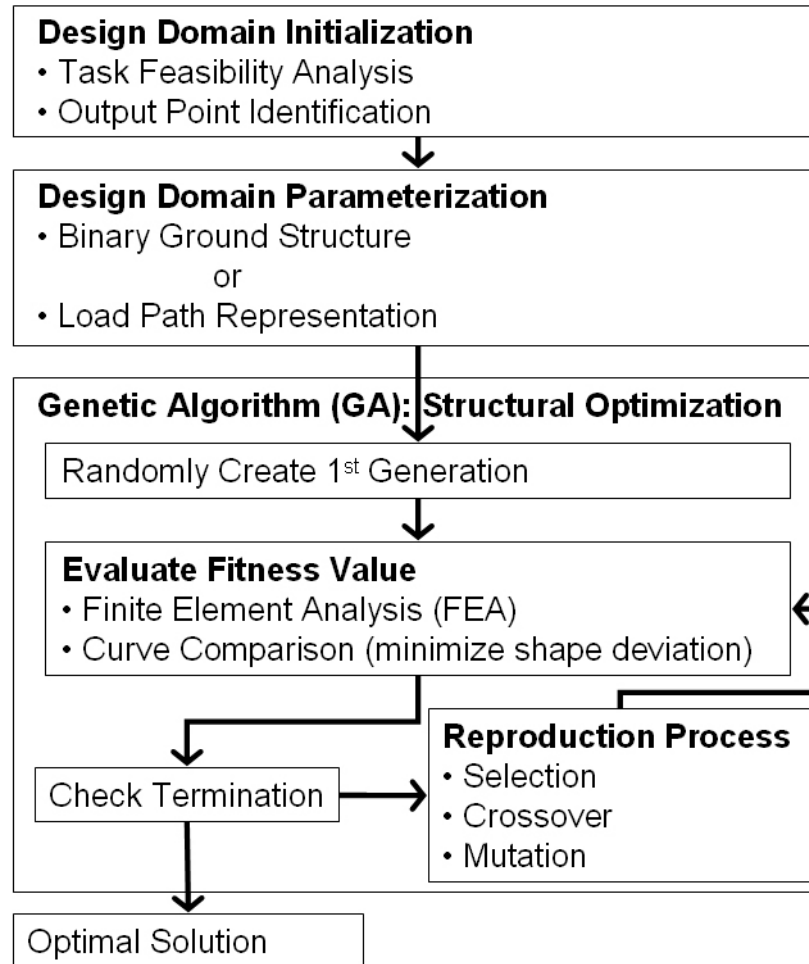
Figure 7-1: Flowchart of the systematic synthesis approach for shape morphing compliant mechanisms, using either binary ground structure parameterization or load path representation.

7.2 Morphing Aircraft

A morphing aircraft structure such as a wing is an excellent example to demonstrate the advantage of shape morphing. Changing wing shape in response to the flying condition can potentially produce maximum lift and reduce drag, thus increasing the fuel economy. Active wing morphing also allows a single aircraft to perform multiple tasks that requires different wing shapes, leading to potential improvements in

maneuverability and performance. Four design examples, involving a morphing leading edge and a morphing trailing edge, under low and high external loads, are introduced in the following to demonstrate the capability of the synthesis approach developed in the proceeding chapters. However, the shapes and the loads are not realistic by any means. They only serve to illustrate a potential real application of the methods developed in this dissertation and also as a source of inspiration.

7.2.1 Morphing Leading Edge (Low External Loads)

A hypothetical airfoil shape morphing with low external load is presented in this section to demonstrate the compliant mechanisms' capability to morph shape. Figure 7-2 shows the required shape morphing of a hypothetical airfoil leading edge. The solid and dash lines represent the initial and target curves respectively, with their sampling point information listed in Table 7-1. The overall dimension is approximately 220mm (8.66inch) by 270mm (10.63inch). The design specifications are listed in Table 7-2. Following the procedure introduced in Chapter 4, the curvature functions ($\kappa_{INI}(l)$ and $\kappa_{TAR}(l)$) and curvature difference function ($d\kappa(l)$) shown in Figure 7-3 are calculated in the design domain initialization. The axial stress and maximum bending stress are 184.6MPa and 134.26MPa respectively, both below the maximum allowable stress. The algorithm then proceeds to identify the locations of potential output points. The binary ground structure and load path approaches are both employed to find the compliant mechanism design that can achieve this shape change. Since there is no symmetry in the problem, LSE deviation is used in both approaches. The GA parameters are also identical in both approaches to facilitate comparison.
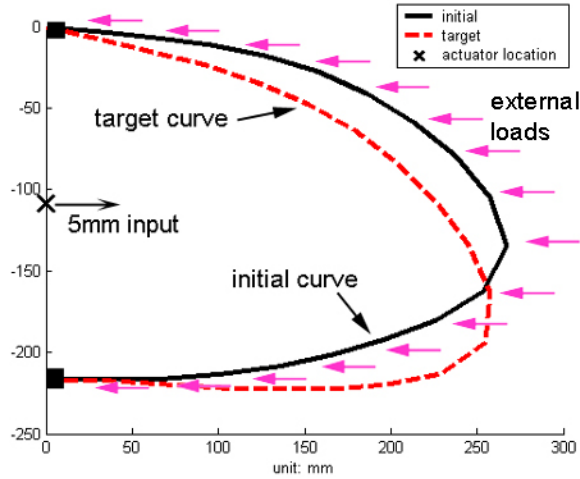
Figure 7-2: Airfoil leading edge shape morphing example.

Table 7-1: Data points along initial and target curves for the morphing leading edge example.

Data point #	Initial Curve Data Points		Target Curve Data Points	
	X (mm)	Y (mm)	X (mm)	Y (mm)
1	0.00	0.00	0.00	0.00
2	31.89	-3.31	31.07	-7.70
3	63.78	-6.69	62.16	-15.35
4	95.53	-11.13	93.00	-23.93
5	126.90	-17.71	123.24	-34.41
6	157.44	-27.43	152.37	-47.66
7	186.46	-40.99	179.70	-64.28
8	213.29	-58.50	204.56	-84.41
9	237.37	-79.62	226.49	-107.70
10	257.30	-104.66	244.87	-133.88
11	267.11	-134.76	257.23	-163.28
12	253.15	-162.54	254.52	-194.43
13	226.35	-179.94	229.30	-212.99
14	196.69	-192.08	198.12	-220.01
15	165.99	-201.30	166.22	-222.58
16	134.73	-208.44	134.21	-222.87
17	103.05	-213.33	102.22	-221.76
18	71.09	-215.78	70.27	-219.72
19	39.04	-216.46	38.36	-217.18
20	6.97	-216.53	6.97	-216.53

Table 7-2: Design Specification and parameters used in GA.

Objective function	minimize LSE deviation
Material	Aluminum E: 69000MPa (10007.6kpsi) σ_{yield}: 227.53MPa (33kpsi)
Beam dimensions	Out-of-plane: 20mm (0.79inch)

	In-plane: 1 ~ 4mm (0.0394 ~ 0.1575inch)	
Boundary conditions	Input displacement: 5mm → (0.1969inch)	
	Input location: (0,-108.263)	
	Fixed point location: (0,0) and (6.973,- 216.53)	
	External loads: multiple point loads of 2N ← (0.45lbf)	
Constraints	$\sigma_{allowable}$: 227.53MPa (33kpsi) (σ_{yield})	
	$d_{allowable}$: 3mm (0.1181inch)	
GA parameters	Population #: 150	Crossover probability: 0.8
	Max. # of generation: 50	Mutation probability: 0.5
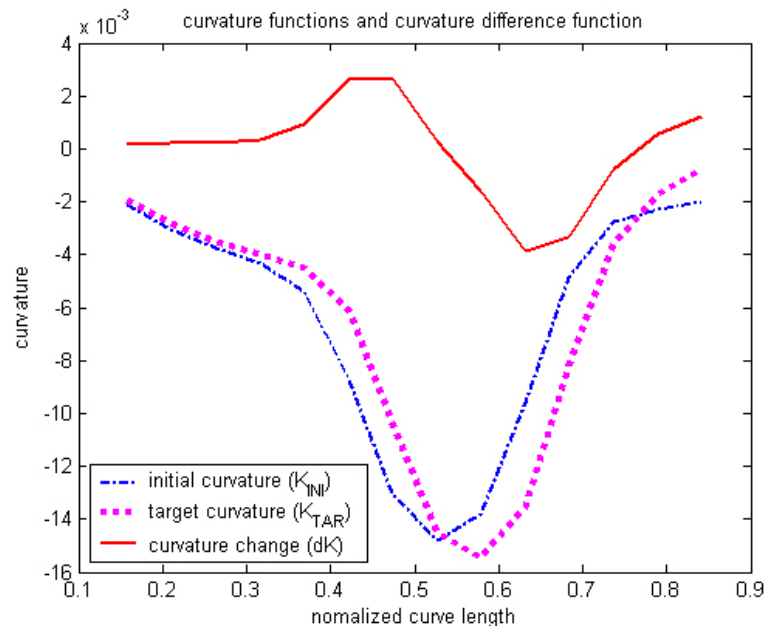
Figure 7-3: The curvature functions of the initial and target curves, and the curvature difference function between them (solid line) for the morphing leading edge example.

Binary Ground Structure Approach

As seen in Figure 7-4, an initial mesh is created by connecting the input to the output points. The output points used in this example are data point number 1, 4, 8, 11, 12, 14, 16, and 20 in Table 7-1. Additional cross elements are included to increase the variety of available topologies. Various mesh configurations can be used; the mesh used here gives an example of a typical configuration. The optimal compliant mechanism (unactuated) obtained from GA is shown in Figure 7-5 with the deviation results shown in Table 7-3. The design in Figure 7-5 has several 'trivial' elements that have one 'free

end.' These elements have no strain/stress in them, thus can be removed in a post-

processing step without affecting the compliant mechanism performance.
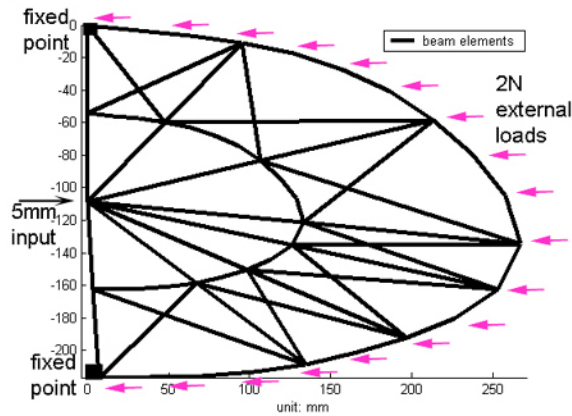
Figure 7-4: The initial mesh used in the binary ground structure approach.
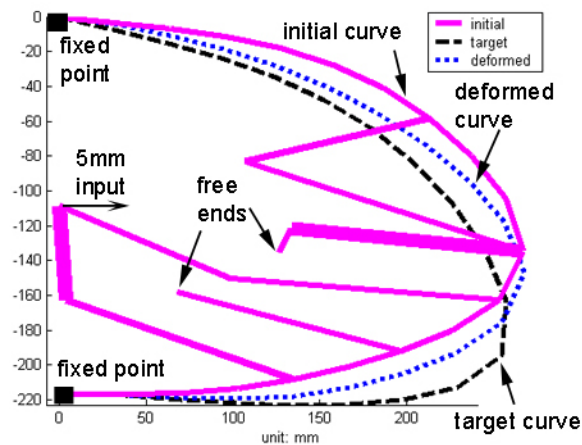
Figure 7-5: The morphing leading edge design obtained from binary ground structure approach.

Table 7-3: Design summary for the morphing leading edge in Figure 7-5.

LSE deviation: 178.4mm (7.02inch)	Maximum stress: -215.80MPa (31.3kpsi)
CPU time: 538sec (8.97min)	Required input force: 23.56N (5.3lbf)

Load Path Approach

Figure 7-6 shows the result obtained from the GA using load path representation

with one output point at data point #13 in Table 7-1. Five intermediate connection ports

are allowed to move within the region bounded by the initial curve and the x-axis. The

design has a LSE deviation of 74.38mm (2.93inch), which 58% smaller than that in

Figure 7-5. The maximum stress and required actuator force are shown in Table 7-4. Note

that the design is well-connected (free of trivial elements) because the topology is now

represented in terms of the load paths, thus eliminating the need of a post-processor.
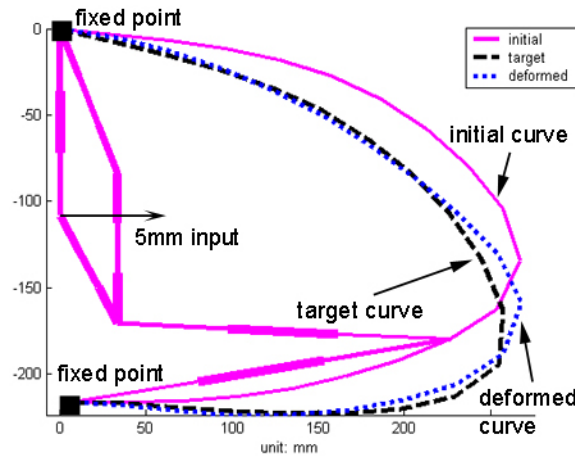
Figure 7-6: The optimal compliant mechanism obtained from ten trial runs of the load path approach for airfoil leading edge shape morphing.

Table 7-4: Design summary for the morphing leading edge in Figure 7-6.

LSE deviation: 74.38mm (2.93inch)	Maximum stress: 227.08MPa (32.93kpsi)
CPU time: 283sec (4.72min)	Required input force: 176.5N (39.68lbf)

Discussion

Since GA is a non-deterministic process, different results can be obtained from

multiple search processes on the same problem. The designs shown in Figure 7-5 and

Figure 7-6 are the best solutions after performing ten trial runs using the binary ground

structure and load path approach respectively. The average LSE deviation and

computation time of the ten trials are shown in Table 7-5. As can be seen, the

performance of the load path approach is better than the binary ground structure

approach; the LSE deviation is almost 30% smaller on average and is 58% smaller when

compared to binary ground structure results (Figure 7-5 and Figure 7-6). This difference

in performance may be due to the available mesh configuration in each approach. Since

117

the mesh is fixed in the binary ground structure, the final design is always a subset of all possible topologies embedded in the initial discretization mesh. However, the *true* optimal solution might not be included in the initial mesh. The selection of the initial mesh is, therefore, critical to the quality of the final solution. The load path approach, on the other hand, allows variable mesh configuration because the locations of the connection ports are part of the design variables. It is thus capable of finding the design in Figure 7-6, which is not included in the initial mesh shown in Figure 7-4.

Table 7-5 also suggests that the load path approach is more computationally efficient. It requires only 50% the computation time of the ground structure approach due to fewer numbers of variables and easier identification of structural connectivity.

Table 7-5: The LSE deviation value and computation time from ten searches using both approaches.

Aircraft Leading Edge Example	Binary Ground Structure	Load Path Representation
LSE dev. of best design	178.39mm	74.38mm
Average LSE dev.	189.08mm	134.77mm
Average CPU time	533sec (8.88min)	274sec (4.57min)

Due to the low external load, this example focuses on the kinematics requirement (morph shape) of the compliant mechanism without emphasizing on providing very high stiffness. The shape morphing in Figure 7-5 and Figure 7-6 is achieved mainly due to the input actuation, while the effect due to external load is relatively small. In a more realistic scenario, however, the external loads are orders of magnitude higher than 2N (0.45lbf multiple point loads), thus requiring designs with higher stiffness. A different leading edge morphing example is, therefore, investigated next to explore higher stiffness designs.

7.2.2 Morphing Leading Edge (Higher External Loads)

A hypothetical leading edge shape morphing is investigated in this section with higher external loads. This example is not intended to capture the 'realistic' aircraft loading condition, but, by applying higher external loads, the example focuses on compliant mechanisms' capability to fulfill both structural (stiffness) and kinematics (shape change) requirements.

Figure 7-7 shows the same shape morphing seen in the previous example (Figure 7-2), but the magnitude is increased to 15N (3.37lbf per arrow) from three different directions. The sampling point information and design specifications are identical to those in Table 7-1 and Table 7-2, except the out-of-plane dimension is increased to 50mm (1.97inch), the input pulls to the left, and the bottom fixed point is now allowed to slide.
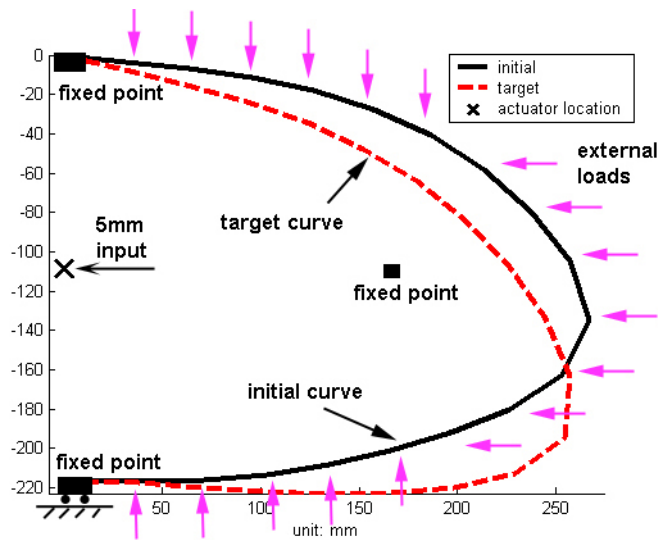
Figure 7-7: Airfoil leading edge shape morphing example with higher external loads.

Binary Ground Structure Approach

The initial mesh is shown in Figure 7-8 with output points at #1, 6, 10, 11, 13, 16, and 20 in Table 7-1. The initial mesh contains more elements than that in Figure 7-4 to

119

begin with a stiffer ground structure. An additional fixed point is included within the

design domain at (171.53,105.86). The design obtained from binary ground structure

approach is shown in Figure 7-9 and Table 7-6.
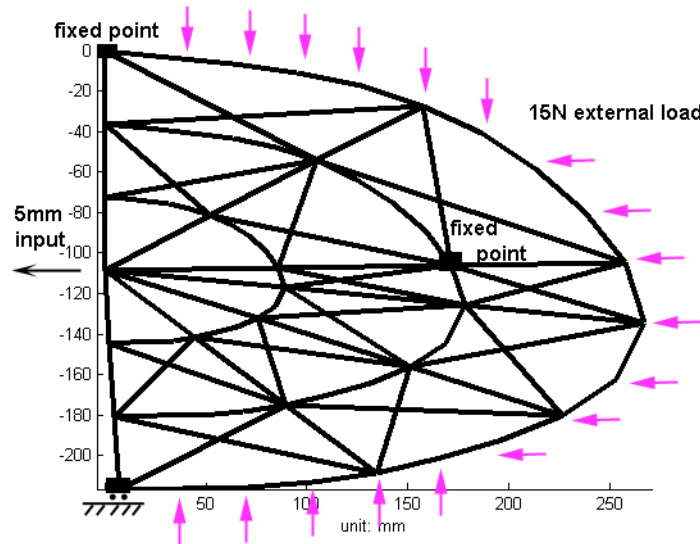
Figure 7-8: The initial ground structure chosen for the higher load leading example.
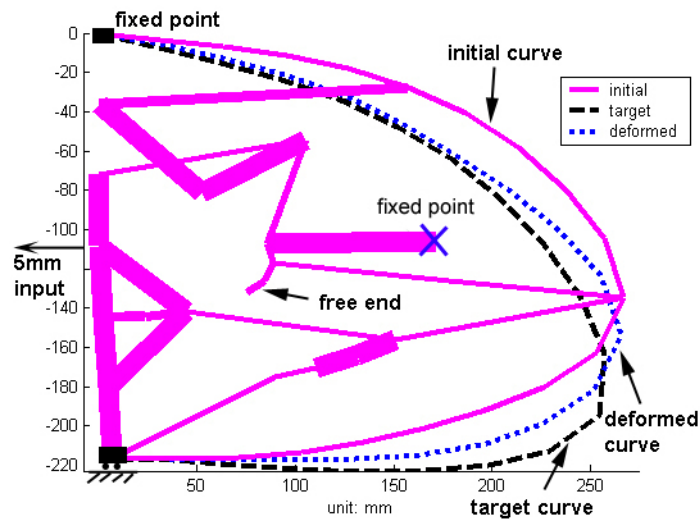
Figure 7-9: The morphing leading edge design obtained from binary ground structure approach with higher external loads.

Table 7-6: Design summary for the morphing trailing edge in Figure 7-9.

LSE deviation: 134mm (5.31inch)	Maximum stress: 227.53MPa (33kpsi)
CPU time: 388.64sec (6.48min)	Required input force: -393.23N (-88.40lbf)

Load Path Approach

Figure 7-10 shows the result obtained from the load path approach with output points at #6, 10, 11, 13, and 16 in Table 7-1. Ten intermediate connection ports are used in this example to allow more complex meshes. Two interior fixed points are included in this design at (80,-100) and (80,-150), but only one fixed point (80,-100) is active in the result (all paths from the other fixed point is eliminated). The deviation values and stress information are shown in Table 7-7.
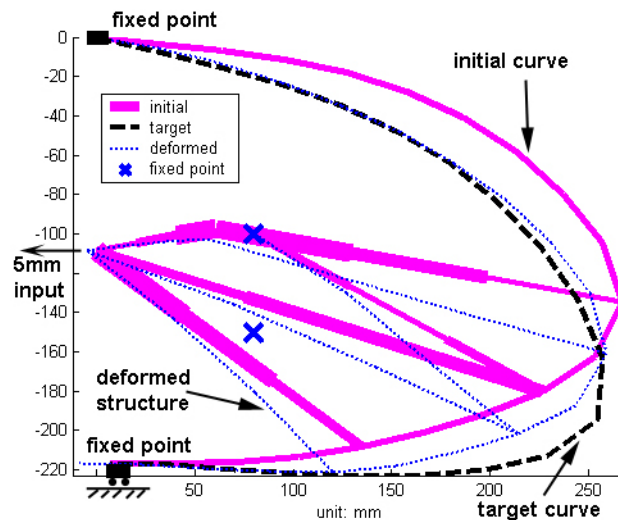
Figure 7-10: The morphing leading edge design obtained from the load path approach with higher external loads.

Table 7-7: Design summary for the morphing trailing edge in Figure 7-10.

LSE deviation: 168.49mm (6.63inch)	Maximum stress: 227.53MPa (33kpsi)
CPU time: 190.7sec (3.18min)	Required input force: -604.2N (-135.8lbf)

Discussion

Although the loading condition prescribed in this example may still be far from the realistic scenario, the designs in Figure 7-9 and Figure 7-10 have demonstrated that the proposed algorithm is capable of creating compliant mechanisms that can achieve the required shape change and withstand higher external loads at the same time. Higher loading conditions have also been investigated to study the performance of these designs.

Using additional size optimization local search algorithm (fmincon in Matlab), we found that the designs in Figure 7-9 and Figure 7-10 can withstand loads more than 3 times the current value (>45N or 10.12lbf multiple loads) with the same topology. Another way to explore higher stiffness design is to prescribe larger external loads in the design specification. However, it turns out that it may be more difficult for the GA to find a working design (especially the topology) with acceptable shape deviation and stress level. It is, therefore, recommended to first apply moderate external loads in the GA synthesis approach to find a working design (topology and rough dimensions). Then, employ a local search algorithm to further optimize the dimensions to sustain larger external loads.

Since the structural deformation is as a result of both the input actuation and external load, the deformed curve profile and stress distribution may change as the external load varies. Additional analyses are, therefore, performed on the two designs in Figure 7-9 and Figure 7-10 to study the effect of external load variation. The external loads are reduced to 10N (2.25lbf) while everything else remains unchanged (including the element dimensions). The results showed that the LSE deviation of the load path design remains almost the same (169mm) without any stress violation (Maximum stress: 224.33MPa). However, the stress in the ground structure design exceeds the allowable value (Maximum stress: 269.36MPa > 227.53MPa), despite the reduction in LSE deviation (124.45mm). This suggests that further consideration needs to be incorporated in the synthesis approach to ensure the robustness of the solution. The design should be insensitive to the variation in external loads within reasonable and prescribed bounds, and the design should at least function for external loads within the designed value (in this

example, loads up to 15N). One potential solution to address this issue is to include appropriate safety factors in the design process. Currently, the safety factor is 1.

By visual comparison between Figure 7-9 and Figure 7-10, the load path design appears to have a better match of the target curve. However, the LSE deviation values in Table 7-6 and Table 7-7 contradict this observation; the ground structure design has a smaller LSE deviation. This inconsistency results from the definition of the LSE deviation. As shown in Figure 7-11, the LSE deviation is the sum of the linear distances of the sampling points along the morphing boundary from their deformed locations ('o') to the corresponding target locations ('x'). As can be seen, the LSE in the ground structure design results mainly from deviation in region A1, while the deviation in the load path design comes from region B1 as well as region B2. Although the deformed points ('o') in region B2 lie closely along the target curve, the point-to-point differences still contribute to the increase in LSE deviation. This suggests future improvements should be made on the curve comparison objective function, such as adding weighting coefficients for points along more critical portions (such as the leading edge regions).
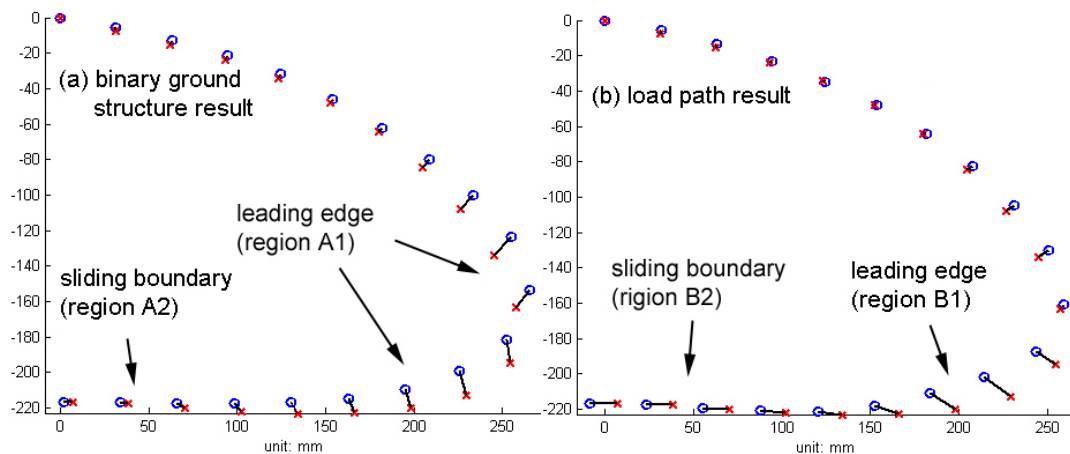
Figure 7-11: The sampling points along the morphing boundary: 'o' represents the deformed locations, and 'x' represents the target locations.

7.2.3 Morphing Trailing Edge (No External Load)

As shown in Figure 7-12, a morphing trailing edge is expected to deflect approximately 10 degrees downwards to potentially enhance the handling and maneuvering capabilities. This specification is interpreted as the target curve in dash line, while the data points are included in Table 7-8. The horizontal dimension for this model is 889mm (35inch) and the vertical dimension is 381mm (15inch). The specifications are shown in Table 7-9. No external loads are applied in this example to first explore the topology required to achieve this shape change (kinematics requirement). The output points are identified using the process described in section 4.2 and are shown as circles in Figure 7-12.
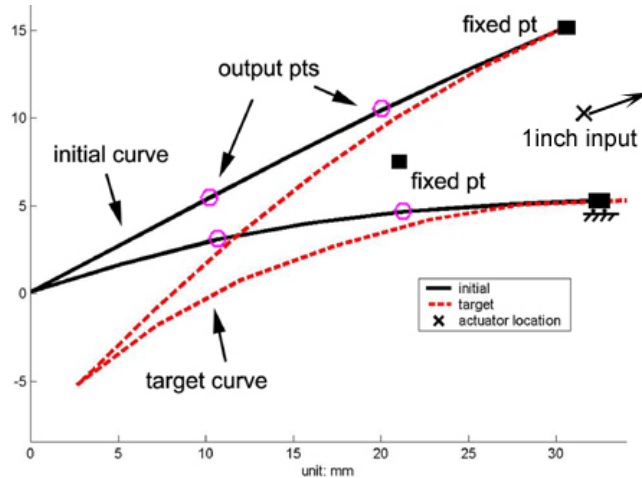
Figure 7-12: Aircraft wing trailing edge shape morphing example.

Table 7-8: Data points along initial and target curves for the morphing trailing edge example.

Data point #	Initial Curve Data Points		Target Curve Data Points	
	X (mm)	Y (mm)	X (mm)	Y (mm)
1	30.52371	15.18214	30.52371	15.18214
2	25.35923	12.94128	25.64791	12.84109
3	20.22761	10.53739	20.86688	10.03123
4	15.12053	8.012576	16.17307	6.789892
5	10.03444	5.383447	11.56465	3.126199
6	4.961688	2.688353	7.036164	-0.9329
7	-0.01605	0.079394	2.6593	-5.21313
8	5.168158	1.667014	7.212793	-1.80662

Data point #	Initial Curve Data Points		Target Curve Data Points	
	X (mm)	Y (mm)	X (mm)	Y (mm)
9	10.50948	3.033582	12.03971	0.776236
10	15.929	4.013375	17.31153	2.683452
11	21.41552	4.661164	22.62322	4.165335
12	26.95363	5.054324	28.05379	5.059115
13	32.52106	5.301909	34.03508	5.301909

Table 7-9: Design specifications and parameters used in GA.

Objective function	minimize LSE deviation	
Material	Aluminum E: 71705.5MPa (10400kpsi) σ_{yield}: 227.53MPa (33kpsi)	
Beam dimensions	Out-of-plane: 25.4mm (1inch) In-plane: 1.32 ~ 2.98mm (0.052 ~ 0.1174inch)	
Boundary conditions	Input displacement: 25.4mm (1inch) ∠11.4287° Input location: (31.5937,10.2586) Fixed point location: (21,7) External loads: none	
Constraints	$\sigma_{allowable}$: 227.53MPa (33kpsi) (σ_{yield}) $d_{allowable}$: 25.4mm (1inch)	
GA parameters	Population #: 120 Max. # of generation: 30	Crossover probability: 0.7 Mutation probability: 0.8

Binary Ground Structure Approach

Figure 7-13 shows the binary ground structure parameterization used in this example. The optimal compliant mechanism obtained from GA is shown in Figure 7-14 with the results summarized in Table 7-10. Trivial elements with free ends can be removed with additional post-processing.
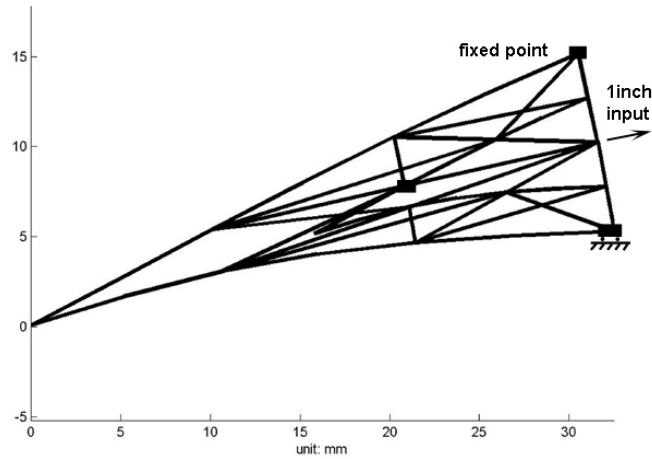
Figure 7-13: The initial binary ground structure.
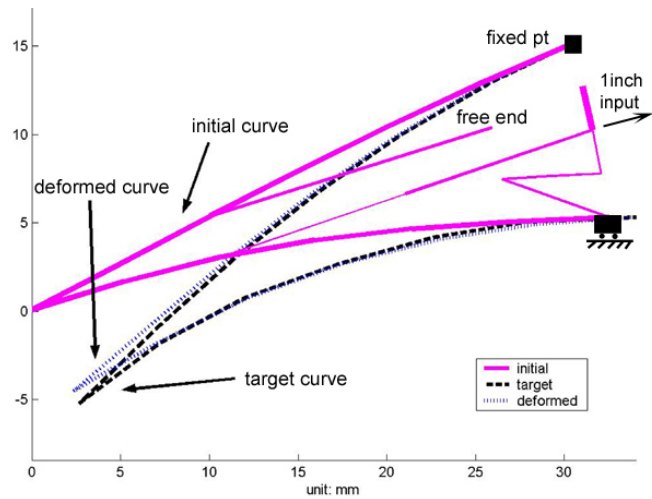
Figure 7-14: The morphing trailing edge design obtained from the binary ground structure approach.

Table 7-10: Design summary for the morphing trailing edge design in Figure 7-14.

LSE deviation: 92.456mm (3.64inch)	Maximum stress: 65.07MPa (9.44kpsi)
CPU time: 246sec (~4min)	Required input force: 10.79N (2.42lbf)

Load Path Approach

Figure 7-15 shows the design obtained from the GA using load path representation. Ten intermediate connection ports are allowed to move within the area bounded by the initial curve. The resulting structure has a simple topology and is well-connected. The results are summarized in Table 7-11.
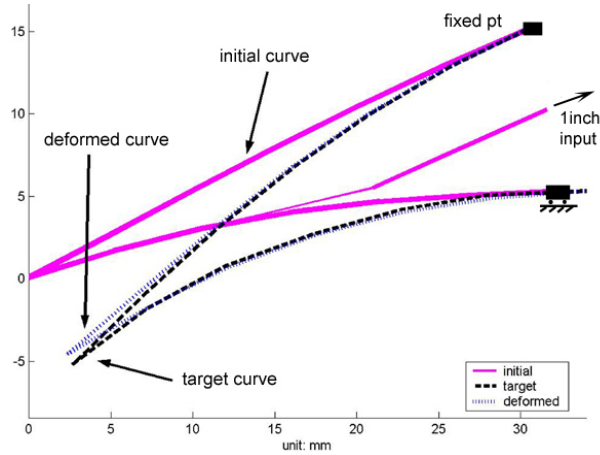
Figure 7-15: The morphing trailing edge design obtained from the load path approach.

Table 7-11: Design summary for the morphing trailing edge design in Figure 7-15.

LSE deviation: 91.42mm (3.6inch)	Maximum stress: -45.21MPa (-6.56kpsi)
CPU time: 38.85sec (<1min)	Required input force: 11.94N (2.68lbf)

Discussion

Although the designs obtained from both approaches have different topologies, the underlying 'mechanism' is very similar. Both designs include a direct connection from the actuator to the same output point on the bottom surface. The design in Figure 7-14 (binary ground structure approach) has one additional connection from input to the slider, but this connection merely pulls the slider to the right; it has no significant effect on the deformed shape except for the force required at the input. As seen in Table 7-10 and Table 7-11, the LSE deviations are very similar for the two designs. In fact, this type of shape morphing is similar to bending of a cantilever beam. As will be shown later in the antenna reflector example, this type of shape morphing does not require complicated intermediate connections to change the 'load direction' (a direct connection from input to output is sufficient). Since the initial ground structure generally starts with connecting the input to all the output points before adding cross members, the direct connection between input and output is always embedded in the initial mesh. Therefore, both approaches are

127

equally effective in finding the required structural topology and dimensions (although binary ground structure approach requires slightly longer computation time).

Another interesting observation is related to the elimination of the fixed point at the center of the design domain shown in Figure 7-12. In Figure 7-14, all the elements connecting to the center fixed point (see Figure 7-13) are eliminated in the GA. Similarly, the binary topology variables are zero for all paths connected to the center fixed point in Figure 7-15. This suggests both approaches are capable of eliminating unnecessary fixed points during the optimization process.

7.2.4 Morphing Trailing Edge (Higher External Loads)

To explore higher stiffness designs for the morphing trailing edge, the same problem is investigated again in this section with higher external loads, as shown in Figure 7-16. The curve information and design specifications are identical to those shown in Table 7-8 and Table 7-9, except the multiple point external load is increased to 15N (3.37lbf per arrow), and the in-plane beam dimension s are allowed to vary between 1 ~ 8.46mm (0.04 ~ 0.33inch).
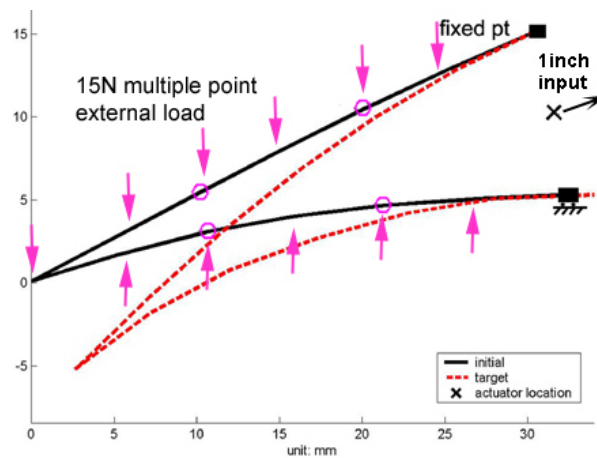
Figure 7-16: Aircraft wing trailing edge shape morphing example with higher external loads.

Binary Ground Structure Approach

As shown in Figure 7-17, more elements are employed in this initial mesh to explore higher stiffness designs. The design obtained from binary ground structure approach is shown in Figure 7-18 and Table 7-12. Similar to the design in Figure 7-14, the direction connection from the input actuator to the bottom surface can be seen again in this design. However, additional elements closer to the trailing edge (left tip) are now included to provide stiffness. Trivial elements (free ends) can also be seen in Figure 7-18, but these elements can be removed from the design without affecting the performance.
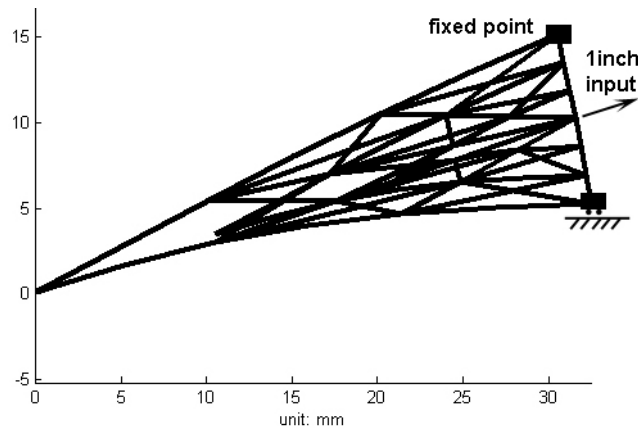
Figure 7-17: The initial binary ground structure with more elements to provide higher stiffness (compared to that in Figure 7-13).
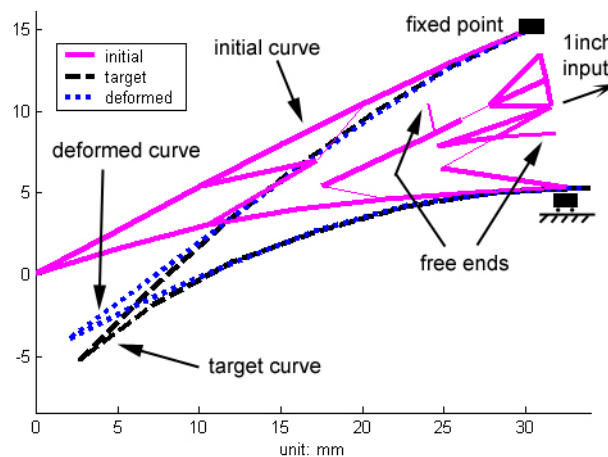
Figure 7-18: The morphing trailing edge design obtained from the ground structure approach with higher external loads.

Table 7-12: Design summary for the morphing trailing edge in Figure 7-18.

LSE deviation: 117.68mm (4.63inch)	Maximum stress: 227.53MPa (33kpsi)
CPU time: 346sec (5.77min)	Required input force: -115.17N (-25.85lbf)

Load Path Approach

Figure 7-19 shows the result obtained from the load path approach. Four

intermediate connection ports are used in this example. The deviation and stress

information are summarized in Table 7-13. Again, the direct connection from the input to

the bottom surface is present in this design. Furthermore, the elements connecting the top

and bottom surfaces provide stiffness against external loads.
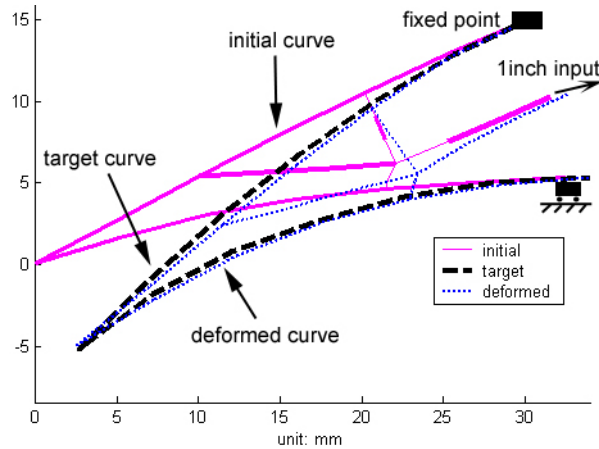
Figure 7-19: The morphing trailing edge design obtained from the load path approach with higher external loads.

Table 7-13: Design summary for the morphing trailing edge in Figure 7-19.

LSE deviation: 115.7mm (4.56inch)	Maximum stress: 181.39MPa (26.32kpsi)
CPU time: 235.97sec (3.93min)	Required input force: -80.95N (-18.17lbf)

Discussion

Both designs in Figure 7-18 and Figure 7-19 have two similar features: the direct

connection from input to the bottom surface, and elements connecting top and bottom

surfaces for stiffness. These results demonstrate the capability of the synthesis approach

to create compliant mechanisms that are compliant to morph shape yet stiff enough to

work against external loads. Using additional local search algorithm, both designs can be further optimized (dimensional optimization) to withstand externals up to entire whole range below the prescribed external load value is still not guaranteed.

7.3 Flexible Antenna Reflector

Antennas and reflective mirrors are another type of applications where shape morphing can enhance the system performance. The shape of the antenna or mirror directly affects the radiation pattern or optical property of the system. Typical contoured reflector antenna is low cost and versatile, but it usually has a fixed shape and can only generate one specific radiation pattern. One approach to generate variable signal pattern include the use of an array antenna, which is an aggregation of radiating elements in an electrical and geometrical arrangement. The arrangement results in the desired radiation characteristics that may not be achievable by a single element. It generates appropriate signal pattern by selective excitation of current distribution of each element. Although the array antenna can change its signal pattern by controlling the excitation current, it generally has higher cost, heavier weight, and lower efficiency (due to heat dissipation).

Recent studies (Washington, 1996; Martin et al., 2000; Yoon, Washington, and Theunissen, 2000; Washington et al., 2002) have shown that antenna reflector adaptation can potentially enhance system performance and increase flexibility, such as changing the signal pattern or coverage area. As opposed to controlling the electronic signals in the array antenna, the reflector adaptation can be achieved mechanically by changing the physical shape of the antenna. Conventional mechanisms and smart materials have both been used in pervious research (see section 1.2). However, the mechanical joints in

conventional mechanisms create discontinuity on the surface and introduce errors due to backlash. The smart material actuators, on the other hand, have more control degrees of freedom, but they generally have limited output displacement that might not be scalable for larger reflectors. The example here will focus on the use of compliant mechanisms for shape morphing antenna reflectors.

The compliant mechanisms provide a smooth reflector surface, as opposed to the discontinuous surface comprised of rigid panels that connected through hinges. The compliant mechanism approach also requires simpler control (fewer actuators) and provides better scalability, compared to the small displacement seen in smart materials (especially piezoelectric materials). The external load is relatively low in this type of application, thus the stiffness consideration is less critical. Two examples are presented in the following to design antenna reflectors that morph to change radiation pattern and signal direction.

7.3.1 Beam Shaping Mode

Figure 7-20 is a cylindrical antenna reflector in its beam shaping mode that changes the focus of the reflector to vary the radiation pattern. The goal is to change the parabolic reflector (initial curve) into a circular one (target curve). Due to symmetry about the y-axis, only the left half of the reflector is modeled. Information of the initial and target curves are shown in Table 7-14, and the design specifications can be seen in Table 7-15. The output points are shown as circles in Figure 7-20 (#1 and #7 in Table 7-14). The binary ground structure and load path approaches are employed in the following to search for the design that can morph the parabolic curve into the circular

target curve. Note that LSE deviation objective function is used in this example, because both the initial and target curves are asymmetric in the half-model.
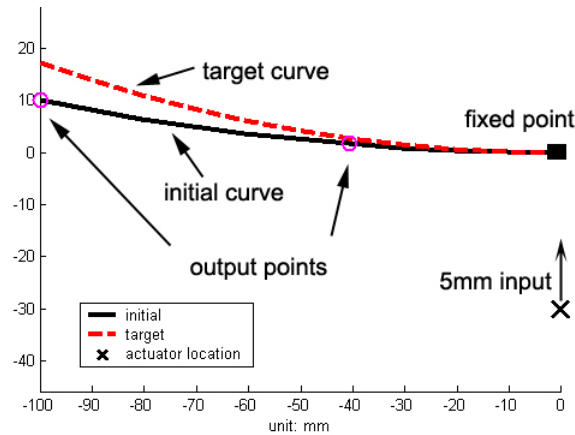
Figure 7-20: An antenna reflector that changes from a parabolic shape into a circular shape.

Table 7-14: Data points along initial and target curves for the beam shaping antenna reflector.

Data point #	Initial Curve Data Points		Target Curve Data Points	
	X (mm)	Y (mm)	X (mm)	Y (mm)
1	-100.0000	10.0000	-100.0000	17.1573
2	-90.3321	8.1599	-90.3321	13.9229
3	-80.5598	6.4899	-80.5598	11.0188
4	-70.6946	4.9977	-70.6946	8.4485
5	-60.7477	3.6903	-60.7477	6.2148
6	-50.7306	2.5736	-50.7306	4.3204
7	-40.6550	1.6528	-40.6550	2.7675
8	-30.5324	0.9322	-30.5324	1.5578
9	-20.3745	0.4151	-20.3745	0.6927
10	-10.1931	0.1039	-10.1931	0.1732
11	0.0000	0.0000	0.0000	0.0000

Table 7-15: Design specifications and GA parameters in the antenna beam shaping example.

Objective function	minimize LSE deviation
Material	ABS plastic (Acrylonitrile-butadiene-styrene) E: 2480MPa (359.7kpsi) σ_{yield}: 34.45MPa (5kpsi)
Beam dimensions	Out-of-plane: 4mm (0.1575inch) In-plane: 1.5 ~ 4mm (0.059 ~ 0.1575inch)
Boundary conditions	Input displacement: 5mm ↑ (0.1969inch) Input location: (0,-30) Fixed point location: (0,0) External loads: multiple point loads of 1N ↓ (0.225lbf)
Constraints	$\sigma_{allowable}$: 34.45MPa (5kpsi) (σ_{yield})

	$d_{allowable}$: 1mm (0.0394inch)	
GA parameters	Population #: 200	Crossover probability: 0.8
	Max. # of generation: 50	Mutation probability: 0.4

From the task feasibility analysis (section 4.1), both the estimated axial and maximum bending stresses are found to be less than the yielding limit of ABS, thus the shape change is considered feasible. The curvature functions ($\kappa_{INI}(l)$ and $\kappa_{TAR}(l)$) and curvature difference function ($d\kappa(l)$) are shown in Figure 7-21.
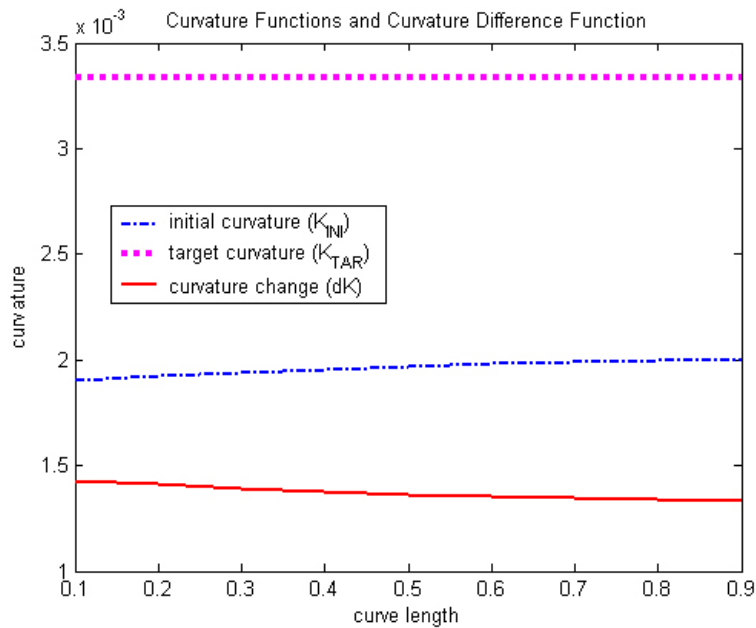
Figure 7-21: The curvature functions of the initial and target curves, and the curvature difference function between them (solid line) for the antenna beam shaping example.

Binary Ground Structure Approach

Figure 7-22 shows the initial ground structure created by connecting the input and output points with a beam element mesh. The horizontal members are included to provide stiffness and alternative connectivity between input and output points. Using the binary ground structure approach, the resulting compliant mechanism is shown in Figure 7-23 with the result summarized in Table 7-16.
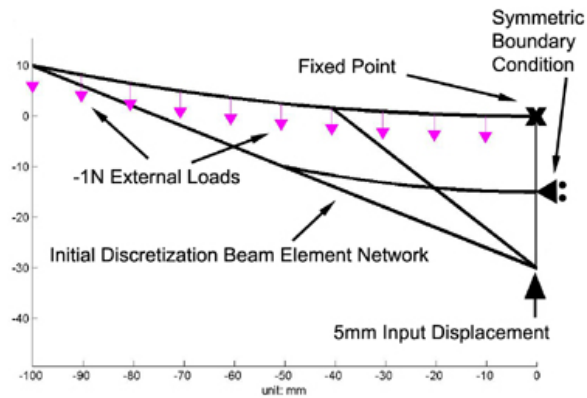
Figure 7-22: Initial ground structure and boundary conditions of the antenna reflector example.
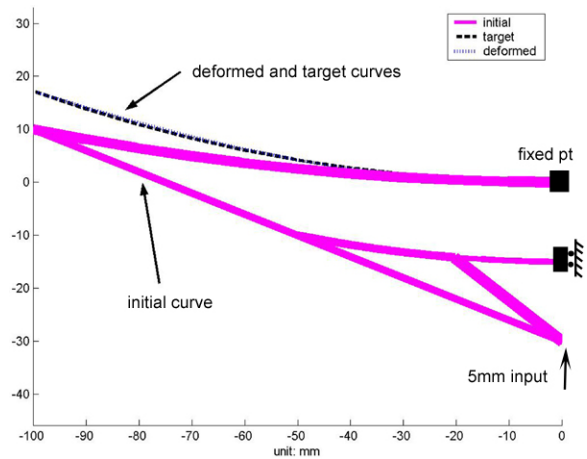
Figure 7-23: The beam shaping antenna design obtained from the binary ground structure approach.

Table 7-16: Design summary for the beam shaping antenna reflector in Figure 7-23.

LSE deviation: 2.97mm (0.12inch)	Maximum stress: -17.64MPa (-2.56kpsi)
CPU time: <15min	Required input force: 8.17N (1.84lbf)

Load Path Approach

Figure 7-24 shows the resulting design obtained from the GA using load path representation. The output points are data point # 1, 7, and 11 in Table 7-14. Five intermediate connection ports are included in this design. The design summary is shown in Table 7-17.
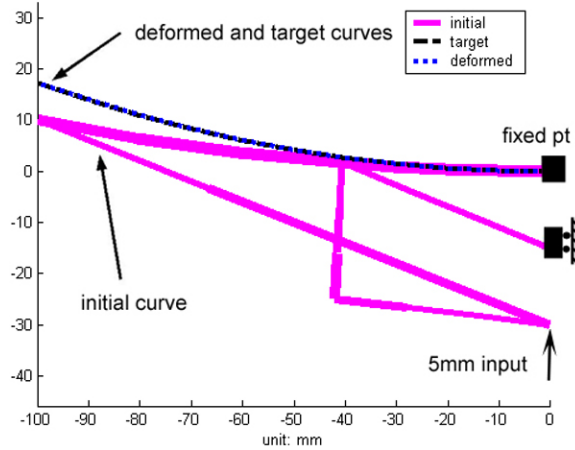
Figure 7-24: The beam shaping antenna design obtained from the load path approach.

Table 7-17: Design summary for the beam shaping antenna reflector in Figure 7-24.

LSE deviation: 2.60mm (0.1inch)	Maximum stress: 30.54MPa (4.43kpsi)
CPU time: 193sec (<3.5min)	Required input force: 9.45N (2.12lbf)

Discussion

The LSE deviation of the two designs in Figure 7-23 and Figure 7-24 are only 15% different from each other. This implies that the two approaches are equally effective in synthesizing the compliant mechanism that morphs the parabolic curve into the circular target curve. Similar to the morphing trailing edge example in Section 7.1.2, the beam shaping mode of this antenna reflector can also be seen as bending of a cantilever beam. The direct connection from input to the output point on the left end appears in both designs. Additional paths deliver force and moment to the middle output point in Figure 7-24 to further modify the shape of the morphing boundary, thus the LSE deviation is slightly smaller than that in Figure 7-23.

7.3.2   Beam Steering Mode

Figure 7-25 is a cylindrical antenna reflector in its beam steering mode that changes the orientation of the reflector to vary the coverage area. In this example, the two

136

tips of the cylindrical reflector are expected to move in opposite directions to simulate a

rotation of 3° (0.05rad) clockwise about the center. The specification is interpreted as the

target curve in dash line (Figure 7-25). The initial and target curve data points are listed

in Table 7-18, and the design specifications are shown in Table 7-19. In the design

domain initialization, the output points are identified along the morphing boundary as #

1, 5, 8, 14, 17, and 21 in Table 7-18. Both binary ground structure and load path

approaches are applied in this problem to synthesize the morphing structure.
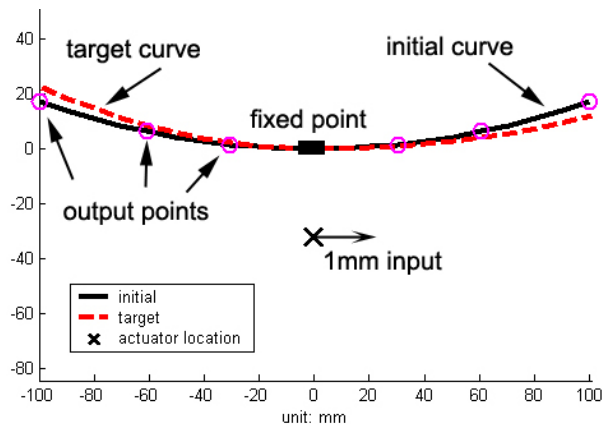
Figure 7-25: A morphing antenna reflector that simulates a rotation about the center to steer the signal 3° to the right.

Table 7-18: Data points along initial and target curves for the beam steering antenna reflector.

Data point #	Initial Curve Data Points		Target Curve Data Points	
	X (mm)	Y (mm)	X (mm)	Y (mm)
1	-70.6946	8.4485	-98.9249	22.1573
2	-60.7477	6.2148	-89.4997	18.1974
3	-50.7306	4.3204	-79.9410	14.5743
4	-40.6550	2.7675	-70.2573	11.3074
5	-30.5324	1.5578	-60.4582	8.4156
6	-20.3745	0.6927	-50.5551	5.9183
7	-10.1931	0.1732	-40.5614	3.8345
8	0.0000	0.0000	-30.4916	2.1827
9	10.1931	0.1732	-20.3623	0.9814
10	20.3745	0.6927	-10.1918	0.2481
11	30.5324	1.5578	0.0000	0.0000
12	40.6550	2.7675	10.1944	0.0983
13	50.7306	4.3204	20.3867	0.4040
14	60.7477	6.2148	30.5732	0.9329
15	70.6946	8.4485	40.7486	1.7005

137

Data point #	Initial Curve Data Points		Target Curve Data Points	
	X (mm)	Y (mm)	X (mm)	Y (mm)
16	80.5598	11.0188	50.9061	2.7225
17	90.3321	13.9229	61.0372	4.0140
18	100.0000	17.1573	71.1319	5.5896
19	-70.6946	8.4485	81.1786	7.4633
20	-60.7477	6.2148	91.1645	9.6484
21	-50.7306	4.3204	101.0751	12.1573

Table 7-19: Design specifications and GA parameters in the antenna beam steering example.

Objective function	minimize FT deviation	
Material	ABS plastic (Acrylonitrile-butadiene-styrene) E: 2480MPa (359.7kpsi) σ_{yield}: 34.45MPa (5kpsi)	
Beam dimensions	Out-of-plane: 4mm (0.1575inch) In-plane: 2 ~ 4mm (0.0788 ~ 0.1575inch)	
Boundary conditions	Input displacement: 1mm $\rightarrow$ (0.0394inch) Input location: (0,-15) Fixed point location: (0,0) External loads: multiple point loads of 1N $\downarrow$ (0.225lbf)	
Constraints	$\sigma_{allowable}$: 34.45MPa (5kpsi) (σ_{yield}) $d_{allowable}$: 1mm (0.0394inch)	
GA parameters	Population #: 60 Max. # of generation: 20	Crossover probability: 0.8 Mutation probability: 0.5

Binary Ground Structure Approach

Figure 7-26 shows initial ground structure and the mesh configuration used in this example. The modified FT objective function is used in this example, since the initial curve is symmetric about y-axis. The obtained result shown in Figure 7-27 is actually a mirror image design that simulates a rotation opposite to the desired direction. Table 7-20 shows the shape deviations between the deformed and target curve using both FT and LSE; the FT deviation is 1.1758mm for this design, but its LSE deviation is approximately 5 times larger (6.0869mm). If LSE deviation were to be used as the objective function, the GA would not be able to find the design in Figure 7-27. This result

simply implies that the desired shape morphing can be achieved by mirroring the current

design.
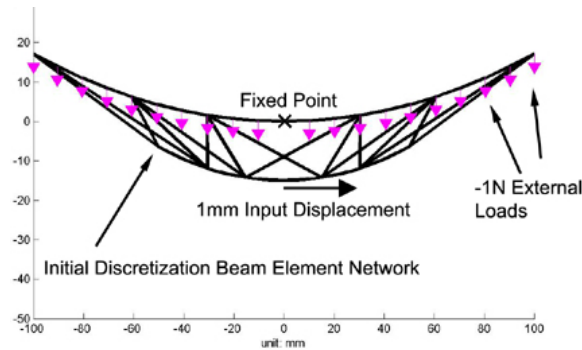
Figure 7-26: Initial discretization element network and input actuation.
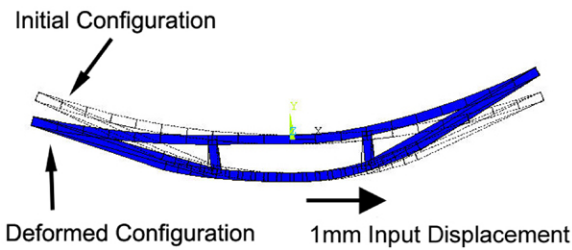
Figure 7-27: The optimized morphing antenna reflector in beam steering mode from binary ground structure approach.

Table 7-20: Design summary of the beam steering antenna reflector shown in Figure 7-27.

FT dev: 1.18mm (LSE dev: 6.09mm)	Maximum stress: -34.15MPa (-4.95kpsi)
CPU time: <10min	Required input force: 17.3N (3.9lbf)

Figure 7-28 shows the mirror image design of Figure 7-27 about the y-axis. As

can be seen in Table 7-21, the FT deviation remains the same (1.18mm), but the LSE

deviation reduces to 0.6801mm. This example suggests another useful aspect of the

modified FT objective function: the resulting design helps identify appropriate actuation

direction when user-specified direction does not allow the shape change in the intended

direction. Unlike the LSE which might prevent GA from finding a feasible solution,

using the modified FT can help identify the mirror solution. Note that the FT deviation

of 1.18mm is obtained after only 20 generations. The deviation can be further reduced by

adding more generations.
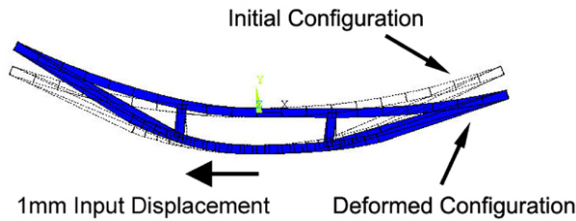
Figure 7-28: The mirror image design of the morphing antenna reflector in Figure 7-27.

Table 7-21: Design summary of the beam steering antenna reflector shown in Figure 7-28.

FT dev: 1.18mm (LSE dev: 0.68mm)	Maximum stress: -34.15MPa (-4.95kpsi)
CPU time: <10min	Required input force: 17.3N (3.9lbf)

Load Path Approach

The load path approach is incorporated here to synthesize the antenna reflector

capable of the shape morphing shown in Figure 7-25. The boundary condition is slightly

different from Table 7-19; the input location is (0,-30) and an additional fixed point is

located at (0,-20). As suggested by the results from the binary ground structure approach,

the input direction is now towards the left. Using LSE deviation and 5 intermediate

connection ports, GA yields the design shown Figure 7-29 with its LSE deviation listed

in Table 7-22.
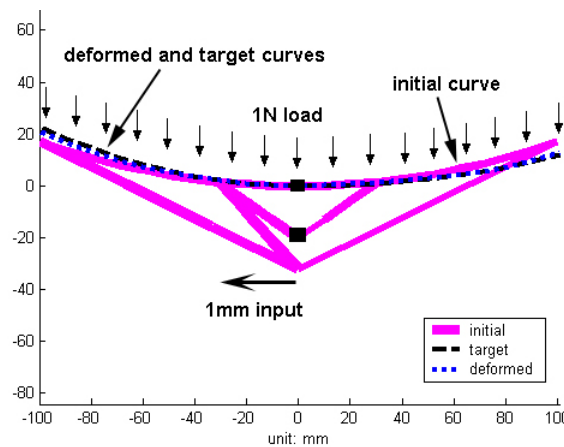
**Figure 7-29: The optimized morphing antenna reflector in beam steering mode obtained from GA
using load path representation.**

Table 7-22: Design summary of the beam steering antenna reflector shown in Figure 7-29.

LSE dev: 0.51mm (0.02inch)	Maximum stress: -24.14MPa (-3.5kpsi)
CPU time: <1min	Required input force: -112.35N (-25.26lbf)

Discussion

The shape morphing required in this example is similar to simple bending of cantilever beams; deflecting the left arm upwards while pulling the right arm downwards. The direct connections from the actuator to the two ends can be seen in both results (Figure 7-28 and Figure 7-29). This suggests that the fixed mesh approach and load path approach are equally effective in finding a design that can achieve the desired shape morphing when it only requires simple bending of cantilever beams. As will be discussed in the next example, the complexity of the shape morphing can be defined by the number of inflection points in the problem. For simple beam bending (no inflection points) seen in antenna morphing or even the trailing edge design in Section 7.1.2, the designer can usually use his/her intuition to choose a good initial ground structure that is likely to include a feasible design (such as direct connection between input and the tip of the beam). However, when the desired shape morphing is no longer simple bending, it would be more difficult to predict the required mesh complexity when choosing an initial ground structure.

7.4 Compliant Lumbar Support

Lower back pain occurs frequently and is one of the most costly health problems affecting industry and society. Lifetime prevalence of 60% to 90% has been reported (Andersson, 1991). Lumbar support is one of the commonly used preventive strategies (Lahad et al., 1994). This example is inspired by the lumbar support system that is

commonly used in car seats and office chairs to prevent lower back pain. The downward 'seating' motion from a person actuates the lumbar support, changing the straight back support into a curved profile. The curved profile should match the natural profile of human spine, which typically includes an inflection point as shown in Figure 7-30.
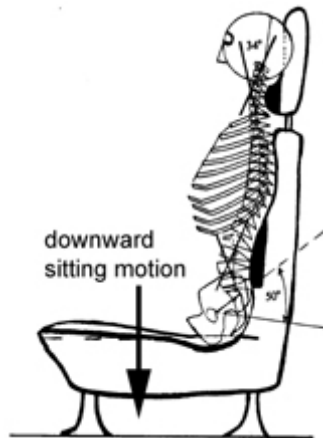
Figure 7-30: Natural sitting spinal model in an ideal driver's seat (Harrison et al., 2000).

The target curve is created to roughly approximate the spinal shape. The initial (straight) and target (spine) curves are shown Figure 7-31 with a 'downward' input motion. The curve information and specifications are shown in Table 7-23 and Table 7-24 respectively.
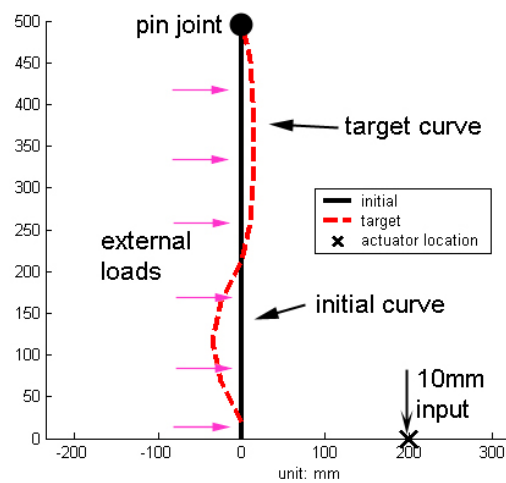
Figure 7-31: The initial and target curves for the lumbar support design.

Table 7-23: Data points along initial and target curves for the lumbar support example.

Data point #	Initial Curve Data Points		Target Curve Data Points	
	X (mm)	Y (mm)	X (mm)	Y (mm)
1	0	0	0	20
2	0	50	-25	68
3	0	100	-35	116
4	0	150	-25	164
5	0	200	0	212
6	0	250	10	260
7	0	300	13	308
8	0	350	15	356
9	0	400	13	404
10	0	450	10	452
11	0	500	0	500

Table 7-24: Design specifications and GA parameters in the lumbar support example.

Objective function	minimize LSE deviation	
Material	ABS plastic (Acrylonitrile-butadiene-styrene) E: 2480MPa (359.7kpsi) σ_{yield}: 34.45MPa (5kpsi)	
Beam dimensions	Out-of-plane: 5mm (0.1969inch) In-plane: 2 ~ 4.5mm (0.0788 ~ 0.1772inch)	
Boundary conditions	Input displacement: 10mm $\downarrow$ (0.394inch) Input location: (200,166.67) Fixed point location: (200,333.33) External loads: multiple point loads of 2N $\rightarrow$ (0.45lbf)	
Constraints	$\sigma_{allowable}$: 34.45MPa (5kpsi) (σ_{yield}) $d_{allowable}$: 5mm (0.187inch)	
GA parameters	Population #: 200 Max. # of generation: 200	Crossover probability: 0.8 Mutation probability: 0.3

Binary Ground Structure Approach

Several different initial mesh configurations have been investigated, but Figure 7-32 only shows the ground structure that has yielded the best result. Figure 7-33 shows the result obtained from GA using this initial mesh, and results are summarized in Table 7-25.
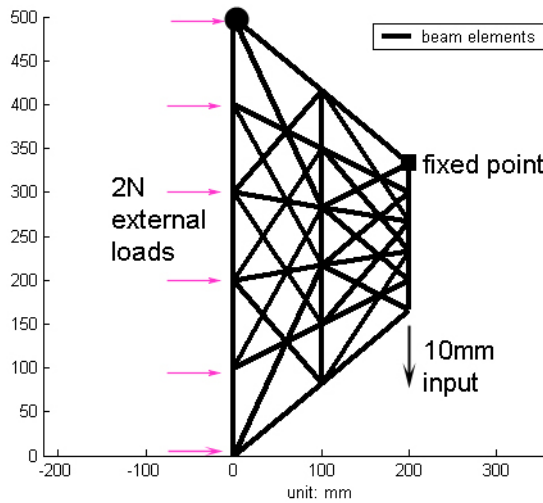
Figure 7-32: The initial binary ground structure of the lumbar support example.
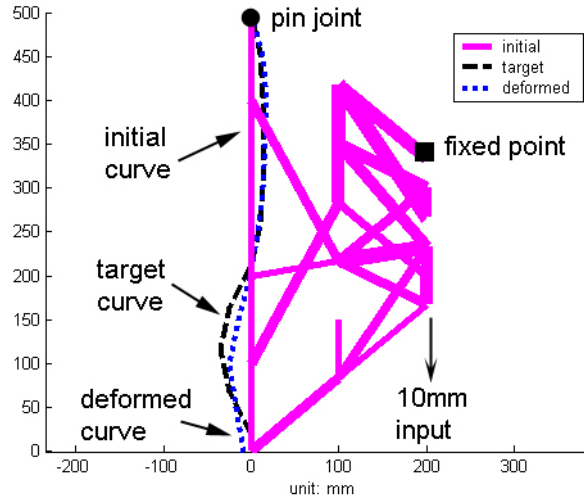
Figure 7-33: The lumbar support design obtained from the binary ground structure approach.

Table 7-25: Design summary of the lumbar support design shown in Figure 7-33.

LSE dev: 11.24mm (0.44inch)	Maximum stress: 31.19MPa (4.5kpsi)
CPU time: 453sec (<8min)	Required input force: 10.46N (2.35lbf)

Load Path Approach

The load path approach is applied to the same lumber support problem with slightly modified boundary conditions. Two fixed points are used here, locating at (200,250) and (200,500); the actuator is moved to (200,0) while the input displacement remains the same. Figure 7-34 and Table 7-26 show the design obtained from GA using 5

intermediate connection ports. The paths are only physically connected at one

intermediate connection port in Figure 7-34; other path intersections are due to

overlapping elements that have relative motion between each other.
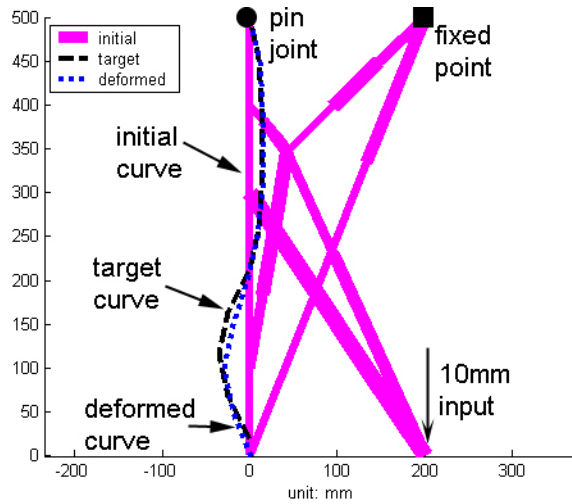
Figure 7-34: The lumbar support design obtained from the GA using load path representation.

Table 7-26: Design summary of the lumbar support design shown in Figure 7-34.

LSE dev: 10.55mm (0.42inch)	Maximum stress: 34.2MPa (4.96kpsi)
CPU time: 249sec (<4.5min)	Required input force: 51.53N (11.58lbf)

Discussion

The shape change required in this example involves creating an inflection point at

the middle of the morphing boundary. As mentioned in the discussion of Section 7.2.2,

creating an inflection point is a more difficult task. Simple cantilever beam bending can

be seen as the beam 'pivoting' about the fixed end. However, creating an inflection point

involves changing the center of curvature from one side to the opposite side of the beam.

Since it requires a moment or some opposite (pushing and pulling) motions to generate a

couple at the inflection point, designing such morphing structure is less intuitive,

especially in selecting an initial ground structure.

The two designs in Figure 7-33 and Figure 7-34 might seem very different at a glance, but they do have a similar underlying topology; both designs have an X-shaped topology consisting of overlapping paths from the input and fixed point to opposite sides of the inflection point. As can be seen in Figure 7-34, the paths from input transmit the pulling motion to the right of the inflection point while the path from fixed point provides stiffness to support the left tip, thus creating a moment about the inflection point. A similar X configuration can also be seen vaguely embedded in the final topology in Figure 7-33. This suggests that the ground structure is as effective in identifying the fundamental topology required to generate an inflection point. However, if this X configuration is not included in the initial mesh, the algorithm might not at all be able to find a design that can create an inflection point. The initial mesh in Figure 7-32 was chosen by studying results from the load path approach, but this kind of information is generally unavailable at the outset. Therefore, it is recommended to employ the load path approach when inflection points are involved in the required shape morphing.

Although the two LSE deviations in Table 7-25 and Table 7-26 are only 6% different from each other, the deformed curve do match the target curve in the load path result. This may result from the insufficient numbers of data points used for curve comparison. There are currently 11 data points along the curve, if more data points were used, the LSE deviation could capture the shape difference more accurately, leading to more significant difference of the LSE deviation in the two designs.

7.5 Single Input Single Output (SISO) Examples

The load path representation developed in this research provides a novel way to represent structural topologies. Although it is originally developed to address problems with multiple output points, the load path representation is a general representation scheme and can be applied to problems not specific to shape morphing. Two SISO compliant mechanisms and two typical structural design problems will be investigated in the following to further explore the capability of the load path approach.

7.5.1 Displacement Amplifier

One of the benchmarking problems for compliant mechanism design is to create a displacement amplifier. Many different designs have been created in previous research (Joo, Kota, and Kikuchi, 2001; Kota, Rodgers, and Hetrick, 2001; Hetrick, Joel and Kota, 2003). The compliant mechanism serves as a transmission so that the input displacement is amplified at the output port. This is typically characterized by the geometric advantage (GeoA). Figure 7-35 shows the design domain defined in this example. The goal is to create a high GeoA compliant amplifier that the output port can work against 1N (0.225lbf) external load with 1mm (0.04inch) input downwards actuation. The overall design domain is 240mm by 100mm (9.45inch by 3.94inch). To ensure linear motion at the output port, the design is chosen to be symmetric about the y-axis. Thus, only the right half of the design domain is considered in the synthesis process. Two fixed points are included in this example, located at (60,0) and (120,50). Since there is only a single output port, the preprocessing step can be neglected. Furthermore, the original curve comparison objective function is replaced by maximizing the GeoA, defined as output

displacement divided by input displacement. Since input displacement is prescribed in this example, maximizing GeoA is essentially the same as maximizing the output displacement.
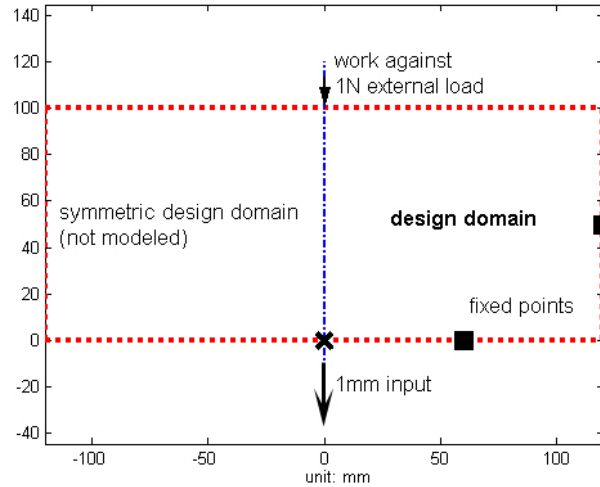
Figure 7-35: Design domain for the displacement amplifier. Due to symmetry about y-axis, only the right half is modeled in the synthesis process.

With 8 intermediate connection ports, a compliant amplifier with geometric advantage of 27 is created using the load path approach, shown in Figure 7-36 and Table 7-27. The full model of the displacement amplifier is shown in Figure 7-37. This design is very similar to the device described in (Kota, Rodgers, and Hetrick, 2001; Hetrick, Joel and Kota, 2003), which was developed based on intuition. The result in Figure 7-36 demonstrates that the load path approach can create topologies that confirm with design intuition.
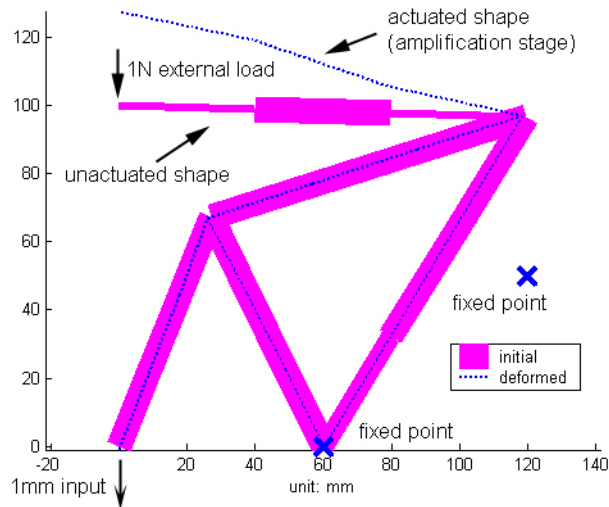
Figure 7-36: A displacement amplifier with loaded geometric advantage of 27 (right half of the design) based on linear analysis.

Table 7-27: Design summary of the displacement amplifier shown in Figure 7-36.

Geometric Advantage: 27.6	Maximum stress: 30.17MPa (4.38kpsi)
CPU time: 194sec (3.23min)	Required input force: -98.7N (-22.19lbf)
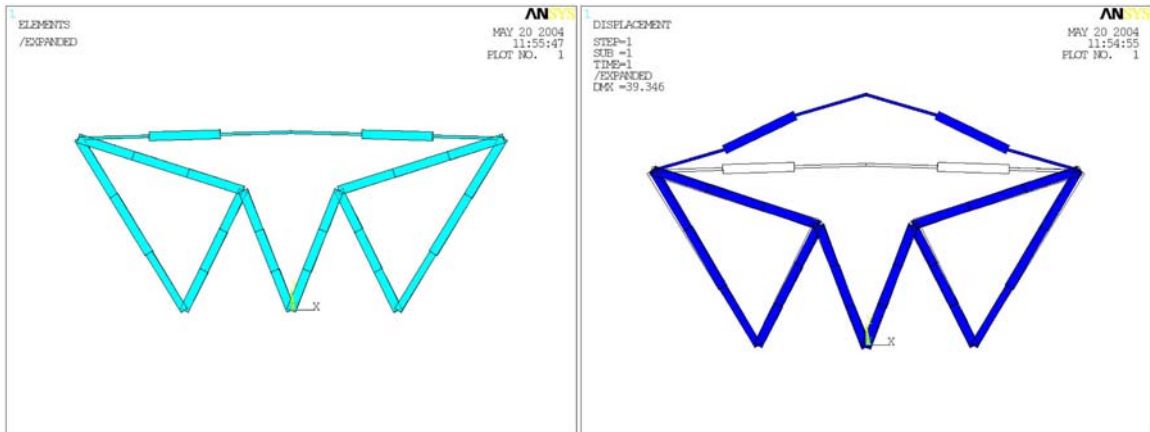
Figure 7-37: The full model of the displacement amplifier in its inactive mode (left) and amplifying mode (right).

7.5.2 Compliant Gripper

The compliant gripper design is also one of the most commonly seen benchmark problems and has been investigated in many previous literatures (Frecker et al., 1997; Hetrick, J. and Kota, 2000; Joo, Kota, and Kikuchi, 2000; Saxena, A. and Ananthasuresh, 2001; Parsons and Canfield, 2002; Saxena, Rajat and Saxena, 2003; Wang, Wang, and

Mei, 2004). The goal is to design a compliant mechanism that deforms to grip an object

and has appropriate stiffness to take the reaction force upon gripping the object (8N or

1.8lbf in this example). Figure 7-38 shows the design domain and boundary conditions,

including the 2mm input at (50,0), and two fixed points located at (0,20) and (0,40). The

overall design domain is 100mm by 80mm (3.94inch by 3.15inch). The gripper is

designed to symmetric about the x-axis, so that the output ends will close by input

actuation and grip the hypothetical object placed at (100,0). Due to symmetry, only the

upper half of the design domain is modeled with a single output point located at (100,20).

Again, the design domain initialization can be deactivated since there is only one output

point.
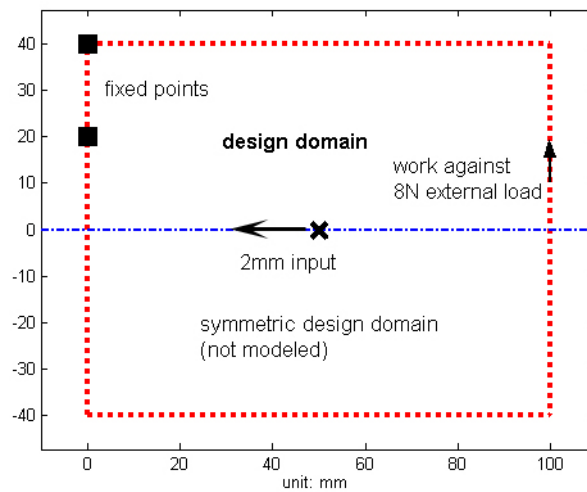
Figure 7-38: The design domain for a compliant gripper. Due to symmetry about the x-axis, only the upper half is modeled in the synthesis process.

Although various formulations have been developed to characterize the gripper

problem, the objective function used in this example is merely maximizing the output

displacement (or GeoA). Using 8 intermediate connection ports, the design in Figure 7-39

is created from the load path approach. To avoid the overlapping elements, the design is

modified as that shown in Figure 7-40 by moving one fixed point to (10,30). The

modified design has an 8.35 geometric advantage, summarized in Table 7-28. The full

model is shown in Figure 7-41 to help visualize how the gripper works.
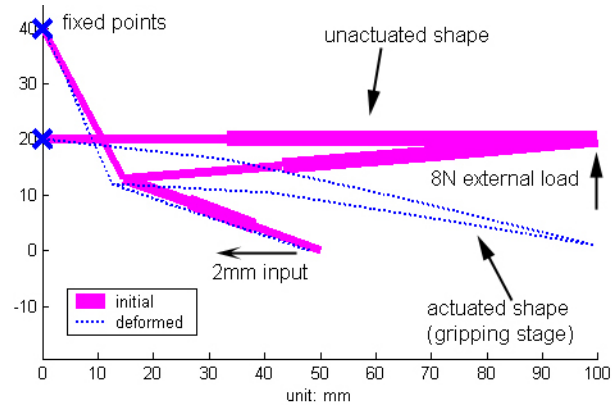
Figure 7-39: A compliant gripper obtained from the load path approach (upper half of the gripper).
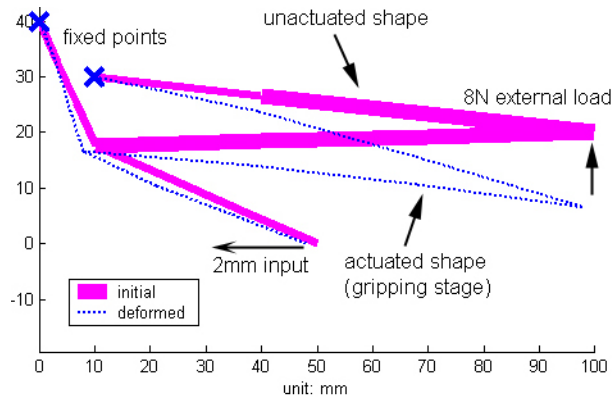
Figure 7-40: The modified compliant gripper from Figure 7-39 to avoid element overlapping.

Table 7-28: Design summary of the compliant gripper shown in Figure 7-40.

Geometric Advantage: 8.35	Maximum stress: 34.45MPa (5kpsi)
CPU time: 51.48sec (0.86min)	Required input force: -85.18N (-19.15lbf)
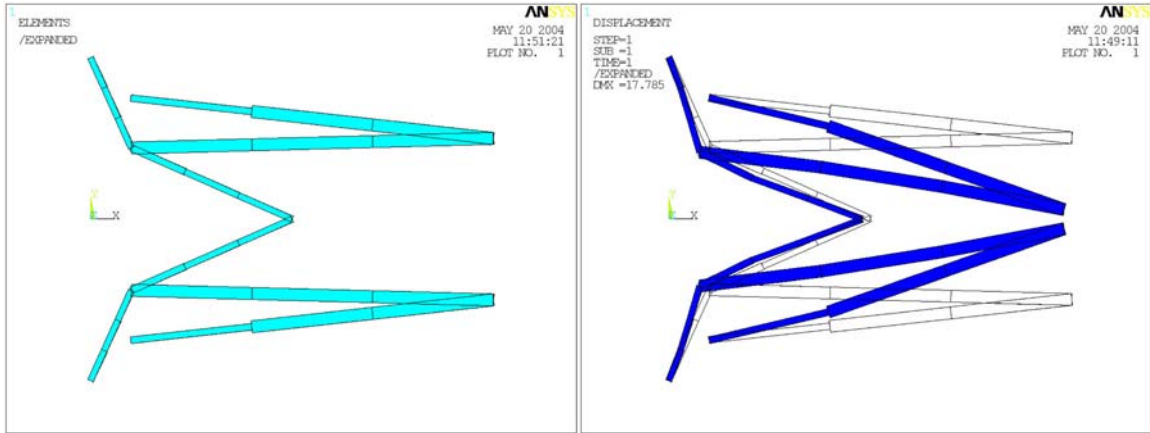
Figure 7-41: The full model of the compliant gripper in its inactive mode (left) and gripping mode (left).

7.5.3   Cantilever Beam

In traditional structural topology optimization, the design goal is to find the stiffest structure that uses the least amount of material (lightest design). This is achieved by minimizing the mean compliance (i.e. the strain energy) while constraining the volume. Since the load path representation provides a novel means to describe structural topologies, a cantilever beam design is investigated in this section to explore load path approach's application in structures.

Figure 7-42 shows the design domain of the cantilever beam. The fixed boundary condition is modeled as two fixed points located at the upper and lower corners on the left. The external load is applied at the lower corner of the free end.
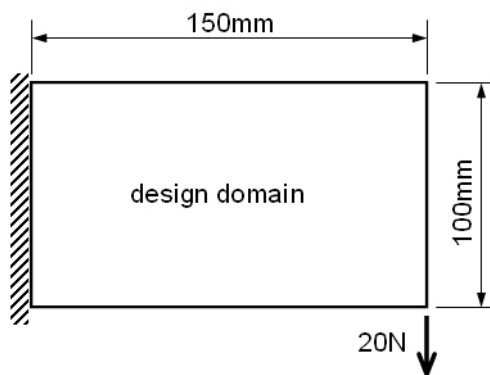
Figure 7-42: Design domain for a short cantilever beam.

Figure 7-43 shows three sample designs obtained from the load path approach where the objective is to minimize strain energy storage in the structure. Figure 7-43(a) is the same as the classical truss solution obtained from other design approaches, such as the SIMP method (Sigmund, 2001). The designs in Figure 7-43(b) and (c) have higher stiffness than (a) though these designs are heavier. As a side note, the designs in Figure 7-43(b) and (c) both contain overlapping elements; they are not included in the solution space of the homogenization approach, which is strictly two-dimensional.
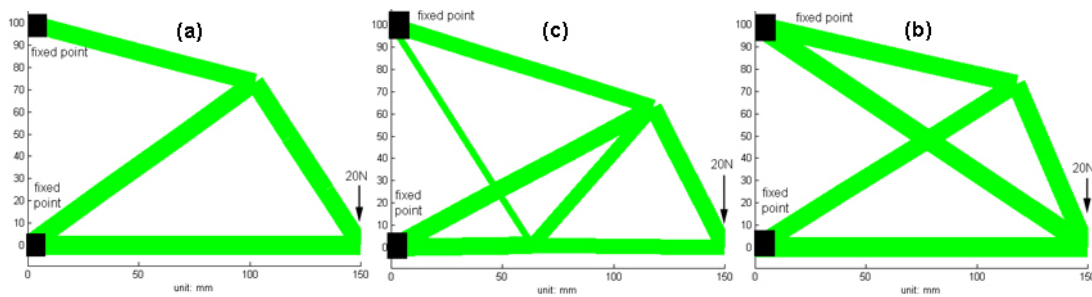
Figure 7-43: Three sample designs from the load path approach: (a) the classical truss solution; (b) and (c) two stiffer designs with higher weight.

7.5.4 Simply Supported Beam

Another standard problem commonly seen in structural topology optimization is the design of a center-loaded simply supported beam. The goal is, again, to design the stiffest and lightest structure that can withstand the applied load. The design domain and boundary conditions are shown in Figure 7-44. Due to symmetry of the problem, only the right half is considered the design domain (the center line is replaced by symmetric boundary conditions using two sliding ground points on the top and bottom of the beam).
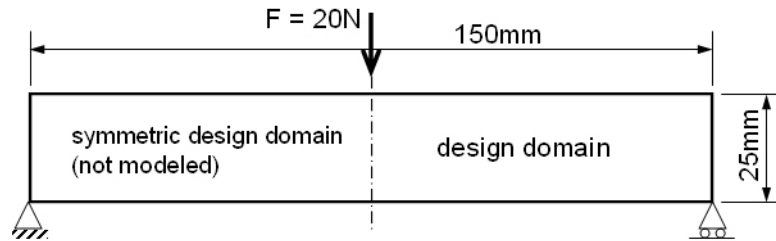
Figure 7-44: Design domain for a center loaded simply supported beam. Due to symmetry, only the right half is modeled in the synthesis process.

Using 4 intermediate connection ports, the load path approach creates several different designs with low strain energy. Two sample designs are shown in Figure 7-45. Figure 7-45(a) is the classical truss design seen in previous research using other design approach (Sigmund, 2001). The design in Figure 7-45(b) is a stiffer but heavier design (with one overlapping element).
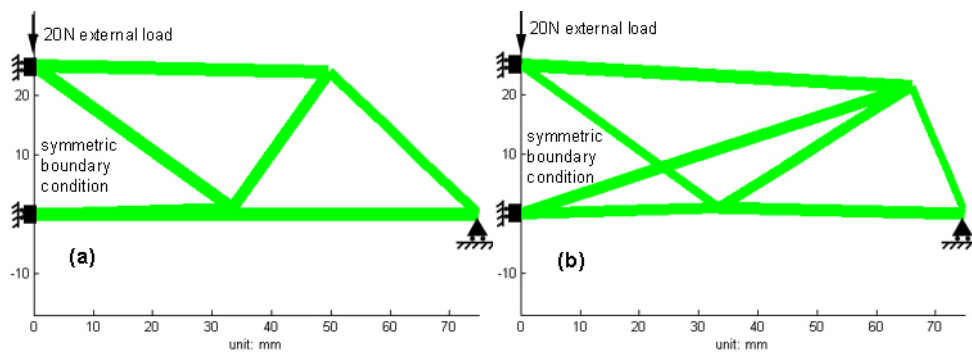
Figure 7-45: Two sample designs from the load path approach: (a) the classical truss solution, and (b) a stiffer design with higher weight.

The results presented in section 7.5 suggest that the load path approach is a versatile design approach that can be generalized to address problems other than shape morphing. The results might not guarantee global optimality, but the approach is capable of exploring a wide variety of designs and finally arrives at several sub-optimal design alternatives. It renders a systematic approach not only for designing compliant mechanisms, but the alternative designs also provides valuable design intuition that is valuable to designers.

CHAPTER 8

CONCLUSIONS AND FUTURE WORK

8.1 Summary

Compliant mechanisms provide a viable means to morph shape due to their smooth structural deformation for the wide range of applications including large scale aerospace structures and MEMS systems. The smooth shape and scalability overcome the limitations seen in shape morphing designs using rigid link mechanisms (joints and seams on surface) and smart material actuators (poor scalability). Previous research has developed various methods to design single input-single output (SISO) compliant mechanisms. However, these existing approaches do not apply to shape morphing problems because of the multiple output points presented in the system. In this dissertation, a systematic approach is developed to synthesize compliant mechanisms that can achieve desired shape morphing between two given shapes. The design problem is formulated into an optimization problem where the goal is to minimize the shape deviation between the desired target shape and the actual shape achieved by the compliant mechanism. The synthesis approach is divided into three major steps: feasibility estimation (preprocessing), design domain parameterization, and design optimization.

8.1.1 Design Domain Initialization

The synthesis approach starts with a design domain initialization that evaluates the feasibility to morph between the two given shapes and identifies the output points along the morphing boundary to facilitate further synthesis. The task feasibility analysis first estimates the differences in curvature and in curve length between the initial and target curves, in order to determine the bending and axial stresses resulting from this shape deformation. The shape morphing is considered feasible only if both stresses stay within the allowable stress level of the selected material.

In the output point identification, the algorithm then proceeds to identify the number and locations of the output points for a feasible shape morphing. This is achieved through a piecewise linear approximation of the curvature difference function (defined in Section 4.1), and the end points of each linear segments are identified as the output points. In order to reduce the design complexity, an optimization routine is implemented to minimize the number of required output points while constraining curve fitting error under an acceptable value. The output points can be seen as the connections that transmit the remote input actuation to the boundary. They are the potential locations along the morphing boundary where a load or a moment can be applied to most effectively deform the initial curve into the target shape. They also provide the basic framework for the design domain parameterization.

8.1.2 Parameterization

The design domain parameterization is the symbolic representation of various physical structures. The symbols, or parameters, are regarded as the design variables later

in the optimization. Previous research utilizing continuous variable representation generally suffered from the "gray area" issue (section 2.3.2), leading to ambiguity in the final topology interpretation. Binary variables are, therefore, incorporated in this research to address the topology synthesis in its natural, discrete form. Two parameterization methods have been introduced: one using a binary ground structure, and the other using a load path representation. Both approaches combine binary and continuous variables to simultaneously address the topology and dimensional aspects of the compliant mechanisms.

In the binary ground structure parameterization, the design domain is first discretized with an initial beam element mesh. The initial mesh configuration and resolution are typically chosen based on intuition. Two design variables are assigned to each beam element: a binary variable to represent the presence or removal of the element, and a real, continuous variable to describe the cross section dimension. In other words, the binary variables control the topology, and the real variables determine the dimensions of the compliant mechanism. However, the structural topologies described by this representation can include disconnected structures that need to be excluded from the solution space. Since the structural connectivity information is not readily available in the design variables, additional verification algorithm is required to 'search for' the invalid designs, thus leading to inefficiency in the synthesis approach. Moreover, the design insight needed to select an "appropriate" initial mesh is subjective and not always available for inexperienced designers. The load path representation is, therefore, developed to overcome these issues.

In the load path representation method, the structural topology and dimensions are represented as a graph. The topology is created by connecting the input, output, and ground points using load paths. Binary variables are used to control the presence of each individual path, rather than controlling only one individual element as in the binary ground structure. The load path representation creates well-connected structural topologies and effectively eliminates the infeasible designs from the solution space. A set of intermediate connection ports and their locations (geometry of the structure) are also treated as design variables. This allows a large variety of topologies without the need to pre-specify an initial mesh based on intuition.

8.1.3 Optimization

The parameterization methods are incorporated into a genetic algorithm (GA) based optimization process to find the design that can achieve the desired shape morphing with minimum errors. Various designs are created in GA and the structural deformation of each design (due to input actuation) is solved for using finite element analysis (FEA). The deformed boundary shape is extracted from the FEA result and compared to the target shape. Two curve comparison objective functions have been introduced to evaluate the performance of each design. A least square error (LSE) and a modified Fourier Transformation (FT) are formulated to quantify the difference between the deformed and target curves. The LSE deviation captures the point-to-point deviation between the curves, while the FT deviation captures the difference in shape regardless of the location, orientation, and size of the two shapes being compared. Although FT deviation is useful to identify mirror images and other symmetric features of a given

curve, LSE deviation is recommended in most problems due to its simplicity, effectiveness, and efficiency. Using the curve comparison objective functions, GA can effectively identify the required mechanism topology and dimensions to achieve the desired shape morphing. Additional local search following GA is also included to refine the dimensions and accelerate the convergence to the nearby local optimum.

Several design examples are shown in Chapter 7 to demonstrate the capability of the GA based synthesis approach. The results have shown that the synthesis approach can successfully generate compliant mechanisms capable of morphing structures under external loads into desired shapes. The resulting shape morphing is smooth, and the design approach can be applied to problems at various scales (micro to macro). The results also suggested that the load path representation can effectively identify the topology required for a particular shape change. With the floating intermediate connection ports as part of the design variables, the load path representation allows variable mesh configuration, relying less on design intuition. Although binary ground structure parameterization has yielded successful results in some examples, the quality of the shape morphing depends greatly on the selection of the initial mesh. If the selected initial mesh does not contain any acceptable design, the approach may fail to find a working compliant mechanism. On the other hand, the load path approach provides a more systematic and objective means to design shape morphing compliant mechanisms without requiring an initial mesh.

8.2 Contributions

A systematic synthesis approach is introduced in this dissertation for designing shape morphing compliant mechanisms. The major contributions are summarized below.

- Development of a Genetic Algorithm based synthesis approach incorporating load path representation scheme. It offers an effective, efficient, and a systematic means to design shape morphing compliant mechanisms.

- The load path representation with binary variables addresses several fundamental issues encountered in many previous synthesis approaches: (1) it ensures structural connectivity, thereby excludes infeasible designs from the design space, (2) it allows variable mesh configuration, and (3) it creates designs free of gray areas.

- The Genetic Algorithm based load path approach can be further generalized to design structures as well as traditional SISO compliant mechanisms.

Some additional insight and contributions are included in the following.

- The development of a unified synthesis approach is essential to the shape morphing problem. Because matching the exact shape is a quantitative goal, the topology and dimensions of the compliant mechanism were addressed simultaneously.

- Both LSE and FT deviations offer an objective measure to quantify the similarity between two curves. However, LSE proves to be sufficient for comparing shapes achievable from structural deformation. Its simple formulation also makes it favorable over FT deviation.

- The selection of the initial mesh is critical in the binary ground structure parameterization. Since the final design is always a subset of all possible element combination in the initial mesh, it is important to start with a mesh with sufficient complexity. For any given shape morphing, however, the required mesh complexity is generally unknown a priori. The load path representation that does not require an initial mesh is, therefore, considered a more desirable parameterization.

- When large external loads are presented, the synthesis approach may find it difficult to converge to a feasible design. It is recommended to start with moderate external loads to first identify the required mechanism topology. Then, a local search can be employed to optimize the dimensions under increased external loads.

8.3 Future Research Directions

The future research can be divided into three main directions: (1) improving current methods and developing new synthesis approaches that are more effective and robust; (2) developing a set of design rules; and (3) exploring areas of applications in shape morphing and compliant mechanisms in general.

8.3.1 Synthesis Approach

The synthesis approach developed in this research focuses on morphing between two given shapes. For multi-stage shape morphing or for continuously morphing through a set of different shapes, the compliant mechanism could require more than one actuator.

It is, therefore, essential to investigate the minimum number of required actuators and the optimal actuator placement to effectively increase the degrees of freedom of the compliant mechanism for more complex morphing. Actuator stiffness matching is also essential in making the synthesis approach truly applicable to practical engineering problems, especially from system efficiency perspective. The relationship between the available design domain (physical design space), support, and actuator locations should be investigated to more realistically determine the feasibility of any given shape morphing.

External loads should also be considered in the design domain initialization. In this research, the output points are identified mainly from the kinematics standpoint; they are seen as locations where forces can be applied to most effectively deform the curve into the desired shape. However, it is very likely that additional output points are required to allow load paths serving mainly as structural support (stiffness). It is, therefore, essential to refine the output point identification process to explore load-bearing output points.

Since the behavior of a compliant mechanism is largely dictated by its topology, it is important to improve the topology synthesis algorithms. The topology includes not only the structural connectivity, but it also involves the relative locations of the essential nodes and the orientations of the beams connecting them. Therefore, the effect of the boundary conditions such as essential node locations should be investigated in the future to understand their significance in structural topology, hence the mechanism function.

More refined finite element analysis including nonlinearity and fluid-structure interaction can be included to more accurately predict the morphing behavior. The

synthesis approach developed in this dissertation should be extended in the future to address more generalized design problems in compliant mechanisms or structures.

8.3.2 Design Rules

Analysis of computer-generated designs can greatly enhance the understanding of the mechanism and structural characteristics of the compliant mechanisms. Systematic analysis of alternative designs can help develop design rules or identify basic building blocks, which can be extremely useful in conceptual design of compliant mechanisms. The increased knowledge in conceptual design rules will also assist the development of more effective synthesis approaches.

8.3.3 Areas of Applications

Last but not the least, new applications that can benefit from compliant mechanism should be explored to take full advantage of the design theories developed thus far and employ compliant mechanisms to practical applications. New materials and manufacturing methods should also be investigated to develop high performance compliant mechanisms.

BIBLIOGRAPHY

BIBLIOGRAPHY

Adalsteinsson, D. and Sethian, J.A., 1995, "A Fast Level Set Method for Propagating Interfaces," Journal of Computational Physics, **118**(2):2690277.

Akhtar, S., Tai, K., and Prasad, J., 2002, "Topology Optimization of Compliant Mechanisms Using Evolutionary Algorithm with Design Geometry Encoded as a Graph," ASME 2002 Design Engineering Technical Conferences, Montreal, Canada, **DETC2002**:DAC-34147.

Ameduri, S., Esposito, C., and Concilio, A., 2001, "Active Shape Airfoil Control through Composite-Piezoceramic Actuators," Smart Structures and Materials 2001: Smart Structures and Integrated Systems, Newport Beach, CA, March 4-8, 2001, **4327**:641-650.

Ananthasuresh, G.K., Kota, S., and Kikuchi, K., 1994, "Strategies for Systematic Synthesis of Compliant Mems," 1994 International Mechanical Engineering Congress and Exposition, Chicago, IL, November 6-11, 1994, **55**:677-686.

Ananthasuresh, G.K. and Saggere, L., 1994, "A Single-Piece Compliant Stapler," ASME Mechanisms Conference: Student Design Competition, Minneapolis, MN, September, 1994,

Andersson, G., 1991, "The Epidemiology of Spinal Disorders," Lippincott Williams & Wilkins, 107-146.

Angelino, M. and Washington, G., 2001, "Point Actuated Aperture Antenna Development," Proceedings of SPIE, **4334**:147-155.

Austin, F., Siclari, M.J., Van Nostrand, W., Weisensel, G.N., Kottamasu, V., and Volpe, G., 1997, "Comparison of Smart Wing Concepts for Transonic Cruise Drag Reduction," SPIE Proceedings, **3044**:33-40.

Austin, F. and Van Nostrand, W., 1995, "Shape Control of an Adaptive Wing for Transonic Drag Reduction," SPIE Proceedings, **2447**:45-55.

Bein, T., Hanselka, H., and Bereitbach, E., 2000, "An Adaptive Spoiler to Control the Transonic Shock," Smart Materials and Structures, **9**(2):141-148.

Bendsoe, M.P., 1989, "Optimal Shape Design as a Material Distribution Problem," Structural Optimization, **1**:193-202.

Bendsoe, M.P., 1995, "Optimization of Structural Topology, Shape, and Material," Springer.

Bendsoe, M.P., Guedes, J.M., Haber, R.B., Pedersen, P., and Taylor, J.E., 1994, "An Analytical Model to Predict Optimal Material Properties in the Context of Optimal Structural Design," Journal of Applied Mechanics, **61**:930-937.

Bendsoe, M.P. and Kikuchi, N., 1988, "Generating Optimal Topologies in Structural Design Using a Homogenization Method," Computer Methods in Applied Mechanics and Engineering, **71**:197-224.

Bendsoe, M.P. and Sigmund, O., 1999, "Material Interpolations in Topology Optimization," Archive of Applied Mechanics, **69**(9-10):635-654.

Birkemeyer, J., Rosemann, H., and Stanewsky, E., 2000, "Shock Control on a Swept Wing," Aerospace Science and Technology, **4**(3):147-156.

Chapman, C.D., Saitou, K., and Jakiela, M.J., 1994, "Genetic Algorithms as an Approach to Configuration and Topology Design," ASME Journal of Mechanical Design, **116**:1005-1012.

Chu, D.N., Xie, Y.M., Hira, A., and Steven, G.P., 1996, "Evolutionary Structural Optimization for Problems with Stiffness Constraints," Finite Elements in Analysis and Design, **21**:239-251.

Cui, G.Y., Tai, K., and Wang, B.P., 2002, "Topology Optimization for Maximum Natural Frequency Using Simulated Annealing and Morphological Representation," AIAA Journal, **40**(3):586-589.

Deb, K. and Gulati, S., 2001, "Design of Truss-Structures for Minimum Weight Using Genetic Algorithms," Finite Elements in Analysis and Design, **37**(5):447-465.

Diaz, A. and Sigmund, O., 1995, "Checkerboard Patterns in Layout Optimization," Structural optimization, **10**:40-45.

Duysinx, P. and Bendsoe, M.P., 1998, "Topology Optimization of Continuum Structures with Local Stress Constraints," International Journal for Numerical Methods in Engineering, **43**:1453-1478.

Erdman, A.G. and Sandor, G.N., 1991, "Mechanism Design: Analysis and Synthesis," Prentice-Hall International, Inc.

Fourie, P.C. and Groenwold, A.A., 2002, "The Particle Swarm Optimization Algorithm in Size and Shape Optimization," Structural and Multidisciplinary Optimization, **23**:259-267.

Frecker, M., 1997, "Optimal Design of Compliant Mechanisms," PhD Dissertation, Department of Mechanical Engineering, University of Michigan, Ann Arbor.

Frecker, M., Kikuchi, K., and Kota, S., 1999, "Topology Optimization of Compliant Mechanisms with Multiple Outputs," Structural Optimization, **17**(4):269-278.

Frecker, M.I., Ananthasuresh, G.K., Nishiwaki, S., Kikuchi, N., and Kota, S., 1997, "Topological Synthesis of Compliant Mechanisms Using Multi-Criteria Optimization," ASME Journal of Mechanical Design, **119**(2):238-245.

Gere, J.M. and Timoshenko, S.P., 1984, "Mechanics of Materials," Brooks/Cole.

Goldberg, D., 1989, "Genetic Algorithms in Search, Optimization, and Machine Learning," Addison-Wesley.

Hajela, P. and Lee, E., 1995, "Genetic Algorithms in Truss Topological Optimization," International Journal of Solid Structures, **32**(22):3341-3357.

Hamda, H., Jouve, F., Lutton, E., Schoenauer, M., and Sebag, M., 2002, "Compact Unstructured Representations for Evolutionary Design," Applied Intelligence, **16**(2):139-155.

Harrison, D.D., Harrison, S.O., Croft, A.C., Harrison, D.E., and Troyanovich, S.J., 2000, "Sitting Biomechanics, Part Ii: Optimal Car Driver's Seat and Optimal Driver's Spinal Model," Journal of Manipulative and Physiological Therapeutics, **23**(1):37-47.

Her, I. and Midha, A., 1987, "A Compliance Number Concept for Compliant Mechanisms and Type Synthesis," ASME Journal of Mechanisms, Transmissions and Automation in Design, **109**(3):348-355.

Hetrick, J. and Kota, S., 1999, "An Energy Formulation for Parametric Size and Shape Optimization of Compliant Mechanisms," ASME Journal of Mechanical Design, **121**:229-234.

Hetrick, J. and Kota, S., 2000, "Topology and Geometric Synthesis of Compliant Mechanisms," 2000 ASME Design Engineering Technical Conference, Baltimore, MD, September 13-16, 2000, **DETC2000**:MECH-14140.

Hetrick, J. and Kota, S., 2003, "Displacement Amplification Structure and Device," United States Patent No. 6,557,436.

Hetrick, J.A., 1999, "An Energy Efficiency Approach for Unified Topological and Dimensional Synthesis of Compliant Mechanisms," Ph.D. Dissertation, Department of Mechanical Engineering, University of Michigan, Ann Arbor.

Holland, J.H., 1975, "Adaptation in Natural and Artificial Systems," The University of Michigan Press.

Howell, L.L., 2001, "Compliant Mechanisms," John Wiley and Sons, Inc.

Howell, L.L. and Midha, A., 1994, "A Method for the Design of Compliant Mechanisms with Small-Length Flexural Pivots," ASME Journal of Mechanical Design, **116**(1):280-290.

Howell, L.L. and Midha, A., 1995, "Parametric Deflection Approximations for End-Loaded, Large-Deflection Beams in Compliant Mechanisms," ASME Journal of Mechanical Design, **117**(1):156-165.

Howell, L.L. and Midha, A., 1996, "Loop-Closure Theory for the Analysis and Synthesis of Compliant Mechanisms," ASME Journal of Mechanical Design, **118**(1):121-125.

Howell, L.L., Midha, A., and Norton, T.W., 1996, "Evaluation of Equivalent Spring Stiffness for Use in a Pseudo-Rigid-Body Model of Large-Deflection Compliant Mechanisms," ASME Journal of Mechanical Design, **118**(1):126-131.

Jensen, B.D. and Howell, L.L., 2000, "Identification of Compliant Pseudo-Rigid-Body Mechanism Configurations Resulting in Bistable Behavior," ASME Design Engineering Technical Conferences, Baltimore, Maryland, September 10-13, 2000, **DETC2000**:MECH-14147.

Jensen, B.D., Parkinson, M.B., Kurabayashi, K., Howell, L.L., and Baker, M.S., 2001, "Design Optimization of a Fully-Compliant Bistable Micro-Mechanism," 2001 ASME International Mechanical Engineering Congress and Exposition, New York, NY, November 11-16, 2001, **IMECE2001**:MEMS-23852.

Jones, D.R., Perttunen, C.D., and Stuckman, B.E., 1993, "Lipschitzian Optimization without the Lipschitz Constant," Journal of Optimization Theory and Applications, **79**(1):157-181.

Joo, J., 2001, "Nonlinear Synthesis of Compliant Mechanisms: Topology and Size and Shape Design," PhD Dissertation, Mechanical Engineering, University of Michigan, Ann Arbor.

Joo, J., Kota, S., and Kikuchi, N., 2000, "Topological Synthesis of Compliant Mechanisms Using Linear Beam Elements," Mechanics Based Design of Structures and Machines, **28**(4):245-280.

Joo, J., Kota, S., and Kikuchi, N., 2001, "Large Deformation Behavior of Compliant Mechanisms," ASME 2001 Design Engineering Technical Conference, Pittsburg, PA, **DETC2001**:DAC-21084.

Kawamura, H., Ohmori, H., and Kito, N., 2002, "Truss Topology Optimization by a Modified Genetic Algorithm," Structural and Multidisciplinary Optimization, **23**:467-472.

Kennedy, J. and Eberhart, R., 1995, "Particle Swarm Optimization," IEEE International Conference on Neural Networks, 1995, 1942-1948.

Kikuchi, N., Nishiwaki, S., Fonseca, J.S.O., and Silva, E.C.N., 1998, "Design Optimization Method for Compliant Mechanisms and Material Microstructure," Computer Methods in Applied Mechanics and Engineering, **151**(3-4):401-417.

Kota, S., 1999, "System for Varying a Surface Contour," United States Patent No. 5,971,328.

Kota, S., 2002, "System for Varying a Surface Contour," United States Patent No. 6,491,262.

Kota, S., Joo, J., Li, Z., Rodgers, S.M., and Sniegowski, J., 2001, "Design of Compliant Mechanisms: Applications to Mems," Analog Integrated Circuits and Signal Processing, **29**(1-2):7-15.

Kota, S., Rodgers, M.S., and Hetrick, J.A., 2001, "Compliant Displacement-Multiplying Apparatus for Microelectromechanical Systems," United States Patent No. 6,175,170.

Kudva, J.N., Appa, K., Jardine, A.P., and Martin, C.A., 1997, "Overview of Recent Progress on the Darpa/Usaf Wright Laboratory Smart Materials and Structures Development - Smart Wing Program," San Diego, CA, March 4, 1997, **3044**:24-32.

Lahad, A., Malter, A.D., Berg, A.O., and Deyo, R.A., 1994, "The Effectiveness of Four Interventions for the Prevention of Low Back Pain," Journal of the Amareican Medical Association, **272**(16):1286-1291.

Larsen, U.D., Sigmund, O., and Bouwstra, S., 1997, "Design and Fabrication of Compliant Micromechanisms and Structures with Negative Poisson's Ratio," Journal of Microelectromechanical systems, **6**(2):99-106.

Lawson, P.R. and Yen, J.L., 1988, "A Piecewise Deformable Subreflector for Compensation of Cassegrain Main Reflector Errors," IEEE Transactions on Antennas and Propagation, **36**(10):1343-1350.

Lutz, T., 2000, "Subsonic and Transonic Airfoil Design Applying Numerical Optimization Techniques," Conference on Actual Problems of Mathematics and Machanics, Kazan State University, Kazan, Russische Goderation, October 1-3, 2000,

Martin, C.A., Jasmin, L., Flanagan, J., Appa, K., and Kudva, J.N., 1997, "Smart Wing Wind Tunnel Model Design," SPIE Proceedings, **3044**:41-47.

Martin, J.W., Main, J.A., and Nelson, G.C., 1998, "Shape Control of Deployable Membrane Mirrors," ASME Adaptive Structures and Materials Systems Conference, **ad57/md83**:217-223.

Martin, J.W., Redmond, J.M., Barney, P.S., Henson, T.D., Wehlburg, J.C., and Main, J.A., 2000, "Distributed Sensing and Shape Control of Piezoelectric Bimorph Mirrors," Journal of Intelligent Material Systems and Structures, **11**:744-757.

Mattheck, C., 1998, "Design in Nature: Learning from Trees," Springer-Verlag.

Metropolis, N., Rosenbluth, A., Rosenbluth, M., Teller, A., and Teller, E., 1953, "Equation of State Calculations by Fast Computing Machine," journal of Chemistry and Physics, **21**:1087-1092.

Mlejnek, H.P., 1992, "Some Aspects of the Genesis of Structures," Structural Optimization, **5**:64-69.

Murphy, M.D., Midha, A., and Howell, L.L., 1996, "The Topological Synthesis of Compliant Mechanisms," Mechanism and Machine Theory, **31**(2):185-199.

Nishiwaki, S., Frecker, M.I., Min, S., and Kikuchi, N., 1998, "Topology Optimization of Compliant Mechanisms Using the Homogenization Method," International Journal for Numerical Methods in Engineering, **42**(3):535-559.

Ohsaki, M., 1995, "Genetic Algorithm for Topology Optimization of Trusses," Computers and Structures, **57**(2):219-225.

Parsons, R. and Canfield, S.L., 2002, "Developing Genetic Programming Techniques for the Design of Compliant Mechanisms," Structural and Multidisciplinary Optimization, **24**:78-86.

Prager, W., 1970, "Optimization of Structural Design," Journal of Optimization Theory and Applications, **6**(1):1-21.

Prager, W., 1977, "Optimal Layout of Cantilever Trusses," Journal of Optimization Theory and Applications, **23**(1):111-117.

Rajan, S.D., 1995, "Sizing, Shape, and Topology Design Optimization of Trusses Using Genetic Algorithm," Journal of Structural Engineering, **121**(10):1480-1487.

Rajeev, S. and Kirishnamoorthy, C.S., 1997, "Genetic Algorithms-Based Methodologies for Design Optimization of Trusses," Journal of Structural Engineering, **123**(3):350-358.

Saggere, L., 1997, "Static Shape Control of Smart Structures: A New Approach Utilizing Compliant Mechanisms," Ph.D. Dissertation, Department of Mechanical Engineering, University of Michigan, Ann Arbor.

Saggere, L. and Kota, S., 1999, "Static Shape Control of Smart Structures Using Compliant Mechanisms," AIAA Journal, **37**(5):572-578.

Saxena, A., 2002, "On Multiple-Material Optimal Compliant Topologies: Discrete Varialbe Parameterization Using Genetic Algorithm," ASME 2002 Design Engineering Technical Conference, Motreal, Quebac, Canda, September 29 - October 2, 2002, **5**:85-96.

Saxena, A. and Ananthasuresh, G.K., 2001, "Topology Optimization of Compliant Mechanisms with Strength Considertations," Mechanics of Structures and Machines, **29**(2):199-221.

Saxena, R. and Saxena, A., 2003, "On Honeycomb Parameterization for Topology Optimziation of Compliant Mechanisms," ASME 2003 Design Engineering Technical Conferences, Chicago, IL, September 2-6, **DETC2003**:DAC-48806.

Sethian, J.A. and Wiegmann, A., 2000, "Structural Boundary Design Via Level Set and Immersed Interface Methods," Journal of Computational Physics, **163**(2):489-528.

Shim, P.Y. and Manoochehri, S., 1997, "Generating Optimal Configurations in Structural Design Using Simulated Annealing," International Journal for Numerical Methods in Engineering, **40**:1053-1069.

Shrestha, S.M. and Ghaboussi, J., 1998, "Evolution of Optimum Structural Shapes Using Genetic Algorithm," Journal of Structural Engineering, **124**(11):1331-1338.

Sigmund, O., 1994, "Materials with Prescribed Constitutive Parameters: An Inverse Homogenization Problem," International Journal of Solids and Structures, **31**(17):2313-2329.

Sigmund, O., 2001, "A 99 Line Topology Optimization Code Written in Matlab," Structural and Multidisciplinary Optimization, **21**(2):120-127.

Sigmund, O. and Petersson, J., 1998, " Numerical Instabilities in Topology Optimization: A Survey on Procedures Dealing with Checkerboards, Mesh-Dependencies and Local Minima," Structural Optimization, **16**(1):68-75.

Sigmund, O. and Torquato, S., 1999, "Design of Smart Composite Materials Using Topology Optimization," Smart Materials and Structures, **8**:365-379.

Slocum, A.H., 1992, "Precision Machine Design," Prentice Hall.

Smith, S.T., 2000, "Flexure: Elements of Elastic Mechanisms," Gordon and Breach Science Publishers.

Smith, S.T. and Chetwynd, D.G., 1992, "Foundations of Ultraprecision Mechanism Design," Gordon and Breach Science Publishers.

Sobel, D., 1995, "Longitude: The Story of a Lone Genius Who Solved the Greatest Scientific Problem of His Time," Walker and Company.

Tai, K. and Chee, T.H., 2000, "Design of Structures and Compliant Mechanisms by Evolutionary Optimization of Morphological Representations of Topology," ASME Journal of Mechanical Design, **122**:560-566.

Tai, K., Cui, G.Y., and Ray, T., 2002, "Design Synthesis of Path Generating Compliant Mechanicms by Evolutionary Optimization of Topology and Shape," Journal of Mechanical Design, Transactions of the ASME, **124**(3):492-500.

Topping, B.H.V., Khan, A.I., and Leite, J.P.D.B., 1996, "Topological Design of Truss Structures Using Simulated Annealing," Structural Engineering Review, **8**(2-3):301-304.

Wadehn, W., Sommerer, A., Lutz, T., Fokin, D., Pritschow, G., and Wagner, S., 2002, "Structural Concepts and Aerodynamic Design of Shock Control Bumps," 23rd ICAS Congress, Toronto, Canada, September 8-13, **66R1.1**:66R1.1-66R1.10.

Wang, M.Y., Wang, X., and Mei, Y., 2004, "Design of Multi-Material Compliant Mechanisms Using Level Set Methods," ASME Journal of Mechanical Design, **(in review)**

Washington, G., 1996, "Smart Aperture Antennas," Journal of Smart Materials and Structures, **5**(6):801-805.

Washington, G., Yoon, H.S., Angelino, M., and Theunissen, W.H., 2002, "Design, Modeling, and Optimization of Mechanically Reconfigurable Aperture Antennas," IEEE Transactions on Antennas and Propagation, **50**(5):628-637.

Webb, G.V., Lagoudas, D.C., and Kulkarini, M., 1999, "Adaptive Shape Control for an Sme-Actuated Aerofoil Rib Structure," Proceedings of IMECE, **59**:205-212.

Yoon, H.S. and Washington, G., 1998, "Piezoceramic Actuated Aperture Antennae," Journal of Smart Materials and Structures, **7**(4):537-542.

Yoon, H.S., Washington, G., and Theunissen, W.H., 2000, "Analysis and Design of Doubly Curved Piezoelectric Strip-Actuated Aperture Antennas," IEEE Transactions on Antennas and Propagation, **48**(5):755-763.

Zhou, M. and Rozvany, G.I.N., 1991, "The Coc Algorithm, Part Ii: Topological, Geometry and Generalized Shape Optimization," Computer Methods in Applied Mechanics and Engineering, **89**:197-224.